

Cambrian evolution of the Earth's system:
integrated chemostratigraphy and geochronology
of Cambrian sequences in the East Warburton
Basin, South Australia

Word Count: 7,968

Thesis submitted in accordance with the requirements of the University of
Adelaide for an Honours Degree in Geology

Josh Craig Watson
November 2019



THE UNIVERSITY
of ADELAIDE

CAMBRIAN EVOLUTION OF THE EARTH'S SYSTEM: INTEGRATED CHEMOSTRATIGRAPHY AND GEOCHRONOLOGY OF CAMBRIAN SEQUENCES IN THE EAST WARBURTON BASIN, SOUTH AUSTRALIA

RUNNING TITLE

Chemostratigraphy and Geochronology of Cambrian Aged Carbonates and Volcanics in East Warburton Basin, South Australia

ABSTRACT

The early Paleozoic Warburton Basin is considered the economic basement to the stacked petroleum producing Cooper-Eromanga system. However, is one of the least studied subsurface basins in Australia regarding its depositional, stratigraphic and tectonic histories. This study provides enhanced chronostratigraphic resolution and constraints on surficial and crustal processes, including depositional environment, palaeo-redox and basin restriction through utilising high resolution stable and radiogenic isotope proxies ($\delta^{13}\text{C}$, $^{87}\text{Sr}/^{86}\text{Sr}$) and major/trace elemental analysis on Cambrian aged marine carbonates from two petroleum wells (Gidgealpa 7 and Kalladeina 1) in East Warburton Basin. U/Pb zircon geochronology on the unconformably underlying Cambrian Mooracoochie Volcanics provided additional, absolute chronological constraints. $^{87}\text{Sr}/^{86}\text{Sr}$ isotopes and REE analysis were used to assess the controversial vuggy dolomite found in Gidgealpa wells to determine origin of dolomitization. $\delta^{13}\text{C}$ results provide enhanced chronostratigraphic resolution for both wells for throughout the middle-late Cambrian (~510 to ~495 Ma), through identification of a number of globally recognised Cambrian carbon isotope excursions (CIE's), (i.e., SPICE, DICE and ROECE). Coupled with sedimentary/gamma logs, this study puts forward evidence for a transgression during the SPICE. $^{87}\text{Sr}/^{86}\text{Sr}$ isotope data is extremely locally radiogenic compared to that of expected coeval Cambrian paleo-seawater, suggesting basin restriction, and REE analysis suggests oxic conditions. Absolute age constraints from U/Pb zircon geochronology yielded best ages of 509.1 ± 2.1 Ma and 510.8 ± 3 for Gidgealpa 7 and Kalladeina 1, respectively. Lastly, this study puts forward evidence for both karstification (marine/meteoric isotope signature) and hydrothermal fluid dolomitization (Eu anomalies) for origin of the vuggy dolomite. Overall, this study provides unprecedented constraints on the geochronostratigraphic framework of the East Warburton Basin through the identification of a number of global Cambrian CIE's and U/Pb geochronology on Cambrian aged sequences, with evidence for basin restriction, oxic conditions and a complex interplay between karstification and hydrothermal fluid dolomitization for origin of vuggy dolomite.

KEYWORDS

Warburton Basin, Cambrian, Chemostratigraphy, Geochronology, Palaeo-Redox, Kalladeina Formation, Mooracoochie Volcanics

TABLE OF CONTENTS

Cambrian evolution of the earth's system: integrated chemostratigraphy and geochronology of Cambrian Sequences in the east warburton basin, south australia	i
Running title	i
Abstract	i
Keywords	i
List of Figures and Tables	3
1. Introduction	5
2. Geological Background	9
3. Methods	14
3.1 Isotope Chemostratigraphy – Carbon & Strontium	15
Sample Selection: Cuttings	15
3.1a Carbon Isotopes: $\delta^{13}\text{C}$	15
Sample preparation	15
3.1b Radiogenic Strontium Isotopes: $^{87}\text{Sr}/^{86}\text{Sr}$	16
Sample Preparation	16
Chromatographic purification of Strontium	16
TIMS Analysis of $^{87}\text{Sr}/^{86}\text{Sr}$	17
Correction of $^{87}\text{Sr}/^{86}\text{Sr}$ for in-situ ^{87}Rb Decay	17
3.2 Geochronology - U/Pb Zircon Dating	18
Sample Selection	18
3.3 Elemental Analysis	19
Major and Trace Element Concentration Analysis	19
Rare Earth Elements (REE)	19
3.3 'Vuggy' Dolomite	20
4. Results	21
4.1 Isotope Chemostratigraphy	21
4.1a Carbon Isotope ($^{13}\text{C}/^{12}\text{C}$) Analysis	21
4.1b Strontium Isotope ($^{87}\text{Sr}/^{86}\text{Sr}$) Analysis	24
4.2 Elemental Analysis	25
4.3 Rare Earth Elements (REE)	30
4.4 Geochronology – U/Pb Zircon Dating	32
Igneous Zircon Analyses	36
4.5 Vuggy Dolomite	41
5. Discussion	42

5.1 Carbon Isotope Record of Carbonates from the Kalladeina Formation: Implications on Primary Productivity, Organic Burial and Chemostratigraphy	42
SPICE (Steptoean Positive Carbon Isotope Excursion)	43
DICE (Drumian Carbon Isotope Excursion)	48
ROECE (Redlichiiid-Oleneliid Extinction Carbon Isotope Excursion)	49
5.2 Assessment of Diagenesis and Clay Contamination on $^{87}\text{Sr}/^{86}\text{Sr}$	51
5.3 Comparison of $^{87}\text{Sr}/^{86}\text{Sr}$ Values: Implications on Paleo-Depositional Environment	57
5.4 Rare Earth Element (REE) Constraints on Paleo-Redox and Hydrothermalism	58
5.5 Geochronological Constraints on Early Cambrian Mooracoochie Volcanics	61
5.6 Vuggy Dolomite: Isotope Constraints on the Origin of Dolomitization	62
6. Conclusions	65
Acknowledgments	68
References	68
Appendix A: Extended Methods	74
Isotope Chemostratigraphy – Carbon & Strontium	74
Carbon Isotopes: $\delta^{13}\text{C}$	74
Radiogenic Strontium Isotopes: $^{87}\text{Sr}/^{86}\text{Sr}$	75
Geochronology – U/Pb Zircon Dating	76
Appendix B: Full Dataset	78
Major and Trace Element Data Sets for Gidgealpa 7 and Kalladeina	78
Carbon Isotope ($\delta^{13}\text{C}$) Datasets	99
Sr Isotope ($^{87}\text{Sr}/^{86}\text{Sr}$) Datasets	106

LIST OF FIGURES AND TABLES

Figure 1. a) Global marine carbon isotope ($\delta^{13}\text{C}$) reference curve for throughout the Cambrian. b) Global palaeo-seawater Sr isotope curve for throughout the Cambrian-Ordovician.....	7
Figure 2. a) A palaeoceanographic reconstruction of Australia during Paibian with respect to other Cambro-Ordovician basins and the stacked Warburton-Cooper-Eromnaga system. b) Regional stratigraphic log of stacked Warburton-Cooper-Eromnaga basin system.....	9
Figure 3. Warburton Basin map displaying structural geology and location of studied wells.....	10
Table 1. Summary of East Warburton Basin Cambrian sequences.....	12
Figure 4. Images and descriptions of different facies observed in the Kalladeina Formation.....	13
Figure 5. Images of “Vuggy Dolomite” from base of Kalladeina Formation with brief description.....	14
Table 2. Detailed description of 3 step leaching procedure used for all carbonates.....	16
Table 3. Description of parameters used to calculate in-situ ^{87}Rb decay in carbonates..	18
Figure 6. $\delta^{13}\text{C}$ data from this study versus stratigraphic depth	22
Figure 7. $^{87}\text{Sr}/^{86}\text{Sr}$ data from this study versus stratigraphic depth.....	23
Table 4. Summaries of elemental concentrations and ratios in Gidgealpa 7 and Kalladeina 1.....	25
Figure 8. Sr concentrations and Rb/Sr ratio versus stratigraphic depth.....	26
Figure 9. Sr/Mn ratio and Mg concentrations versus stratigraphic depth.....	27
Figure 10. Ce and Pr anomaly data (Ce/Ce* and Pr/Pr*) versus stratigraphic depth.....	29
Figure 11. Eu anomaly data (Eu/Eu*) versus stratigraphic depth.....	31
Table 5. Summary of concordant U/Pb zircons and associated ages obtained from all Mooracoochie Volcanic samples analysed.....	36
Figure 12. CL images of igneous zircons from Mooracoochie Volcanics.....	37
Figure 13. Concordia plots for sample G7U for all/concordant grains with weighted means plot.....	38
Figure 14. Concordia plot for sample K1A for all grains.....	39
Figure 15. Concordia plots for sample K1B for all/concordant grains with weighted means plot.....	40
Table 6. Displays all $^{87}\text{Sr}/^{86}\text{Sr}$ values and Eu/Eu* anomalies for analysed “Vuggy Dolomite” samples.....	41
Figure 16. REE distribution pattern for Gidgealpa 5 “Vuggy Dolomite” samples.....	42
Figure 17. Sedimentary/gamma logs provided by SANTOS with interpreted sequence stratigraphy for Gidgealpa 7 and Kalladeina 1 wells.....	45
Figure 18. $\delta^{13}\text{C}$ data integrated with sedimentary logs from Copp (2019).....	47
Figure 19. ROECE ($\delta^{13}\text{C}$) excursion comparisons between published data (Guo et al. 2010) and this study.....	50
Figure 20. Cross plot of shale-normalized (PAAS) Ce/Ce* and Pr/Pr* anomalies for ROECE excursion in Gidgealpa 7.....	51
Table 7. Elemental statistical summary for the SPICE interval between Gidgealpa 7 and Kalladeina 1 for meteoric diagenesis and clay contamination indices and Sr isotope signature.....	54

Figure 21. Seismic cross-section of Gidgealpa 7 and Kalladeina 1 wells with interpreted sequence stratigraphy.....55

Figure 22. Cross plot of elemental concentrations (Al) and ratios (Rb/Sr & Sr/Mn) versus Sr isotope signature.....56

Figure 23. Cross plot of corrected $^{87}\text{Sr}/^{86}\text{Sr}$ versus Rb/Sr ratio for all Kalladeina 1 and Gidgealpa 7 samples.....58

Figure 24. Cross plot of shale-normalized (PAAS) Ce/Ce* and Pr/Pr* anomalies for all Gidgealpa 7 and “least altered” Kalladeina 1 samples.....59

Figure 25. Cross plot of corrected $^{87}\text{Sr}/^{86}\text{Sr}$ versus Rb/Sr ratio for all analysed limestones and dolomites.....63

1. INTRODUCTION

The hydrocarbon province comprising the Cooper and Eromanga Basins is the most productive onshore petroleum province in Australia (Radke, 2009; Hallman et al., 2006). Considered the economic basement to this stacked petroleum producing system is the unconformably underlying Cambro-Ordovician Warburton Basin (Roberts et al., 1990; Hallman et al., 2006; Sun 1996). Despite its economic potential, the Warburton Basin is one of the least studied subsurface basins in Australia in regard to its depositional, stratigraphic and tectonic histories, stemming from a lack of surface exposure, limited core material and a lack of high-quality seismic information (Sun 1996, 1998; Gatehouse 1986). The drilling of Innamincka 1 in 1959, in conjunction with seven more dry holes in 1963 targeting Permian strata but penetrated Warburton Basin stratigraphy, represented the onset of exploration in this petroleum supersystem, and also provided us with most of what we know about the basin (Gatehouse 1986; Roberts et al., 1990; Carr et al., 2016; Hallman et al., 2006; Alexander, 2008; Sun 1996).

The Warburton Basin represents a window into one of the most critical intervals in Earth history, being deposited during the major biological event known as ‘The Cambrian Explosion’, represented by the emergence and diversification of multicellular animals and the appearance of the first mineralised skeletons during the Cambrian period (Peters & Gaines 2012; Peng et al., 2012; Zhuravlev & Wood 2018). This biological radiation of the ‘Cambrian Explosion’ was also accompanied with a range of climatic and environmental changes, which are reflected in changes in the isotopic composition of the Cambrian oceans, the latter recorded in marine carbonates

(Zhuravlev & Wood 2018; Zhang & Shu 2014). Such global geochemical and environmental change, in conjunction with the correlative complexities associated with the Warburton Basin (i.e., lack of core material and subsurface data) reiterate the potential and need for future chemostratigraphic studies in this relatively underexplored depositional system (Jones et al., 2010; Wright et al., 2010). For example, recent carbon (C) and strontium (Sr) chemostratigraphic studies based on well-preserved marine carbonates from major Phanerozoic and Precambrian depositional systems have documented significant systematic C and Sr isotopic variation during key intervals of geologic time, providing enhanced chronostratigraphic resolution and unprecedented quantitative constraints on the surficial and crustal processes that govern them (Montañez et al., 2000; Kouchinsky et al., 2008; Schmid 2017).

Changes in the ratio of stable carbon isotopes (i.e., $^{13}\text{C}/^{12}\text{C}$ ratio, expressed also as $\delta^{13}\text{C}$) in global oceans (preserved in marine carbonate) are related to changes in the global biogeochemical carbon cycle, driven by processes such as; primary productivity, organic carbon burial, continental weathering, volcanic CO_2 emissions, ocean circulation and global sedimentation rates (Montañez et al., 2000; LeRoy & Gill 2019). There is a range of studies from different regions around the world that document temporal changes in $\delta^{13}\text{C}$ of Cambrian aged marine carbonates with regard to the Cambrian (Chang et al., 2017; Ahlberg et al., 2009; Howley et al., 2010; Kouchinsky et al., 2008; Saltzman et al., 2000; 2004; Schmid 2017; Woods et al., 2011, Fan et al., 2011). These studies identified a number of globally recognised carbon isotope excursions (CIE's), including the Steptoean Positive Isotope Excursion (SPICE), the Redlichiiid-Olenellid Extinction Carbon Isotope Excursion (ROECE), and/or the

Drumian Carbon Isotope Excursion (DICE), for details see also the global marine carbon isotope reference curve for the Cambrian period (see Figure 1a), (Saltzman et al., 2000). More importantly, the SPICE among other large-scale CIE's coincide with chronostratigraphic boundaries related to mass extinctions, global paleoclimate and sea-level fluctuations, herein lying their chronologic and correlative potential (Zuo et al., 2018; Saltzman et al., 2000).

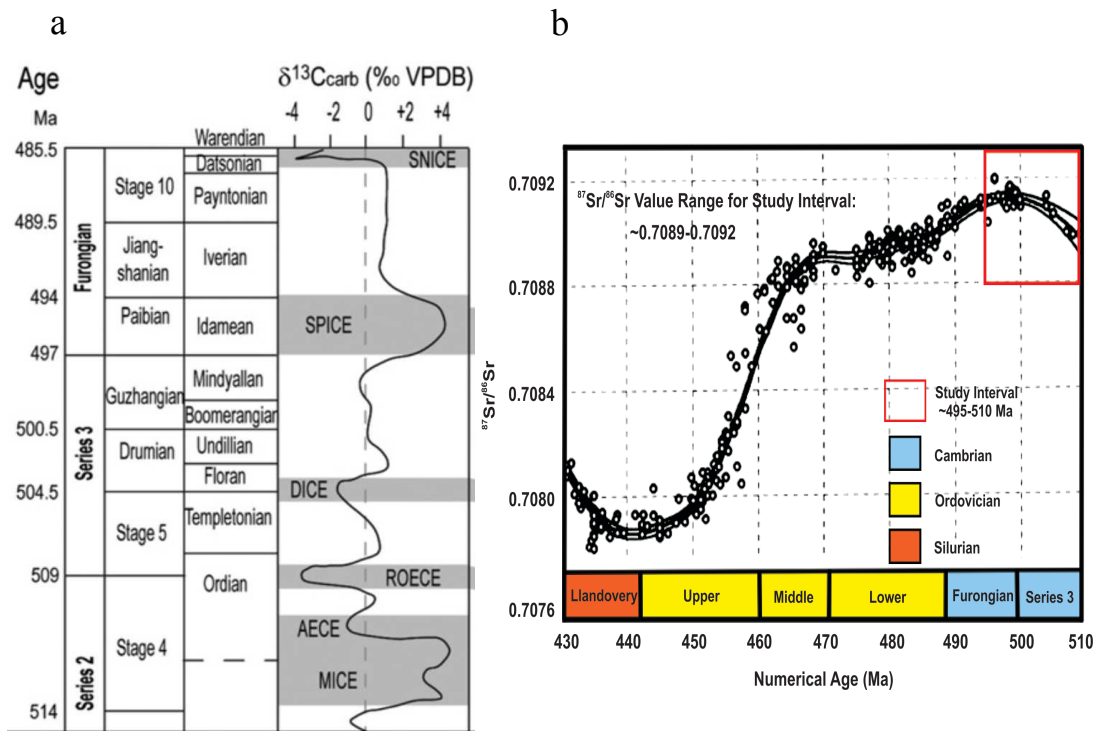


Figure 1. a) Global marine carbon isotope ($\delta^{13}C$) reference curve for throughout the Cambrian by Peng et al. (2012). b) Expected global palaeo-seawater Sr isotope curve for throughout the Cambrian, indicated by McArthur et al., 2012; Montañez et al., 1996; Peng et al., 2012; Kouchinsky et al., 2008, modified from McArthur et al. (2012).

Variations of radiogenic Sr isotopes ($^{87}Sr/^{86}Sr$) in the oceans and thus in marine carbonate archives are regulated predominantly between the balance of Sr fluxes to the ocean from either continental weathering, or hydrothermal inputs via fluid-rock (i.e., seawater-basalt) interactions. As highly complementary marine isotope proxies, this

study aims to couple high resolution $^{87}\text{Sr}/^{86}\text{Sr}$ and $\delta^{13}\text{C}$ records from Gidgealpa 7 and Kalladeina 1 wells drilled in the East Warburton Basin (Figure 3) for intra and interbasinal correlations and chronological constraints on Cambrian carbonate sequences, with implication for global palaeoceanographic and biogeochemical events. Additionally, because of the unique stratigraphic framework and geological/tectonic history of this basin, the underlying volcano-sedimentary sequences called the Mooracoochie Volcanics (see 'Geological Background'), will integrate absolute age constraints derived from U-Pb zircon geochronology to better refine the geochronostratigraphic framework of this unique and poorly explored Cambrian basin.

Lastly, this study also aims to use the analysis of rare earth elements (REE's) in leached limestones and dolostones to i) reconstruct the palaeo-redox conditions during deposition of Cambrian marine carbonates using cerium (Ce/Ce^*) anomaly, and also ii) identify evidence for hydrothermal fluid dolomitization of marine carbonates, possibly related to Mooracoochie Volcanics, with the application of europium (Eu/Eu^*) anomaly. The unique chemistry of Ce whereby its valence and solubility changes as a function of oxidising conditions allows it to be a proxy for determining depositional redox conditions, particularly when coupled with praseodymium (Tostevin et al., 2016; Hua et al., 2013). Additionally, enrichments in REE's and Eu anomalies in seawater or marine carbonates can be used to identify hydrothermal fluid component (Olivarez & Owen 1991).

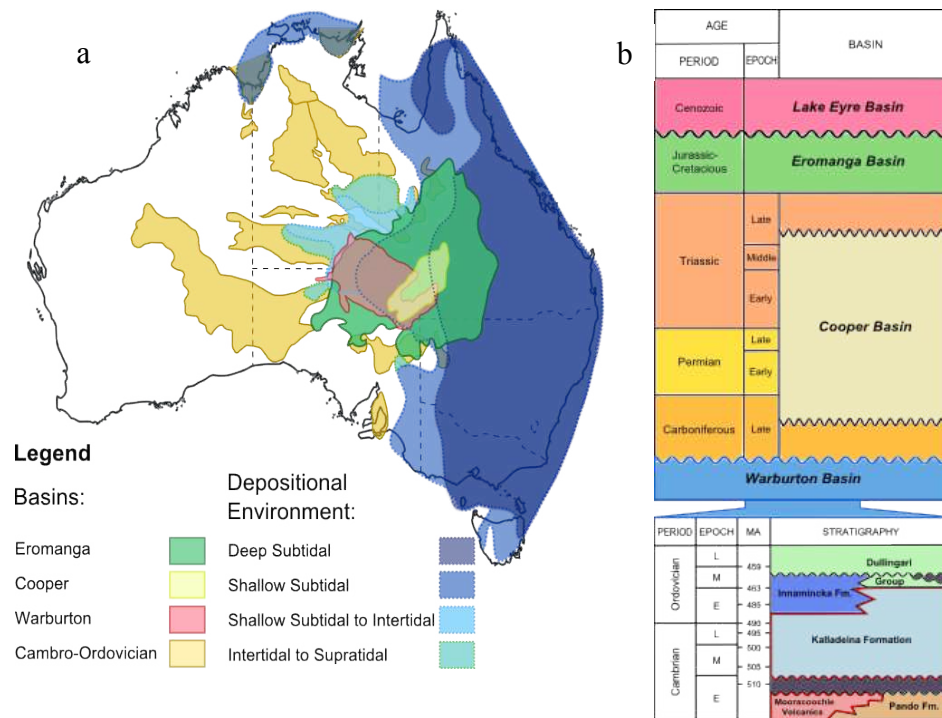


Figure 2. Figure a) is a palaeoceanographic reconstruction of interpreted depositional environment during the Cambrian (495 Ma) for Australia. Displays layout of Australian Cambro-Ordovician basins and the stacked Warburton-Cooper-Eromanga system, represented by the red-yellow-green colour scheme, from which an interplay between the Warburton Basin and depositional environment can be inferred (modified from (Schmid et al., 2018)). Figure b) represents a stratigraphic log of the region; the stacked Warburton-Cooper-Eromanga system, with a more detailed log of the relevant Warburton Basin. The red outline of Warburton Basin formations indicates those addressed in this study (modified from (Sun 1996; Khair et al., 2013)).

2. GEOLOGICAL BACKGROUND

The Warburton Basin is located in north east South Australia, neighbouring parts of the Northern Territory and Queensland, unconformably underlying the Permian-Triassic Cooper and Mesozoic Eromanga Basin respectively. Geographically, the Warburton basin is bound by a number of neighbouring structures, including the Arunta block to the north, the Musgrave block to the west and the Muloorina ridge to the south. Interpreted to have originally formed in a back-arc basin setting on the eastern margin of Gondwana, the Warburton Basin is subdivided into 2 sections, the western and eastern. The boundary between the two is approximated by the Birdsville Track Ridge in a north-east trend across the basin (Ambrose 2007 & 2008). The Western Warburton

is the larger portion of the basin, however despite this has attracted little seismic and exploration drilling in comparison to the eastern part, consequently less is known about it.

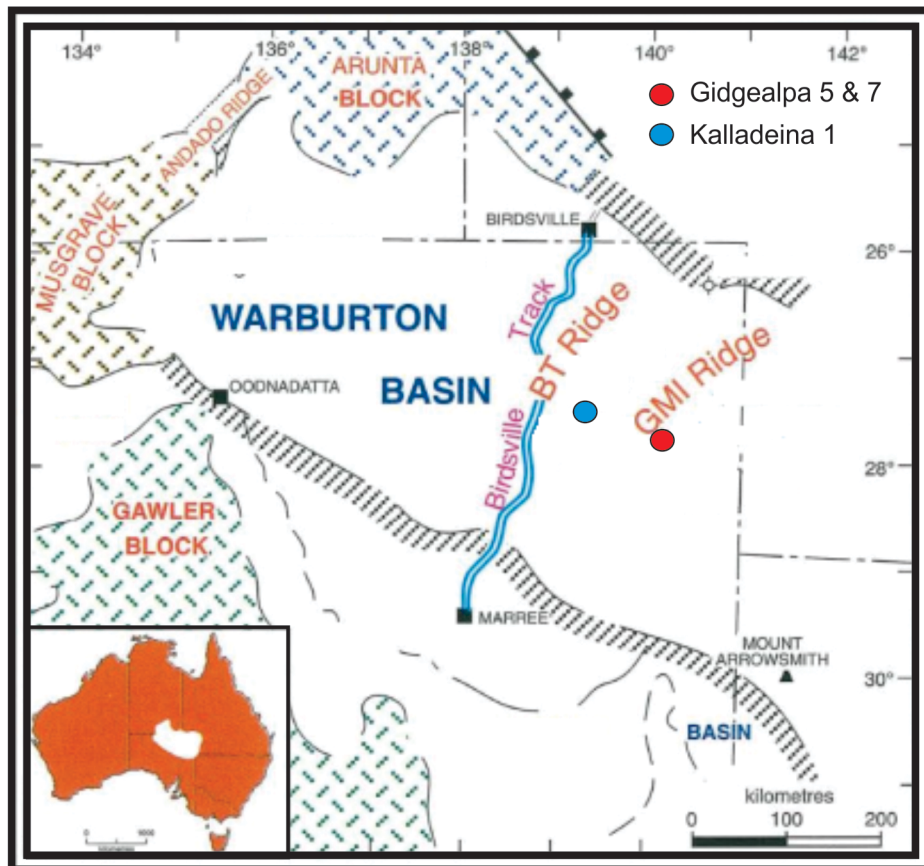


Figure 3. Displays the structural geology of the study site, includes the Warburton Basin and neighbouring structures/basins, including the Gawler, Musgrave and Arunta Block and the Officer and Arrowie Basin. The subdivision between the West and East Warburton is indicated by the blue, linear Birdsville Track ridge. The wells driving this study in the Kalladeina 1 and Gidgealpa 7 are indicated by the blue and red circles respectively, approximately 90kms from one another. Geographical coordinates, scale and basin context with respect to Australia is included (modified from (Sun 1996; Copp 2019).

The Warburton Basin was defined by Wopfner (1972) and more recently by Gatehouse (1986) as a depositional system containing sediments of lower Cambrian to Devonian age. Gatehouse (1986) formally identified three major stratigraphic units: the Mooracoochie volcanics, the Kalladeina Formation and the Dullingari Group, which

was later revisited and restructured, with the inclusions of the Innamincka and Pando Formations (Sun 1996). The Cambrian aged deposits are represented by the Mooraochie Volcanics and Kalladeina Formation, while the Dullingari Group and Innamincka Formation are slightly younger, Ordovician to possibly Devonian age respectively (see figure 1B), with this study addressing the chronostratigraphy of the Cambrian volcano-sedimentary sequences including the Mooracoochie Volcanics and overlying marine carbonates (i.e., the Kalladeina Formation), (see Table 1 below). The Pando Formation is somewhat more controversial, with its age and position within the basins framework still heavily debated (Sun 1996).

East Warburton Basin Cambrian Stratigraphy – Focus of this Study

Table 1. Provides a range of information on the Cambrian aged formations/sequences being addressed in this study, including the Mooracoochie Volcanics, Kalladeina Formation and “Vuggy Dolomite”. Information includes; definition (Gatehouse et al., 1986; Sun 1996), lithology (Copp 2019; Gatehouse 1986; Sun 1996) and tectonic setting/depositional environment (Roberts et al., 1990; Gatehouse 1986; Sun 1996).

Unit/Formation - Age	Definition	Lithological Description and/or Facies	Tectonic Setting/Depositional Environment
Mooracoochie Volcanics - Published U/Pb zircon age of 517±9Ma (Stewart 2010)	Embraces all the major volcanics encountered in the basin, classified into 2 phases: i) Early Cambrian Felsic Volcanics - namely the Mooracoochie Volcanics (focus of this study) ii) Middle to Late Cambrian Basaltic Volcanics	Mainly felsic to intermediate lava including rhyolite, trachyte, dacite (i) and minor basalt (ii). Includes volcanoclastic rocks; syn-eruptive hyaloclastites and ignimbrites	Two tectonic settings depicted for Gidgealpa arc: a) Volcanic arc setting b) Continental rift setting
Kalladeina Formation – Figure 4 - Defined as Middle-Late Cambrian	Early-Middle to Late Cambrian, carbonate-dominated strata with an early carbonate dominated stage and a late stage consisting of mixed siliciclastic/carbonate lithologies	Comprises of limestones (locally dolomitised), intercalated by siltstone, shale, sandstone and minor tuff, with the following facies recognised: i) <i>Platform facies</i> ii) <i>Slope facies</i> iii) <i>Basinal and distal slope facies</i>	Deposited on a low- to moderate-energy slope adjacent to shallower microbial- and shoal-dominated carbonate platform, where off-platform deposits are typically represented by fine-grained carbonate-rich tempestites.
“Vuggy Dolomite” (Kalladeina Formation) – Figure 5 - Youngest unit of the Kalladeina Formation	A dolomitic layer at the bottom of the Kalladeina Formation containing vuggy and fracture porosity	Complete dolomitization and secondary fabrics make it difficult to identify the precursor rock, but the latter is assumed to be unaltered limestone of the Kalladeina Formation	Depositional environment for precursor rock (i.e., Kalladeina Formation limestone) is mentioned above. Karstification and hydrothermal dolomitization are both suggested models for dolomitization making it the topic of debate amongst the petroleum industry

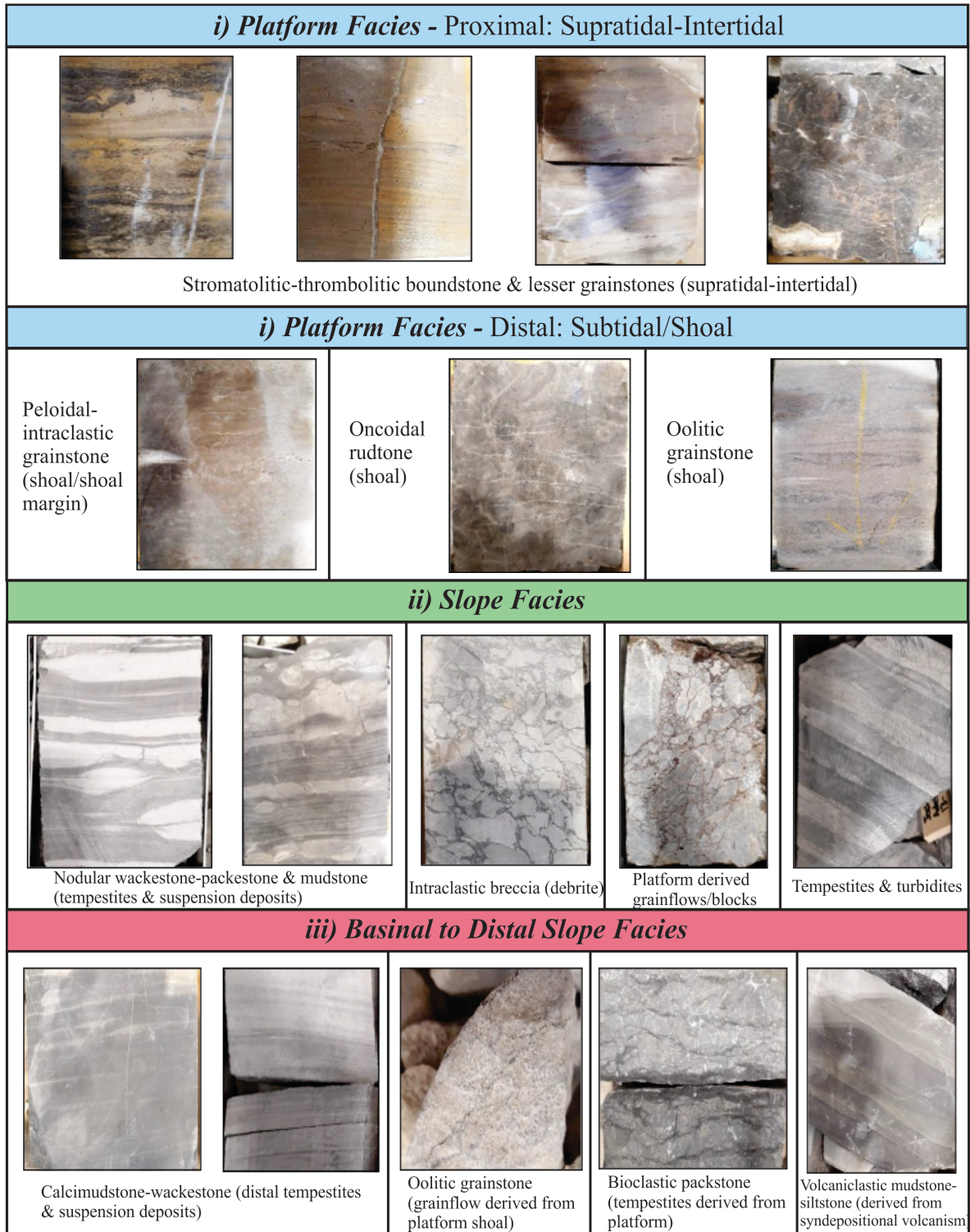


Figure 4. Images and brief descriptions of the different lithologies/facies present in the Kalladeina Formation. The different facies are subdivided into 3 categories; i) Platform facies – proximal & distal, ii) slope facies and iii) basinal to distal slope facies, as mentioned in table 1. Images and descriptions are from Copp (2019).

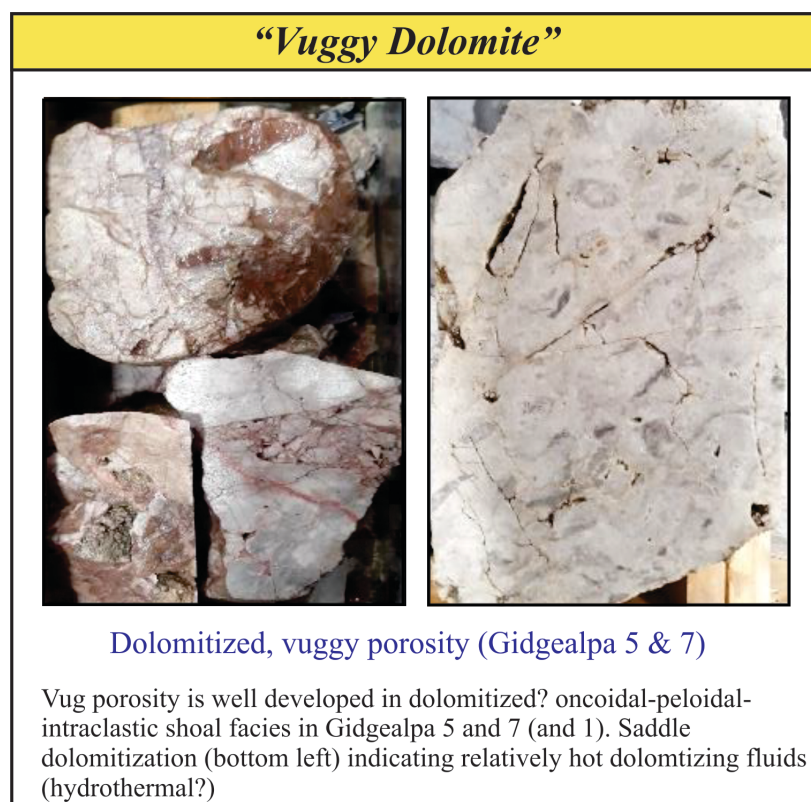


Figure 5. Images of “vuggy dolomite” from the Kalladeina Formation in wells; Gidgealpa 5 and 7, representing a key porous and permeable unit in the East Warburton Basin. Brief description of the rock unit has been provided, as interpreted from Copp (2019), in conjunction with style of dolomitization (i.e., hydrothermal dolomitization?). Images and descriptions from Copp (2019).

3. METHODS

Sections below provide brief summaries of selected techniques and methods used for (i) sample preparation, (ii) elemental/isotope analyses of carbonates, and (iii) geochronology of zircons (volcanic). Detailed description of analytical methods can be found in the Appendix.

3.1 Isotope Chemostratigraphy – Carbon & Strontium

SAMPLE SELECTION: CUTTINGS

The bulk of the geochemical analysis for this study is based on 225 of rock chips (i.e., cuttings) from Kalladeina Formation in Gidgealpa 7 and Kalladeina 1 located in the Eastern Warburton Basin. This study covers the Middle to Late Cambrian period (~510 to 490 Ma), with samples collected from carbonate-rich sections of strata; ~6 to 15-meter resolution. The carbonate-rich sections were identified by HyLogger spectroscopic data (extremely low gamma ray readings) previously undertaken on the cores and provided by SANTOS Ltd. All samples in this study belong to, and are analysed in accordance with SANTOS Ltd.

3.1a Carbon Isotopes: $\delta^{13}\text{C}$

SAMPLE PREPARATION

225 carbonate samples were crushed carefully into powder using a ring mill and tungsten mortar. Homogenised powders were weighed into vials (~2 mg) and sequentially purged and dissolved in phosphoric acid. The fumes from this sample-acid reaction were recorded at the University of Adelaide using the dual inlet elemental IRMS (Isotope Ratio Mass Spectrometer) to determine $\delta^{13}\text{C}$ and $\delta^{18}\text{O}$ values. Measured data was calibrated against standards ANU P3, UAC and NCM.

3.1b Radiogenic Strontium Isotopes: $^{87}\text{Sr}/^{86}\text{Sr}$

SAMPLE PREPARATION

Homogenised samples and/or standard were transferred into plastic centrifuge tubes (~100mg) and sequentially leached following a 3 step-leaching procedure (modified from (Liu et al., 2013) to extract elements associated with the carbonate phase, observed in the table below (Table 2). Supernatants were collected only in the last step and placed into small acid-cleaned Teflon vials for isotopic and elemental analyses.

Table 2. Detailed description of the 3-step leaching procedure (modified from (Liu et al., 2013) used for all carbonate samples (limestones and dolomites) from the Kalladeina Formation.

Leach Step	Acid Used - Amount	Purpose
1	1M ultra-pure ammonium acetate – 3.6 ml	To liberate elements associated with exchangeable sites at clays (Bailey et al., 2000)
Left at room temperature for 1 hour		
Sonicated for 30 minutes		
Centrifuged for 10 minutes		
Acid leach discarded		
2	0.2M ultra-pure acetic acid – 3.6 ml	Secondary leach step to liberate elements associated with the clay phase
Left at room temperature for 1 hour		
Sonicated for 30 minutes		
Centrifuged for 10 minutes		
Acid leach discarded		
3	0.2M ultra-pure acetic acid – 3.6 ml	Final step extracts elements associated with the carbonate phases (Liu et al., 2010)
Left at room temperature for 1 hour		
Sonicated for 30 minutes		
Centrifuged for 10 minutes		
Acid leach COLLECTED		

CHROMATOGRAPHIC PURIFICATION OF STRONTIUM

Leachates from Step 3 were dried and redissolved in 1 ml of 8M Nitric acid SD and passed through Micro Bio-Spin columns filled with specific Sr resin to extract the pure Sr fraction. Columns/resins were washed multiple times using ultra-pure deionised

water and 8M Nitric acid before samples were loaded and 0.05M Nitric acid used to collect the pure Sr fraction. Collected Sr had a drop of 0.1M Nitric Acid added and dried on a hot plate, and a few drops of 15M nitric acid added to oxidise any organics (modified from (Krabbenhöft et al., 2009)).

TIMS ANALYSIS OF $^{87}\text{Sr}/^{86}\text{Sr}$

The pure Sr fraction was dried on a hot plate and loaded onto Rhenium filaments using Brick's solution and the $^{87}\text{Sr}/^{86}\text{Sr}$ ratio measured in a multidynamic mode at the University of Adelaide using the ISOTOPX Phoenix Thermal Ionisation Mass Spectrometer (TIMS). Measurements are normalized using exponential mass fractionation correction. Procedural Sr blanks were measured via isotope dilution using ^{84}Sr spike as a tracer, and determined to be negligible compared to Sr derived from a sample (i.e., ~.083 to 1.83 ng, compared to ~500 to 1000 ng respectively).

CORRECTION OF $^{87}\text{Sr}/^{86}\text{Sr}$ FOR IN-SITU ^{87}Rb DECAY

The content of radiogenic ^{87}Sr may increase over geological time due to the decay of trace amounts of ^{87}Rb present in the bulk carbonate, potentially altering the primary Sr signal in ancient marine carbonates. To combat this, the measured Sr isotopic composition was corrected for in-situ Rb decay using an equation from (Nurgalieva et al., 2007):

$$(^{87}\text{Sr}/^{86}\text{Sr})_0 = (^{87}\text{Sr}/^{86}\text{Sr})_{\text{Measured}} - (^{87}\text{Rb}^*/^{86}\text{Sr}^*) \times (e^{\lambda t} - 1) \quad \text{Eq. 1}$$

Table 3. Description of parameters and values used in the above in-situ ^{87}Rb decay equation (Eq.1).

Parameter	Definition/Value
$(^{87}\text{Sr}/^{86}\text{Sr})_0$	Is the corrected composition for in-situ Rb decay
$(^{87}\text{Sr}/^{86}\text{Sr})_{\text{Measured}}$	Present day isotope composition of carbonates,
$(^{87}\text{Rb}^*/^{86}\text{Sr}^*)$	The molar $^{87}\text{Rb}/^{86}\text{Sr}$ ratio of leached sample
λ	The ^{87}Rb decay constant of $1.393 \cdot 10^{-11} \text{ yr}^{-1}$
t	Time; represented in this study by the geochronological constraint of $\sim 510 \text{ Ma}$.

3.2 Geochronology - U/Pb Zircon Dating

SAMPLE SELECTION

Zircons were picked and analysed from 4 volcanic samples from the unconformably underlying Mooracoochie volcanics, 2 from each well; Kalladeina 1 and Gidgealpa 7. The zircons were separated/picked at the University of Adelaide (see appendix), mounted using epoxy resin and polished exposing the grains. Sequentially, mounts were carbon coated in preparation for cathodoluminescence (CL) imaging, which was done using the FEI Quanta 600 Scanning Electron Microscope (SEM) with attached Gatan CL detector at Adelaide Microscopy (AM). CL images identified the internal structure of the zircons, allowing core-rim structures to be identified and targeted for U/Pb analysis. Analysis took place at AM, programming predetermined laser spots and determining U/Pb concentration using the Laser Ablation Inductively Coupled Plasma-Mass Spectrometer (LA-ICP-MS).

Data was processed using Iolite and plotted using Excel add-in Isoplot (Ludwig, 2003). The GEMOC GJ-1 zircon standard (TIMS normalisation data: $207\text{Pb}/206\text{Pb} = 607.7 \pm 4.3 \text{ Ma}$, $206\text{Pb}/238\text{U} = 600.7 \pm 1.1 \text{ Ma}$ and $207\text{Pb}/235\text{U} = 602.0 \pm 1.0 \text{ Ma}$, Jackson et al., 2004) corrected for mass bias and laser induced fractionation, additionally the Plesovice internal zircon standard ($206\text{Pb}/238\text{U} = 337.13 \pm 0.37$, Slama et al., 2008) assessed accuracy of the analysis. 30 Plesovice internal standards were analysed,

yielding a weighted average $^{206}\text{Pb}/^{238}\text{U}$ age of 342.4 ± 1.8 (95% confidence, MSWD = 0.60). U/Pb geochronology results were plotted on Wetherill plots, typically with respective weighted means plots. Age calculations were derived from grains >90% concordance and weighted average plots of the $^{206}\text{Pb}/^{238}\text{U}$ age plots were used to assess and identify Pb loss. All U/Pb data for igneous samples can be found in the Appendix.

3.3 Elemental Analysis

MAJOR AND TRACE ELEMENT CONCENTRATION ANALYSIS

Carbonate leachates from step 3 were dried on a hotplate and sequentially diluted with ~2% Nitric acid into 1:1,000 aliquots for rare earth and trace element analysis, and 1:10,000 aliquots for major elements. For analysis, the Agilent 8900x (QQQ) Inductively Coupled Plasma Mass Spectrometer (ICP-MS) was used at Adelaide Microscopy to measure the elemental concentration of 202 leached carbonate samples, incorporating JLs-1 standards and acid blanks. All blanks produced elemental concentrations below the detection limit.

RARE EARTH ELEMENTS (REE)

The PAAS (Post Archean Australian Shale) normalized Cerium anomaly (Ce/Ce^*) when coupled with Praseodymium anomaly (Pr/Pr^*) can be a valuable marine redox proxy due to its unique +3 and +4 oxidation states relative to its neighbouring REE's (Tostevin et al., 2016). Additionally Eu anomaly (Eu/Eu^*) can be a valuable indicator for hydrothermal activity in marine settings (Meyer et al., 2012; Tostevin et al., 2016)

To calculate these anomalies, the ‘shale normalized’ to PAAS equation from Taylor & McLennan (1985) was used:

$$\text{Ce/Ce}^* = [\text{Ce/Ce(PAAS)}] / [0.5 \times (\text{La/La(PAAS)}) + 0.5 \times (\text{Pr/Pr(PAAS)})] \quad \text{Eq.2}$$

$$\text{Pr/Pr}^* = [\text{Pr/Pr(PAAS)}] / [0.5 \times (\text{Ce/Ce(PAAS)}) + 0.5 \times (\text{Nd/Nd(PAAS)})] \quad \text{Eq.3}$$

$$\text{Eu/Eu}^* = [\text{Eu/Eu(PAAS)}] / [0.5 \times (\text{Sm/Sm(PAAS)}) + 0.5 \times (\text{Gd/Gd(PAAS)})] \quad \text{Eq.4}$$

3.3 ‘Vuggy’ Dolomite

3 dolomitic drill core samples from Kalladeina Formation in Gidgealpa 5 were sampled and analysed for major/trace element concentration and also $^{87}\text{Sr}/^{86}\text{Sr}$ isotope analysis.

A total of 5 sub-samples (~100mg each sample) were drilled and sequentially leached using the same 3 step leaching procedure mentioned previously. Drilling spots targeted vugs as well as dark/light dolomitized sections, to encompass all observed alteration styles. Similar dilution aliquots of 1:1000 for REE and trace element analysis, and 1:10,000 aliquots for major element analysis. The Agilent 8900x (QQQ) ICP-MS was used at Adelaide Microscopy for elemental analysis on all 5 dolomite samples.

Leachates followed the same $^{87}\text{Sr}/^{86}\text{Sr}$ isotope analysis process previously described in ‘3.1b Radiogenic Strontium ($^{87}\text{Sr}/^{86}\text{Sr}$)’.

4. RESULTS

4.1 Isotope Chemostratigraphy

4.1A CARBON ISOTOPE ($^{13}\text{C}/^{12}\text{C}$) ANALYSIS

185 carbonate samples from Kalladeina Formation were analysed for $^{13}\text{C}/^{12}\text{C}$ ($\delta^{13}\text{C}$) and plotted as a function of depth; 87 from Gidgealpa 7 and 98 from Kalladeina 1. The top of the core in Gidgealpa 7 exhibits a positive $\delta^{13}\text{C}$ excursion from 7701' to 8072', with bimodal peaks of 3.26‰ at 7800' and a more pronounced peak of 3.67‰ at 7940', identified as the SPICE anomaly (~496-499 Ma) with a thickness of 371' (see Figure 6). In Kalladeina 1 the SPICE is also identified at depths 8310' to 9510', exhibiting a more pronounced positive $\delta^{13}\text{C}$ excursion of 5.24‰ at 8460', in conjunction with a 3x larger thickness corresponding to ~1200'.

Below the SPICE in Gidgealpa 7, the $\delta^{13}\text{C}$ record fluctuates between positive to consistently more negative $\delta^{13}\text{C}$ values. At depth 9500', values become increasingly more negative, specifically between 9530'-9580', reaching about -1.71‰, potentially corresponding to the DICE anomaly. In Kalladeina 1 the DICE has been potentially identified at depths 10430' to 10760' (see Figure 6), and similar to SPICE, the DICE is also more pronounced in this well with a negative peak of -3.25‰ at depth 10610'. Another anomaly potentially identified is the ROECE, in Gidgealpa 7 it is a sharp negative excursion identified at 10100' to 10210', with a peak of -2.89‰ at 10110'. Identifying the ROECE in Kalladeina 1 is more problematic and it can either be at depths: i) 11210' to 11330' with a plateaued peak of -3.2‰ at 11240', or alternatively

ii) 11330' to 11450' with a pronounced peak of -4.03‰ at 11390', iii) or a combination of the above.

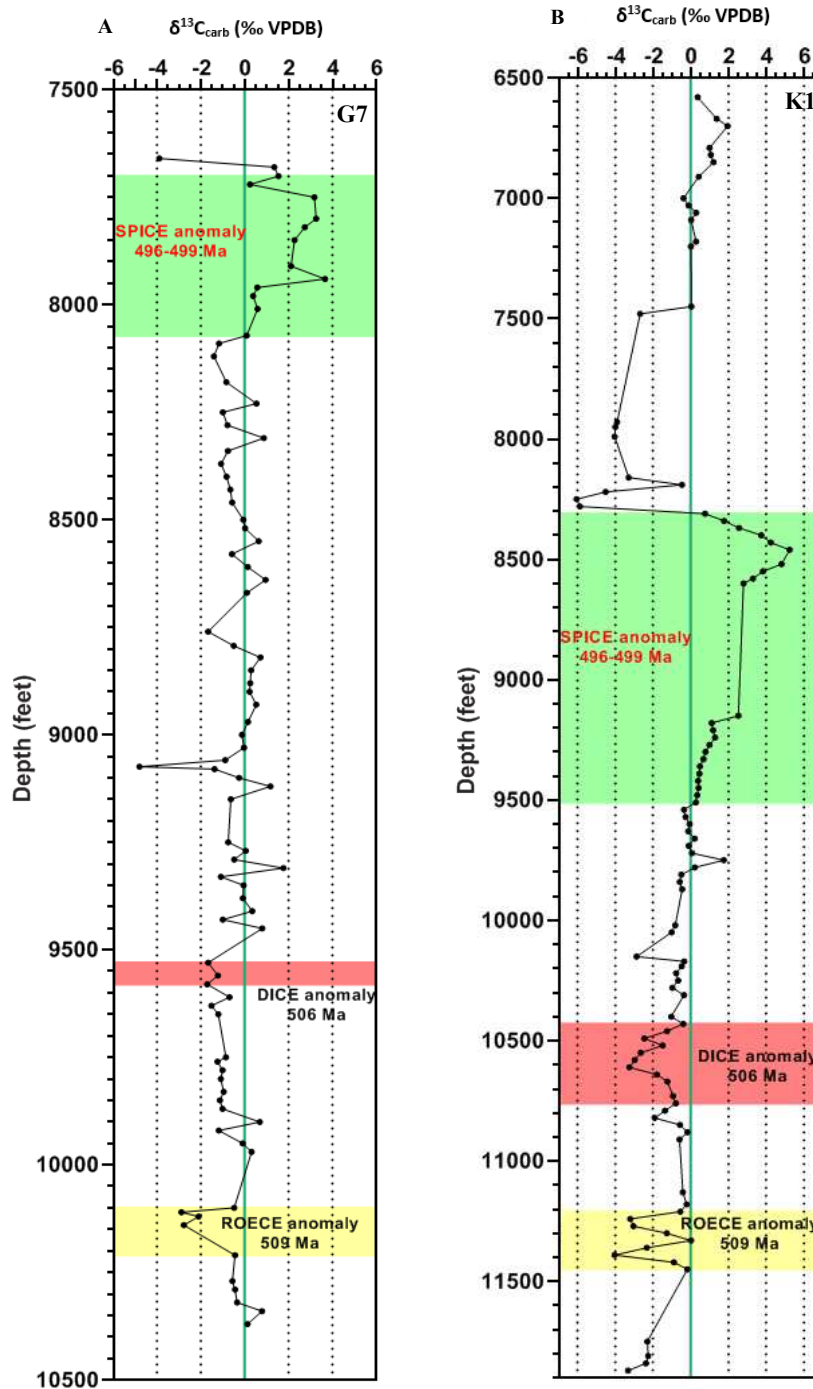


Figure 6. Figure a) is a composite $\delta^{13}\text{C}$ curve for throughout the Cambrian by Fan et al. (2011), with key carbon isotope excursions (CIE's) identified with respect to the geologic timescale. The dashed red box indicates the geologic interval of interest for this study. Figure b) displays the $\delta^{13}\text{C}$ data for Gidgealpa 7 and figure C) displays the $\delta^{13}\text{C}$ data for Kalladeina 1 versus stratigraphic depth (feet). $\delta^{13}\text{C}$ values are 'per mil', standardized to Vienna Pee Dee Belemnite (VPDB). Shaded areas indicate potentially identified CIE's, annotated respectively, including the age. The SPICE excursion at the top, DICE in the middle and ROECE at the base.

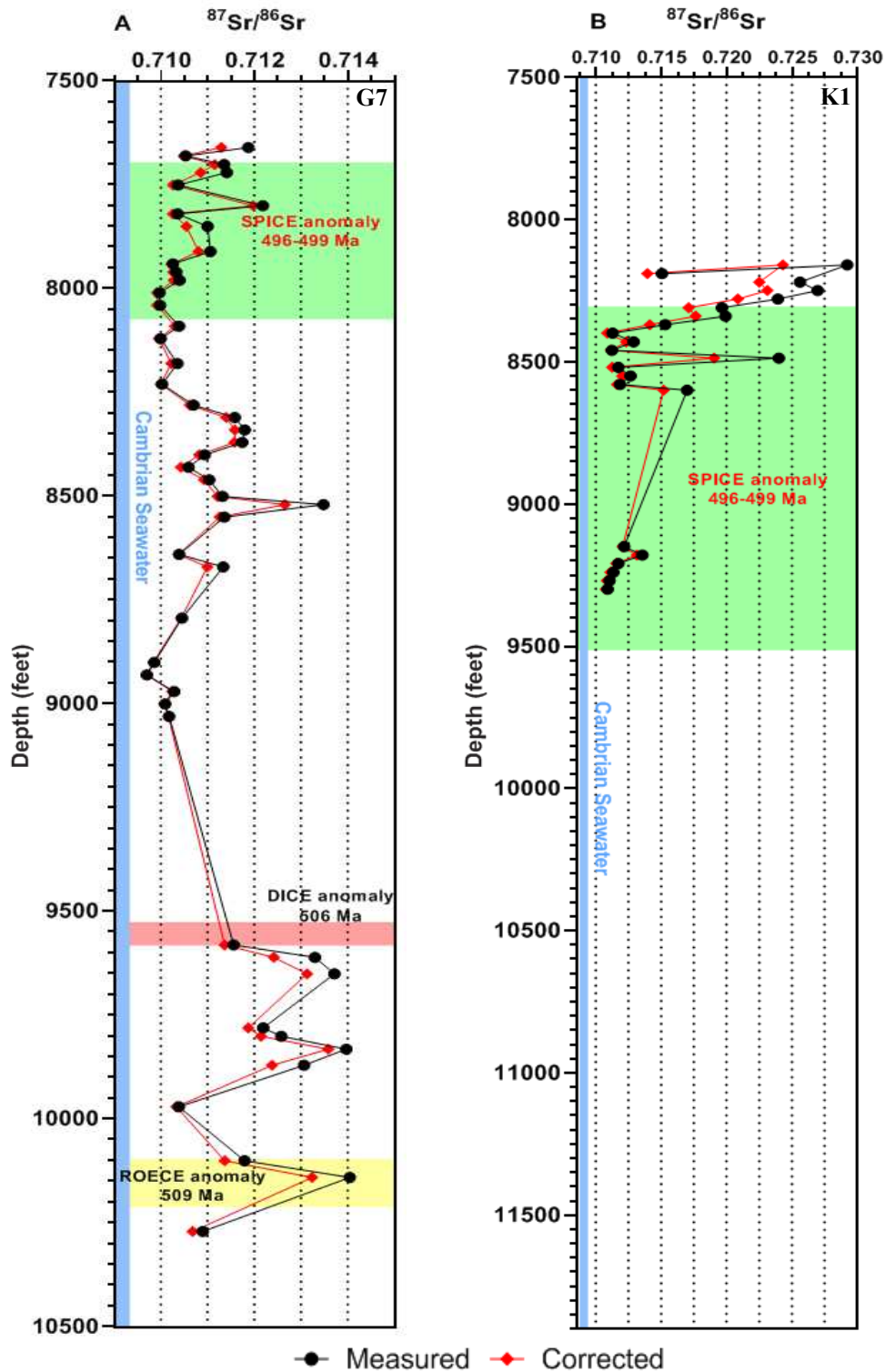


Figure 7. $^{87}\text{Sr}/^{86}\text{Sr}$ values for both Gidgealpa 7 (a) and Kalladeina 1 (b) plotted versus stratigraphic depth (feet). The black data set indicates measured $^{87}\text{Sr}/^{86}\text{Sr}$ values, and the red data set indicates values corrected for in-situ Rb decay (Eq. 1). The blue line represents $^{87}\text{Sr}/^{86}\text{Sr}$ value range expected for Cambrian paleo-seawater at that time (~509 to ~497 Ma; 0.7089-0.7093, indicated by McArthur et al., 2012; Montañez et al., 1996; Peng et al., 2012; Kouchinsky et al., 2008). Shaded intervals indicate identified CIE's, annotated accordingly.

4.1B STRONTIUM ISOTOPE ($^{87}\text{Sr}/^{86}\text{Sr}$) ANALYSIS

69 carbonate samples from Kalladeina Formation were analysed for $^{87}\text{Sr}/^{86}\text{Sr}$ isotope ratios and plotted as a function of depth in Figure 7, 47 from Gidgealpa 7 and 22 from Kalladeina 1. All $^{87}\text{Sr}/^{86}\text{Sr}$ values were corrected for in-situ Rb decay (using Eq. 1), with values ranging from ~ 0.709692 to ~ 0.713585 ($2\text{se} = 0.000004$) in Gidgealpa 7 and ~ 0.710777 to ~ 0.724312 ($2\text{se} = 0.000004$) in Kalladeina 1. As to data coverage, the Sr isotope data from Kalladeina 1 is restricted to the SPICE and above, whereas Gidgealpa 7 $^{87}\text{Sr}/^{86}\text{Sr}$ data is throughout the entire drill hole (see Figure 7). Kalladeina 1 contains the most radiogenic $^{87}\text{Sr}/^{86}\text{Sr}$ values just above the SPICE, and none of the data overlaps with the expected Sr isotope composition of coeval Cambrian seawater (~ 0.7089 to ~ 0.7093 ; expected range for Early to Late Cambrian period; ~ 509 to ~ 497 Ma, as reconstructed by McArthur et al., 2012; Montañez et al., 1996; Peng et al., 2012; Kouchinsky et al., 2008). Interestingly, Gidgealpa 7 data show that $^{87}\text{Sr}/^{86}\text{Sr}$ values get closest to the expected Cambrian seawater at depth of 8930' (~ 0.709692) and just below the SPICE, located between 8010' to 8230' with a minimum $^{87}\text{Sr}/^{86}\text{Sr}$ of ~ 0.709915 (see Figure 7). Radiogenic Sr isotope peaks occur in both the ROECE and DICE, and both wells experience a gradual increase in $^{87}\text{Sr}/^{86}\text{Sr}$ values up through the SPICE, peaking in Kalladeina 1 just above the SPICE (8160') at ~ 0.724312 . However, trends and values are somewhat inconsistent, raising questions as to whether the true $^{87}\text{Sr}/^{86}\text{Sr}$ signal has been preserved.

4.2 Elemental Analysis

202 carbonate samples were analysed for elemental concentrations, including selected indicators for diagenesis (Sr/Mn), dolomitization (Mg), clay contamination (Rb/Sr), and REE-based paleo-environmental proxies such as Ce and Eu anomalies; which are plotted separately as a function of depth in Figures 8 and 9. Elemental analyses (summarised below in Table 3) revealed that Kalladeina 1 contained the lowest Sr values, following a series of jagged peaks and falls throughout the well (Figure 8), with values peaking below the SPICE. Sr concentrations in Gidgealpa 7 are relatively low and constant from the base of the well to depth ~8300', prior to fluctuating significantly throughout the SPICE in excess of 400 ppm between data points, peaking just above the event.

Table 4. Summaries for the selected elemental concentration indicators mentioned above (i.e., Sr, Rb/Sr, Sr/Mn and Mg) for both wells; Gidgealpa 7 and Kalladeina 1. Summaries include the lowest value, an average and highest value for all samples analysed.

Gidgealpa 7											
Sr Concentrations (ppm)			Rb/Sr			Sr/Mn			Mg Concentrations (ppm)		
Low	Ave	High	Low	Ave	High	Low	Ave	High	Low	Ave	High
35	276	1,115	.0009	0.039	0.276	0.198	0.861	3.418	487	7432	76,190
Kalladeina 1											
Sr Concentrations (ppm)			Rb/Sr			Sr/Mn			Mg Concentrations (ppm)		
Low	Ave	High	Low	Ave	High	Low	Ave	High	Low	Ave	High
21	235	652	.004	0.199	0.961	.0198	0.423	2.191	805	5680	45,986

The Rb/Sr ratio in marine carbonates can be used as an index for clay contamination to determine what degree clay minerals have contributed to the radiogenic ^{87}Sr present in bulk samples. Rb/Sr ratio is generally low in Gidgealpa 7 (~0.039), with a few isolated peaks through the well, the latter extremity at the top of the DICE (~0.276), (Figure 8). Alternatively, Kalladeina 1 has significantly higher Rb/Sr ratios (~0.199), including an increased number and intensity of peaks, typically in association with identified CIE's.

Extreme Rb/Sr ratios are observed above the SPICE (~9), which could explain the observed highly radiogenic $^{87}\text{Sr}/^{86}\text{Sr}$ values.

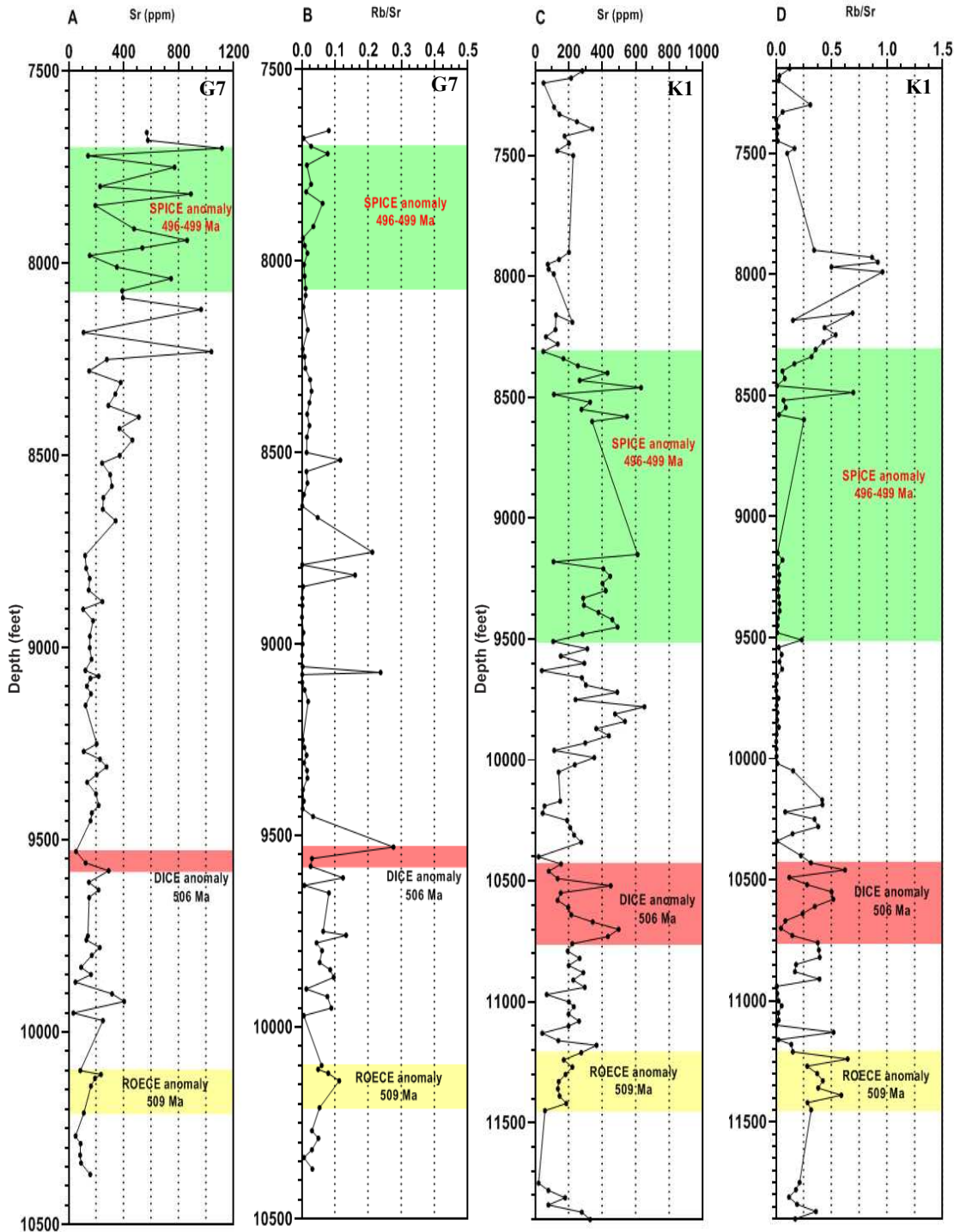


Figure 8. Displays elemental concentrations for Sr and Rb/Sr (ppm) for both wells versus stratigraphic depth (feet). a) Sr concentrations for Gidgealpa 7. b) Rb/Sr ratios for Gidgealpa 7. c) Sr concentrations for Kalladeina 1. d) Rb/Sr ratios for Kalladeina 1. Rb/Sr ratios are used as an indicator for clay contamination. Shaded intervals represent identified CIE's.

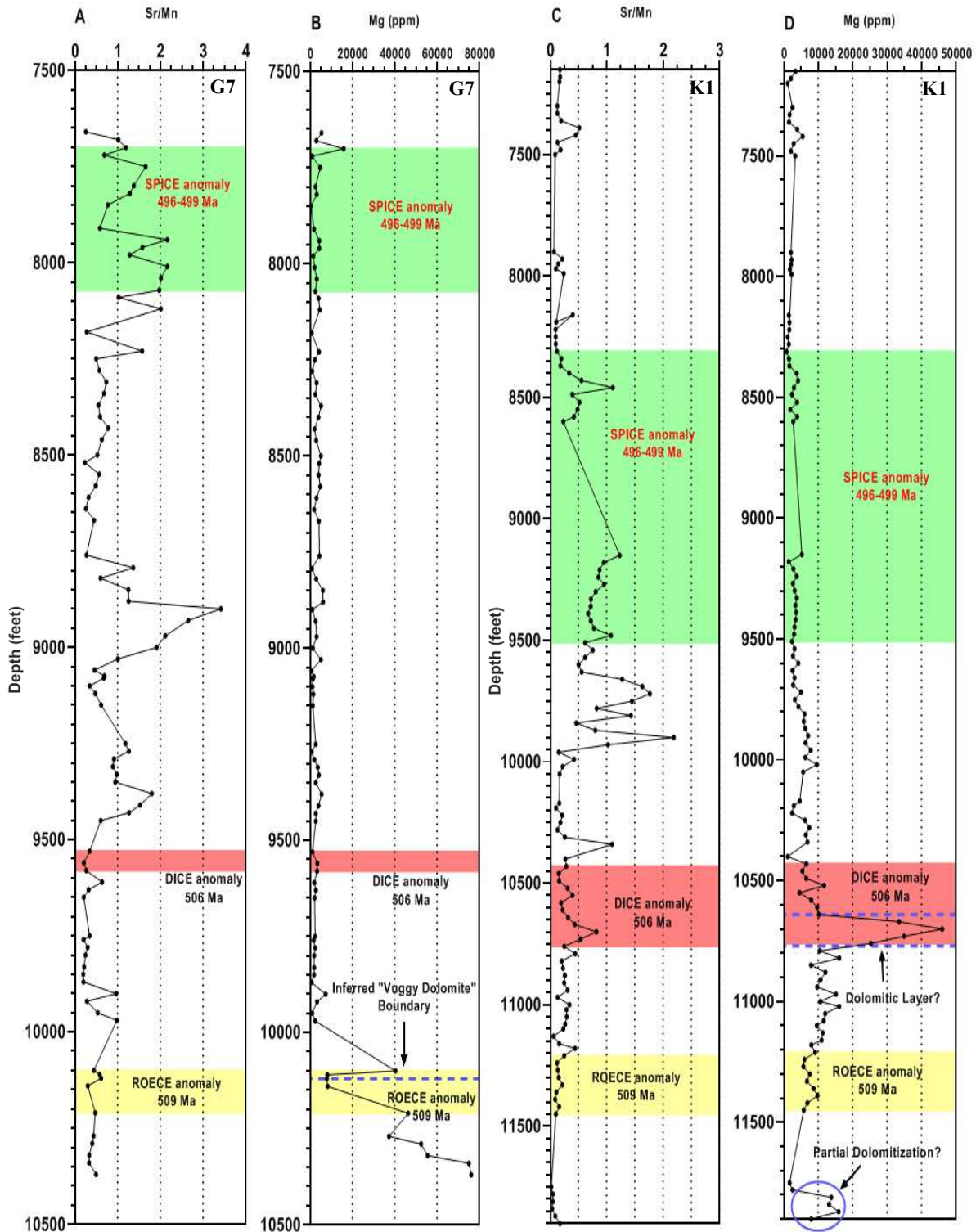


Figure 9. Elemental concentrations, including Sr/Mn and Mg (ppm) for both wells versus stratigraphic depth (feet). a) Sr/Mn ratios for Gidgealpa 7. b) Mg concentrations (ppm) for Gidgealpa 7. c) Sr/Mn ratios for Kalladeina 1. d) Mg concentrations (ppm) for Kalladeina 1. Sr/Mn ratios are used as an indicator of meteoric diagenesis. Concentrations of Mg in these wells, particularly Gidgealpa 7 is likely an indicator for dolomitic carbonate units (Vuggy Dolomite). Shaded intervals represent identified CIE's.

The Sr/Mn ratio in marine carbonates can be an indicator of meteoric diagenesis (Banner & Hansen, 1990), specifically more Sr compared to Mn typically indicates little diagenetic overprint, and vice versa. Both wells have relatively low Sr/Mn ratios, with an average of 0.854 ppm and 0.423 ppm in Gidgealpa 7 and Kalladeina 1 respectively. Both Gidgealpa 7 and Kalladeina 1 also have noticeable Sr/Mn peaks in the “middle depths” of the wells, as well as during the SPICE. Additionally, the Mg concentration in both wells provides a valuable indicator for the transition from a limestone to dolomite. The latter can be observed in both Kalladeina 1 and Gidgealpa 7, with Mg concentrations peaking in Gidgealpa 7 at high levels of 76,190 ppm. The transition is not as significant in Kalladeina 1 and it includes a more dominant peak further up the well at 10700' (~45,986 ppm), (see Figure 9).

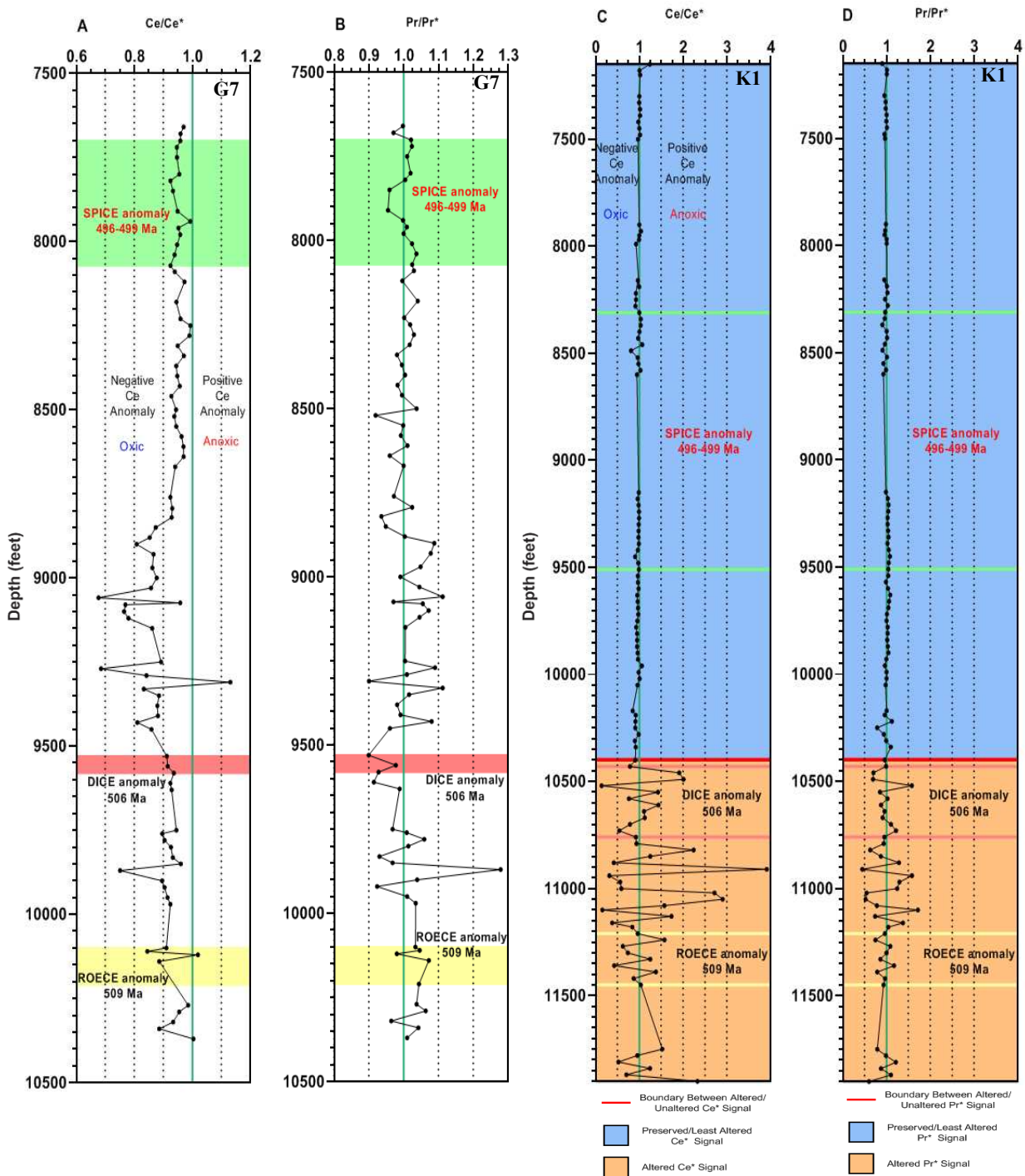


Figure 10. Displays Ce anomalies and Pr anomalies for both wells versus stratigraphic depth. a) Ce/Ce* anomaly for Gidgealpa 7. b) Pr/Pr* anomalies for Gidgealpa 7. c) Ce/Ce* anomalies for Kalladeina 1. d) Pr/Pr* anomalies for Kalladeina 1. Ce anomalies can be used as a redox tool to reconstruct paleo-seawater conditions, negative anomalies associated with oxic conditions, positive anomalies associated with anoxia, as indicated on the figure. Kalladeina 1 wells (C & D) are subdivided into 2 sections based on alteration of REE signal. The upper half (blue) indicates a preserved, or least altered REE signal and alternatively the bottom half (brown) represents the noisy, hydrothermally altered REE signal. The boundary between the two indicated by the red line at 10400'. Redox anomalies were analysed for Kalladeina 1 from the upper, unaltered section of the well. Eq. 2 was used to calculate Ce/Ce* anomalies and Eq. 3 for Pr/Pr* anomalies. Shaded intervals and representative lines indicate identified CIE's.

4.3 Rare Earth Elements (REE)

Redox sensitive rare earth elements (REE), such as cerium (Ce) have a distinct distribution pattern in seawater and marine carbonates and can be used as a valuable proxy for understanding paleo-redox conditions in marine environments (Tostevin et al., 2015). Both Cerium (Ce) and Praseodymium (Pr), the latter used as an indicator of Ce data quality, are plotted as a function of depth. In Gidgealpa 7, the Ce anomaly (Ce/Ce^*) fluctuates strongly with a minimum of 0.677 (i.e., negative Ce anomaly, indicating relatively oxic marine conditions) at the base of the well (8820') and becomes more stable up the stratigraphy with less negative values ($Ce/Ce^* < 1$), peaking at 0.993 in the SPICE. In Kalladeina 1 both Ce and Pr experience significant shifts in values from the base of the well to 10430'. These extraordinary shifts, including Ce anomaly changes exceeding 2, should be treated with caution, with extremely variable values likely the product of diagenesis and secondary alteration. Above 10430', the Ce anomaly in Kalladeina 1 remains stable with a slight mean negative anomaly of ~ 0.973 and an increase in positive anomalies, concentrated in the upper part of the SPICE and above, peaking at ~ 1.241 (increase in reducing conditions). Additionally, Europium (Eu) which is an index for hydrothermal fluid source (Olivarez & Owen 1991), experiences a significant positive anomaly at the base of Kalladeina 1 (Figure 10). Specifically, from 11900' to 11750' there is a sustained positive Eu anomaly peak of ~ 2.011 , before dropping back to ~ 1 , where it remains relatively constant through the rest of the core, with minor positive anomalies at depths 10170', 9210' and 8430'. The Eu anomaly in Gidgealpa 7 fluctuates very significantly between positive and negative values, with the latter concentrated in the upper half of the well.

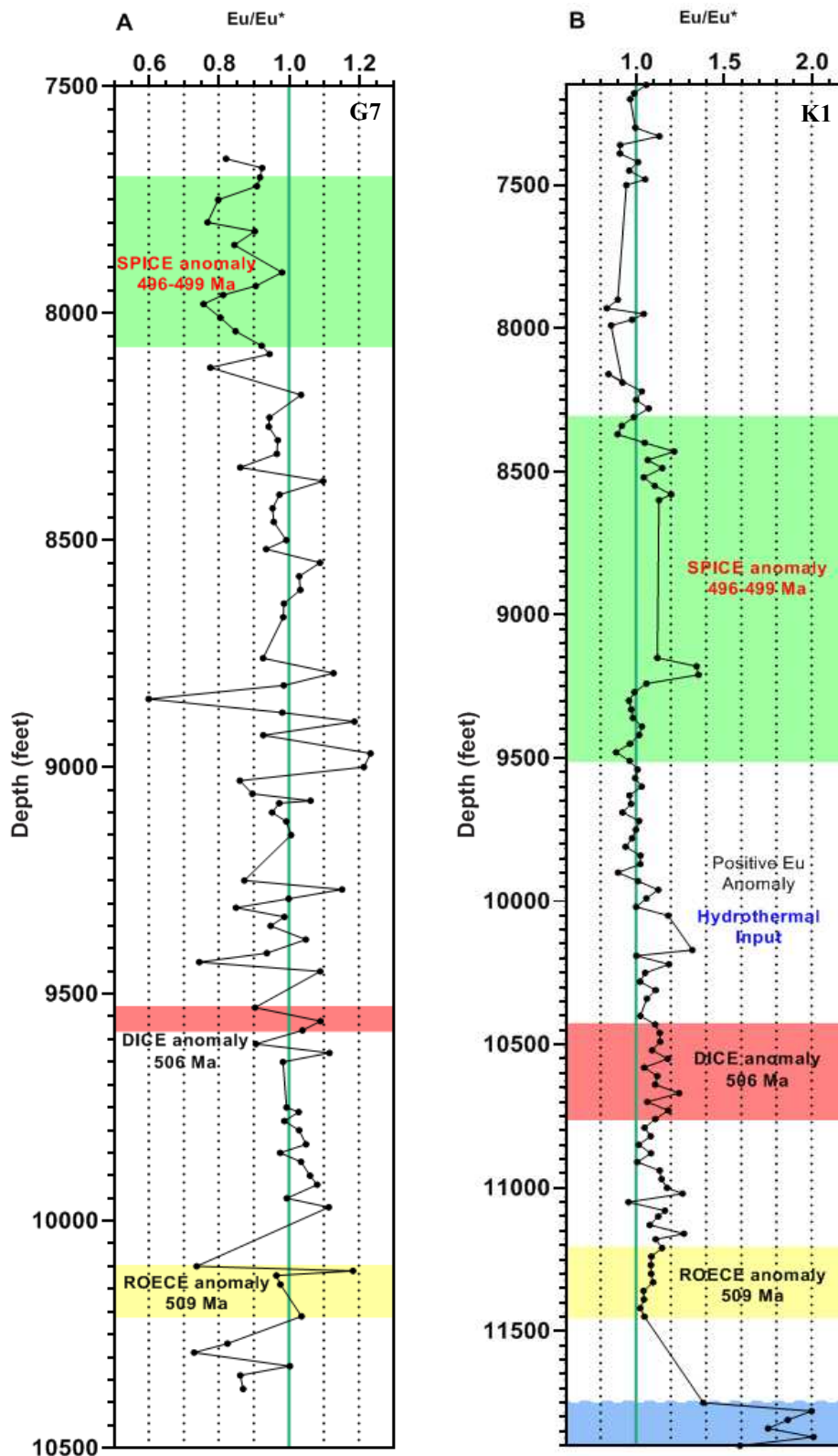


Figure 11. Eu anomaly trends for both wells versus stratigraphic depth. a) Eu anomaly for Gidgealpa 7. b) Eu anomaly for Kalladeina 1. The shaded blue section at the base of Kalladeina 1 indicates an interval that experiences a significant positive Eu anomaly, which is typically a product of hydrothermal fluids, consequently it can be used as a proxy for hydrothermal input. The Eu anomaly was calculated relative to PAAS using Eq. 4.

4.4 Geochronology – U/Pb Zircon Dating

U/Pb zircon ages are derived from 4 samples of the Mooracoochie Volcanics, 2 from Gidgealpa 7 at depths 10567' (G7U) and 10572' (G7L), and 2 from Kalladeina 1 at depths 11821' (K1A) and 11964' (K1B), yielding a combined 279 laser-ablation U/Pb spots. Exact analysis numbers and associated ages for respective wells are displayed below in Table 5. Zircon grains in this study vary in size and shape, but are typically elongated, prismatic grains showing oscillatory zoning under CL imaging, characteristic of volcanics and indicative of growth within a magma chamber (Corfu et al. 2003). The Concordia plot of all analyses shows a distinct Pb-loss trend, specifically the youngest four samples from G7U and the youngest from K1B were excluded due to Pb-loss illustrated in blue in the weighted means plots (i.e., those observed slipping downwards in Figures 13 and 15, respectively). The oldest grain in K1B is considerably older and is interpreted to represent inheritance and excluded accordingly (see Figure 15). All ages and associated MSWD are provided in Table 5 below, for a degree of classifications previously mentioned. Briefly, G7U and K1B yielded the best ages of 509.1 ± 2.1 Ma (MSWD of 1.4) and 510.8 ± 3 Ma (MSWD of 2.2) respectively, and all concordant grains (from all samples, minus exclusions) yielding 510 ± 1.6 Ma (MSWD of 1.8).

IGNEOUS ZIRCON ANALYSES

Constraints on Crystallisation Age of Mooracoochie Volcanics

Sample	Well	Depth (feet)	Total Number of Analysed Grains	Concordant Grains (>90%)	Exclusion + Classification	Age	MSWD
G7U	Gidgealpa 7	10567'	160	27	All Grains	507.1±2.5	2.6
G7U	Gidgealpa 7	10567'	160	23	Excluding bottom 4; Pb loss	509.1±2.1	1.4
G7L	Gidgealpa 7	10572'	10	-	-	-	-
K1A	Kalladeina 1	11820.7'	23	3	All Grains	513±13	1.5
K1B	Kalladeina 1	11964'	86	20	All Grains	510.9±3.5	3.3
K1B	Kalladeina 1	11964'	86	19	Excluding bottom sample; Pb loss	511.6±3.4	3.0
K1B	Kalladeina 1	11964'	86	19	Excluding top sample; inheritance	510.1±3.1	2.5
K1B	Kalladeina 1	11964'	86	18	Excluding top & bottom; Pb loss/ inheritance	510.8±3	2.2
All	K1 & G7	-	279	50	All Grains	508.9±2	3.0
All	K1 & G7	-	279	44	Removing all exclusions	510±1.6	1.8

Table 5. All the U/Pb zircon ages obtained from analysed Mooracoochie Volcanic samples. Displays respective well, depth (feet), total number of zircon grains analysed, number of grains >90% concordance, any exclusion of grains and classification of exclusion, age and MSWD for each respective sample. Samples G7U and K1B have multiple rows due to a degree of classifications specified in the table, yielding a variety of ages and MSWD's. Red columns indicate the best ages for each sample, typically those with exclusions yielding the best ages. Due to no concordant grains, age could not be determined for G7L. "All" represents a collation of all analyses, with ages displayed for all concordant grains and removing all exclusions. The blue column indicates the best age obtained for the U/Pb analysis.



Figure 12. CL images from igneous zircons from Gidgealpa 7 (G7U) and Kalladeina 1 (K1A & K1B) Mooraoochie Volcanics in the East Warburton Basin. Zircon grains are generally prismatic with oscillatory zoning, characteristic of igneous zircons. Positioning of U/Pb laser spots has been indicated with the corresponding age obtained from analysis. Different colours represent the different samples analysed, as depicted in the legend in the top right. Laser spots containing an asterisk (*) indicate those samples excluded from final age constraint due to either; Pb loss or inheritance. Interestingly, of the 3 excluded samples from G7U displayed (4 total), 2 are rims, which characteristically record late stage volcanism. This in conjunction with Pb loss would explain the values observed. The K1B excluded sample yielding an apparently old age contains a number of dark, inherited regions near the positioned laser spot, suggesting a mixed aged. Therefore, has been excluded from final U/Pb ages under conditions of inheritance.

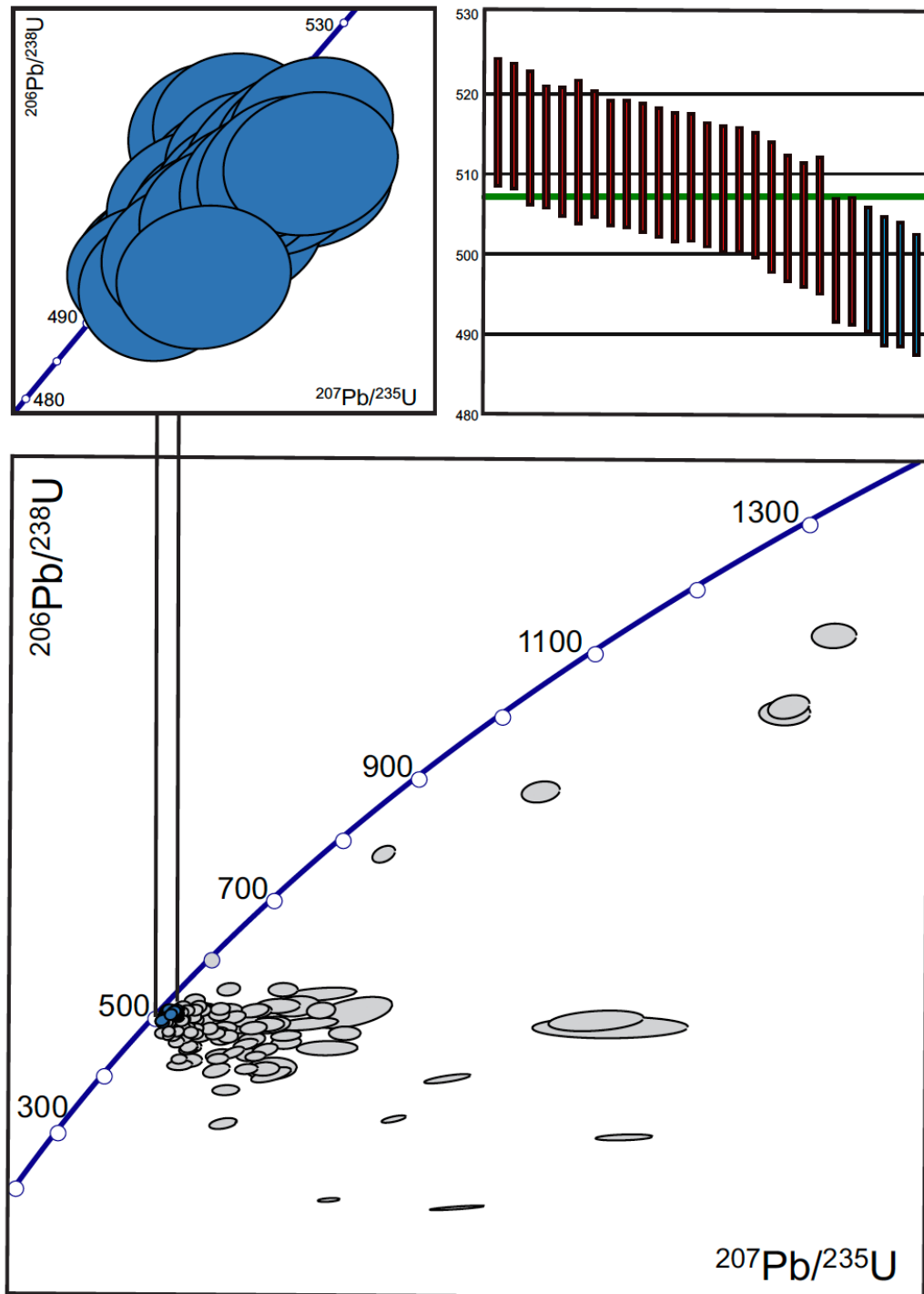


Figure 13. Concordia plot for sample G7U from Gidgealpa 7. The blue line represents the concordant line, samples that locus lie on this yield concordant ages. The centroid of the blue ellipses are >90% confident concordance, represent the samples the ages are derived from. The grey ellipses represent discordant data, representing an open system indicating lead loss from the zircon. The concordant data yields an age of 507.1 ± 2.5 Ma with a MSWD of 2.6. The Concordia to the top left represents only the concordant samples. The top right plot displays a weighted means average of concordant points. Samples in blue indicate those potentially susceptible to lead loss, impacting age of the population. Additional analysis under redefined concordant grains yields an age of 509.1 ± 2.1 Ma with a MSWD of 1.4.

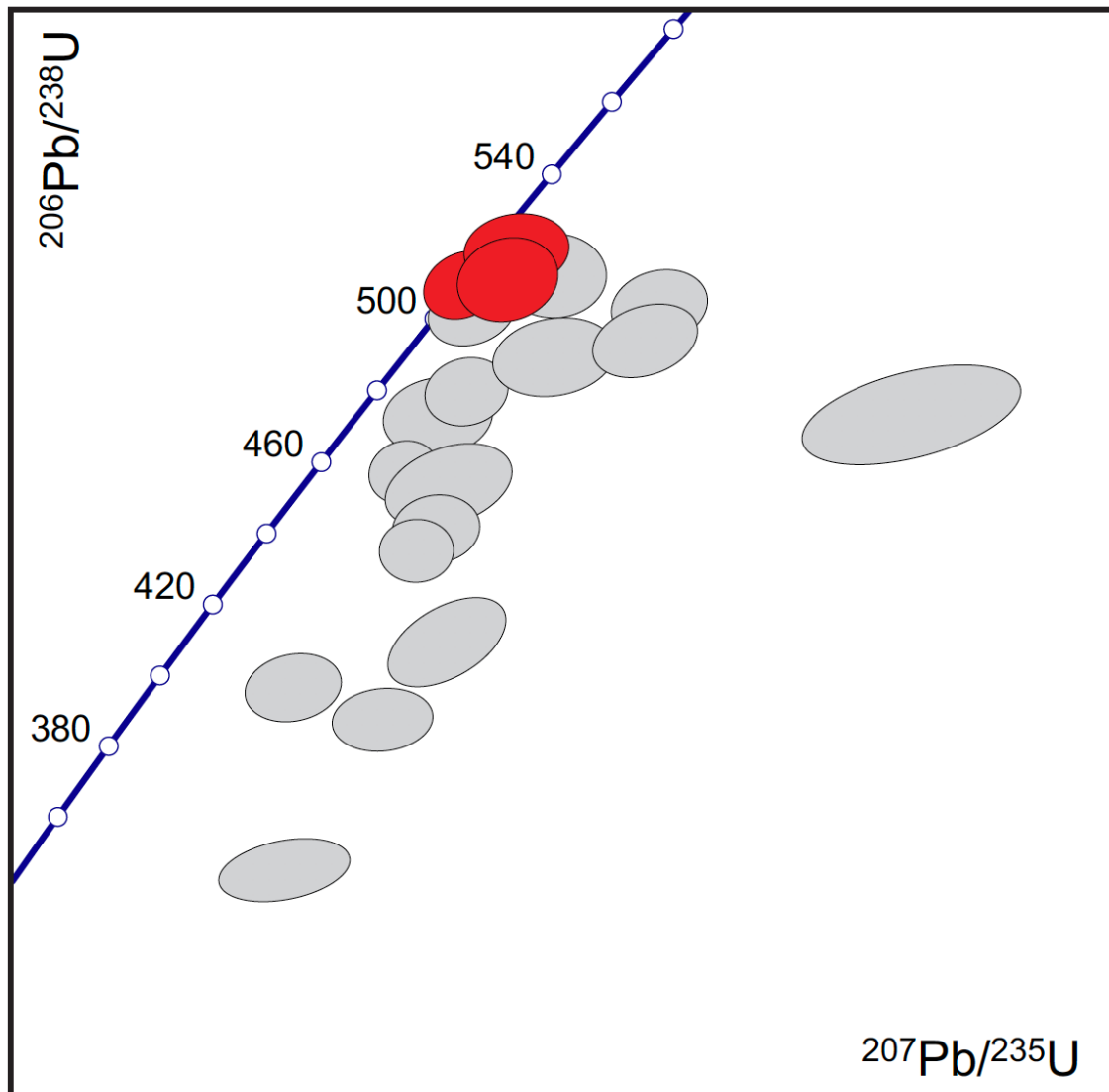


Figure 14. Concordia plot for sample K1A from Kalladeina 1. The blue line represents the concordant line, samples that locus lie on this yield concordant ages. The centroid of the red ellipses are >90% confident concordance, represent the samples the ages are derived from. The grey ellipses represent discordant data, representing an open system indicating lead loss from the zircon. The concordant data yields an age of 513 ± 13 Ma with a MSWD of 1.5.

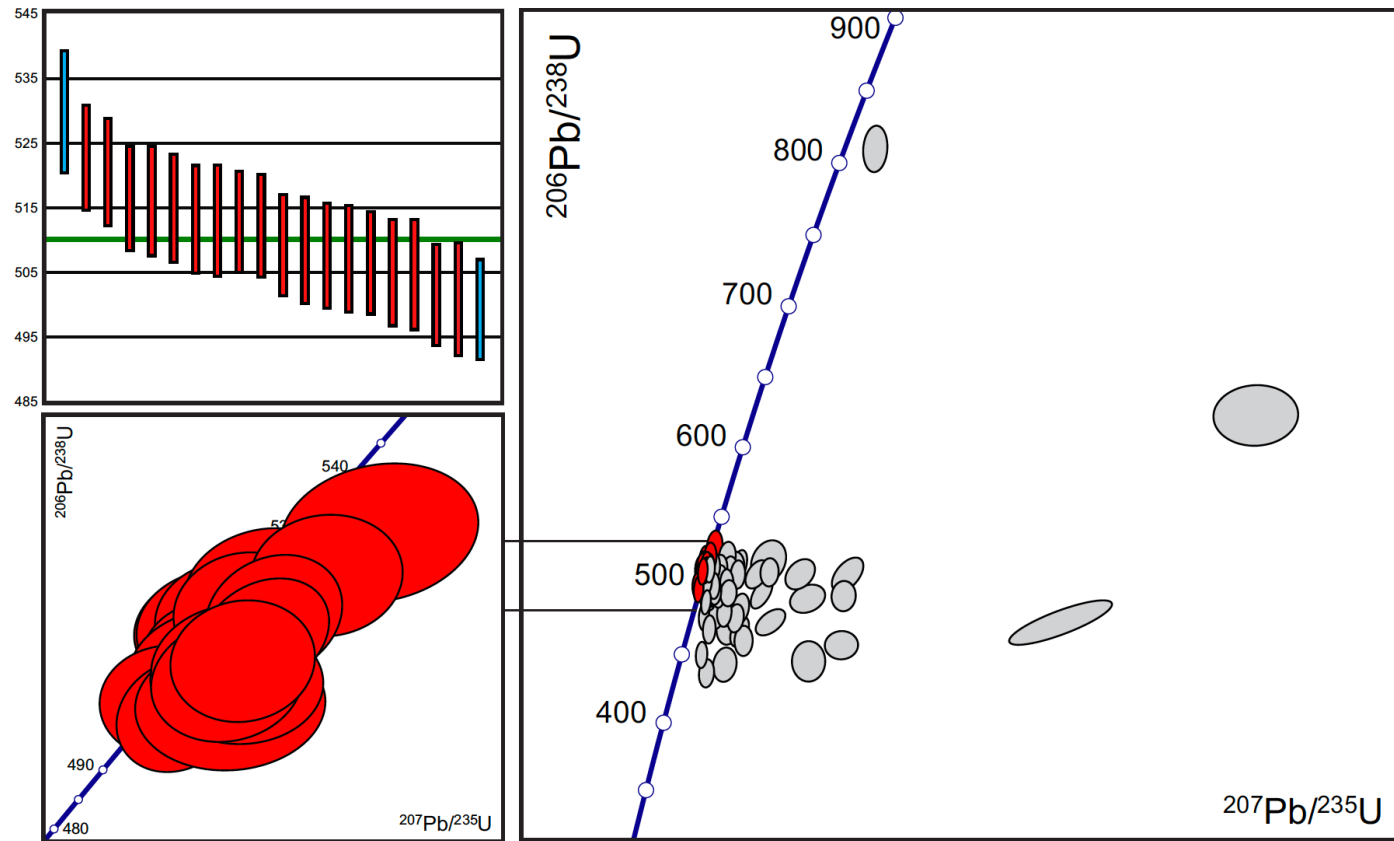


Figure 15. Concordia plot for sample K1B from Kalladeina 1. The blue line represents the concordant line, samples that locus lie on this yield concordant ages. The centroid of the red ellipses are >90% confident concordance, represent the samples the ages are derived from. The grey ellipses represent discordant data, representing an open system indicating lead loss from the zircon. The concordant data yields an age of 510 ± 3.5 Ma with a MSWD of 3.3. The Concordia to the bottom left represents only the concordant samples. The top left plot displays a weighted means average of concordant samples. A) The sample in blue to the bottom right, similarly to G7U, is potentially susceptible to lead loss, impacting age of the population. B) the blue sample to the top left yielding an age ~ 529 Ma is also highlighted as a potential outlier, under conditions of inheritance. Additional analysis under scenario A) yields an age of 511.6 ± 3.4 Ma with a MSWD of 3.0, B) an age of 510.1 ± 3.1 Ma with a MSWD of 2.5. The combined scenario of A & B yield an age of 510.8 ± 3 Ma with a MSWD of 2.2.

4.5 Vuggy Dolomite

5 “vuggy dolomite” sub-samples, derived from 3 slabbed core samples in Kalladeina Formation, Gidgealpa 5 were analysed for major/trace elements and $^{87}\text{Sr}/^{86}\text{Sr}$ isotopes. $^{87}\text{Sr}/^{86}\text{Sr}$ values, as observed in Table 6 range from ~ 0.70988 to ~ 0.71034 ($2\sigma = .000005$), which is slightly higher than Sr composition of expected coeval Cambrian seawater, but similar to the less radiogenic $^{87}\text{Sr}/^{86}\text{Sr}$ data from Gidgealpa 7 samples.

Table 6. Displays all $^{87}\text{Sr}/^{86}\text{Sr}$ values, including error for all dolomite samples analysed from Gidgealpa 5 with respect to stratigraphic depth. “Drill position” refers to the ‘morphology’ of the drilling spots selected from the slabbed core samples (i.e., light and/or dark altered/dolomitized rock and vugs). The Eu/Eu* anomaly has also been displayed for all dolomite samples.

Sample Name	Depth (feet)	Drill Position	$^{87}\text{Sr}/^{86}\text{Sr}$ Value (corrected)	Error	Eu/Eu*
D1	7951'	Vug	0.71004618	.000005	1.19036648
D2	7951'	Light Spot	0.71009626	.000004	1.01534445
D3	8123'	Light/Dark (thin section)	0.70988223	.000003	1.02261681
D4	8123'	Vug	0.71034187	.000003	1.00952634
D5	8123'	Light/Dark	0.7099748	.000003	1.21017974

Trace element/REE analysis of dolomite samples identified negative Ce anomalies for all samples, possibly influenced by the significant La anomalies observed, with the exception of D1. Positive Eu anomalies are identified in samples D1 and D5, with D5 experiencing a number of additional REE anomalies, including a positive Tm anomaly and a negative Yb anomaly.

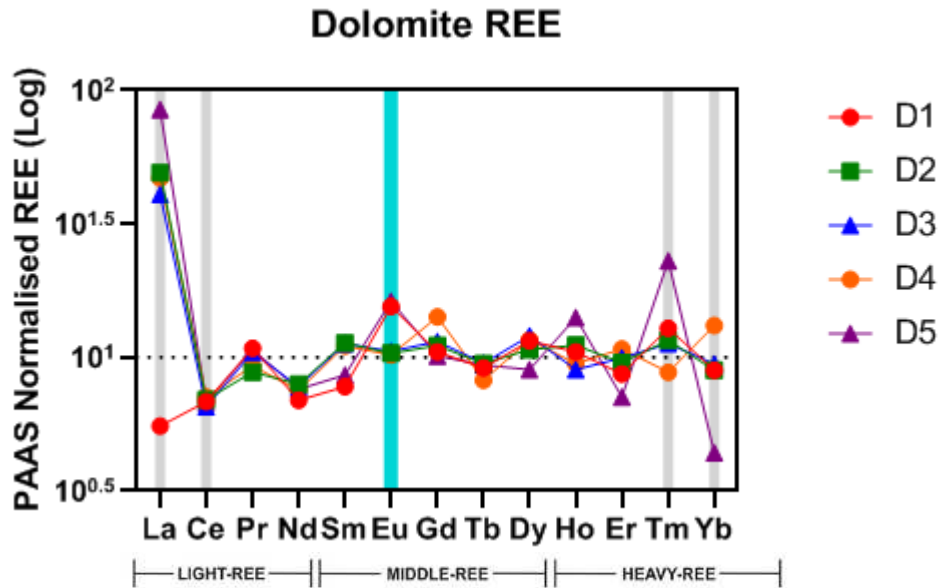


Figure 16. PAAS normalised rare earth element (REE) patterns for all vuggy dolomite samples from the base of the Kalladeina Formation in Gidgealpa 5. Shaded intervals represent anomalies, specifically positive La anomalies for D2, D3, D4, D5, negative La anomaly for D1, negative Ce anomaly for all samples, positive Eu anomaly for D1 and D5, positive Tm anomaly for D5 and negative Yb anomaly for D5. Emphasis has been placed on the Eu anomaly, with its hydrothermal implications a key piece of evidence towards the vuggy dolomite origin. Symbols depicted in the figure legend represent drilling spot; circle = vug, square = light alteration, triangle = light/dark alteration.

5. DISCUSSION

5.1 Carbon Isotope Record of Carbonates from the Kalladeina Formation: Implications on Primary Productivity, Organic Burial and Chemostratigraphy

Excursions of stable carbon isotopes ($\delta^{13}\text{C}$) in marine carbonates represents an increasingly important tool for stratigraphic correlations, especially in Precambrian but also Palaeozoic depositional systems, where their chemostratigraphic (i.e., relative ages) and chronostratigraphic (i.e., absolute ages inferred from global C isotope excursions) potential has been recognised and applied in numerous studies (Peng et al., 2012, and references therein; Woods et al., 2011; Fan et al., 2011). The Middle/Upper Cambrian

contains a number of important stable carbon isotope excursions (CIE's) recognised globally, including the SPICE (Steptoean Positive Isotope Carbon excursion), DICE (Drumian Isotope Carbon Excursion) and ROECE (Redlichiiid-Oleneliid Extinction Carbon Isotope Excursion). These CIE's, among others are typically characterised by global events, including mass extinctions and sea level fluctuations, although the underlying causes and driving mechanism(s) behind these CIE's need further investigation to better understand exact relationships (Saltzman et al., 2000; Zuo et al., 2018; Howley & Jiang 2010).

SPICE (STEPTOEAN POSITIVE CARBON ISOTOPE EXCURSION)

The SPICE, which is the main CIE during the Cambrian period and the primary focus of this study, represents a major positive shift in marine carbon $\delta^{13}\text{C}$ isotope record, which occurred during the Paibian Stage in the Furongian Series (from ca. ~496 to ~499 Ma). This global oceanographic C isotope event has been documented in a range of carbonate successions across the globe, including China, Kazakhstan, Australia, South America, Europe and Antarctica with a typical average $\delta^{13}\text{C}$ amplitude of about $\sim 4\text{‰} \pm 1$, depending also on local depositional settings (Fan et al., 2011; Kouchinsky et al., 2008; Woods et al., 2011; Saltzman et al., 2000). This study documents SPICE peaks recorded in two cores (Gidgealpa 7 and Kalladeina 1) with maximum magnitudes of 3.7‰ and 5.2‰ respectively, the latter comparable only to the SPICE record from Great Basin, USA with $\delta^{13}\text{C}$ excursion of $\sim 5\text{‰}$ (Fan et al., 2011). The difference in excursion intensity between Warburton Basin wells, and other documented excursions worldwide,

likely reflects the local carbon cycling in these different settings, which are often enhanced or modulated by a local basin restriction (Fan et al., 2011; Schmid 2017).

Despite being globally documented, the origin of SPICE and its links to changes in the Cambrian geological, biological and/or climatic processes are still quite uncertain and controversial. One interpretation of the SPICE is attributed to increased burial of organic matter in global oceans, locking away the lighter ^{12}C through fractionation of plants and increasing the amount of ^{13}C in the oceans, shifting the marine $\delta^{13}\text{C}$ signature to heavier values. Alternatively, sea level fluctuations and/or changes in climate, in particular the formation of methane hydrates in response to global cooling, which would efficiently remove ^{12}C from the oceans is considered a possible explanation (Saltzman et al., 2000; Woods et al., 2011; Fan et al., 2011). Additionally, there is controversy surrounding the relationship between SPICE and eustatic sea-level changes, specifically if the event is associated with a global transgressive or regressive event? A recent study by Schmid et al. (2017), which documented the SPICE event across the Amadeus Basin in central Australia, observed an increased ratio of siliciclastic to carbonate rocks towards the peak of SPICE, hypothesised to be the product of marine transgression.

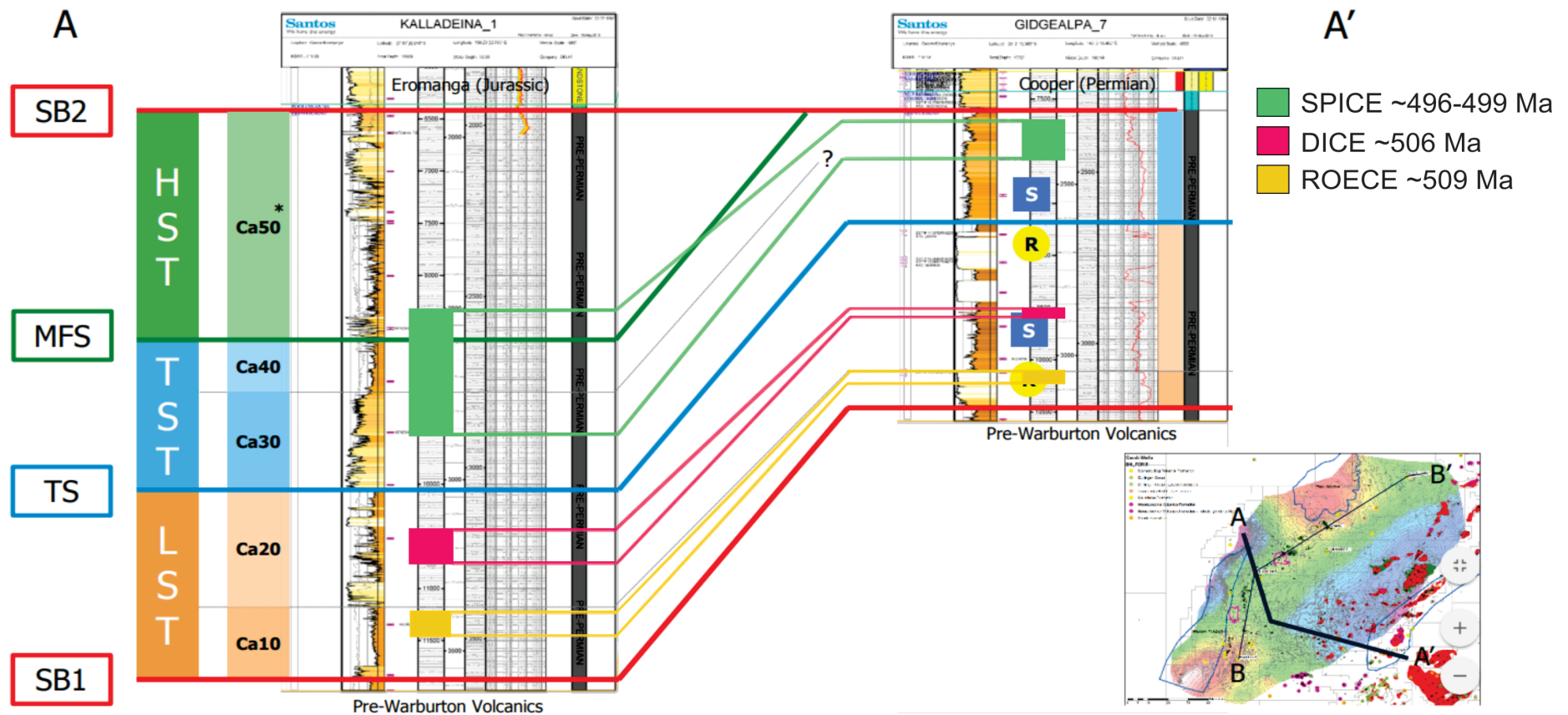


Figure 17. Summary plot showing gamma logs (provided by SANTOS) for two studied wells; Kalladeina 1 on the left and Gidgealpa 7 on the right. Positioning of wells with respect to the basin has been indicated by the map to the bottom right, with the cross-section correlation indicated by the A – A' line. Sedimentological and sequence stratigraphic interpretations have been made for both wells, with indicated eustatic sealevel changes, based on intra-basin correlations of these two wells have been made. Positioning of a Low System Tract (LST), Transgressive System Tract (TST) and Highstand System Tract (HST) have been identified in Kalladeina 1, while the HST is absent in Gidgealpa 7. Smaller sequences (e.g. parasequences) have been also identified within the system tracts, represented by Ca*, indicating distinct boundaries between units. These boundaries can be clearly identified in the gamma logs, with sharp, distinct changes, indicating a change in grain size and/or lithology. Abbreviation S and R represent, respectively “Source” and “Reservoir” units within the Kalladeina Formation, and a local petroleum system.

However, the general consensus in the literature seems to be that the peak of SPICE coincides with a global sea level lowstand, thus the product of a major marine regression (Woods et al., 2011; Saltzman et al., 2000; Fan et al., 2011); and geological record from Cook et al. (1991) and Saltzman et al. (2000) from Kazakhstan and Queensland respectively, support such purported Upper Cambrian regression event (see Woods et al., 2011, and references therein). Additional support for a regression model comes from North America, where peaks in SPICE correspond with a sea-level lowstand exhibited by the Sauck II-Sauck III sequence boundary, a hiatus that exposed large areas of Laurentian craton for the first time in the Cambrian (Montañez et al., 2000; Saltzman et al., 2000; Fan et al., 2011). Alternatively, this study puts forward evidence for a transgression during the SPICE anomaly in the Warburton Basin, complimentary with recent findings from Schmid (2017) in the Amadeus Basin. Integrating sedimentology logs by Copp (2019) with the $\delta^{13}\text{C}$ data from this study indicates basin deepening up through the SPICE, transitioning from a proximal, to a more distal depositional environment. This is also further supported by SANTOS sedimentology/gamma logs (Figure 17), with depth of the Gidgealpa 7 SPICE event interpreted to be a transgression, and similarly in Kalladeina 1 with a medium flooding surface (MFS) and consequently highstand system tract (HST) interpreted towards the top of the SPICE.

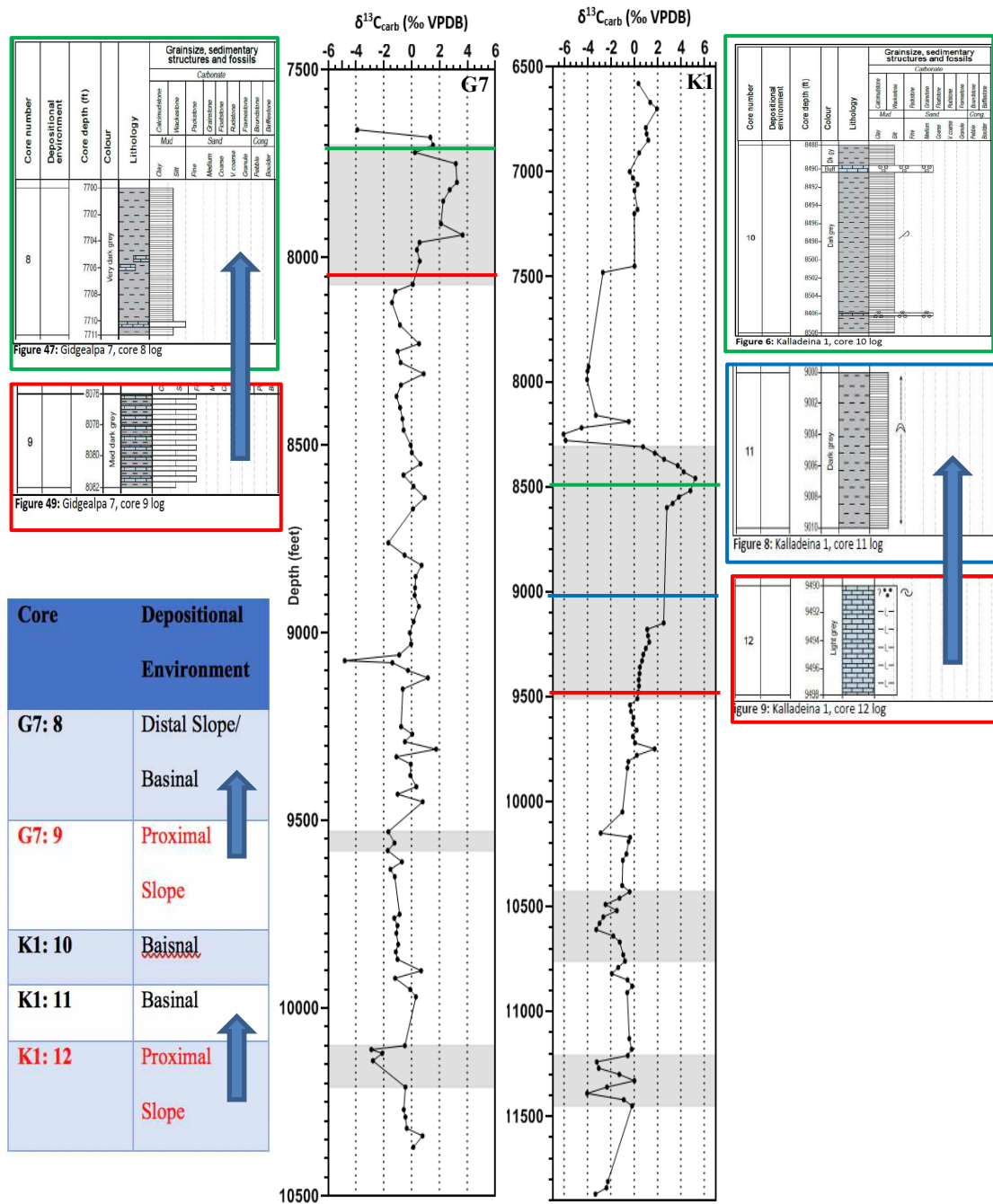


Figure 18. Summary of $\delta^{13}C$ trends with SPICE for both wells; Gidgealpa 7 (G7) and Kalladeina 1 (K1), plotted as a function of stratigraphic depth. Sedimentary logs from Copp (2019) that correspond with the SPICE interval have been included either side of their respective well. A colour coding scheme of green, blue and red has been used to indicate stratigraphic position of all logs, similar colours representing similar ages. The tables in the bottom left indicates depositional environment summaries for respective cores (cores for each sedimentary log displayed in text below logs) as interpreted by Copp (2019). The blue arrows indicate evidence for transgression, which can be observed in both wells throughout the SPICE interval.

DICE (DRUMIAN CARBON ISOTOPE EXCURSION)

The DICE represents another global Cambrian carbon isotope excursion, with a negative peak of about -2 to -3‰, occurring at the base of the Drumian Stage (~506Ma). As is the case with most CIE's, the DICE coincides with a number of biostratigraphic markers, including the FAD (first appearance datum) of trilobite species *Ptychagnostus atavus* and significant changes in conodont and polymerid trilobite faunas (Peng et al., 2012; Howley & Jiang 2010; Zhu et al., 2006; Babcock et al., 2007). Howley & Jian (2010) propose a definition for the DICE, as a negative $\delta^{13}\text{C}$ excursion that occurs superjacent to FAD of *P. atavus* and is associated with transgressive deposits, encompassing the fact that the FAD of *P. atavus* is not homogenous globally. The DICE has been well documented in localities in the USA, including the Great Basin and Utah (Howley & Jiang 2010; Babcock et al., 2007), furthermore in North and South China (Zhu et al., 2019; Howley & Jiang 2010) and also more recently in central Australia (Schmid 2017). The similarity between $\delta^{13}\text{C}$ excursions observed in the Great Basin (-2‰ to -3.6‰) and that observed in the Georgina Basin (-2‰ to -3.2‰) emphasise the potential of this event as a global isotopic correlative tool (Schmid et al., 2017). This study provides first evidence for the DICE in the Warburton Basin, recorded in both Gidgealpa 7 and Kalladeina 1 wells, with a negative excursion of 1.71‰ and 3.25‰ respectively. The latter is thus consistent with documented DICE at other continents and palaeo-locations (USA, China). Interestingly, sedimentary/gamma logs by SANTOS (Figure 17) suggest that the DICE anomaly in the Warburton Basin, and Gidgealpa 7 and Kalladeina 1 records, is associated with a low system tract (LST) prior to a transgression (TST), which is somewhat consistent with literature and published eustatic reconstructions, suggesting the DICE resides in the lower part of a

eustatic rise, although the relationship between the two is still elusive (Pages & Schmid 2017; Babcock et al., 2007; Zhu et al., 2006; Howley & Jiang 2010). As to palaeo-redox reconstructions, due to resetting of the primary REE signal in Kalladeina 1 and anomalous La values in Gidgealpa 7, redox conditions based on Ce/Ce* anomaly data could not be accurately determined for the DICE.

ROECE (REDLICHIID-OLENELIID EXTINCTION CARBON ISOTOPE EXCURSION)

The Lower-Middle Cambrian boundary corresponds with a major negative $\delta^{13}\text{C}$ excursion termed the ROECE, dated at ~509 Ma, which is one of the largest negative C isotope excursions known in the Cambrian, suggesting major palaeo-oceanographic and environmental changes during this time (Peng et al., 2012; Fan et al., 2011; Zhu et al., 2006). The ROECE coincides with a number of trilobite mass extinctions, including the LAD (last appearance datum) of trilobite orders such as Redlichiid and Oleneliid. This major negative shift in marine $\delta^{13}\text{C}$ records has been documented globally, including China, Canada, Russia, Sweden, Siberia and USA, with intensity of excursion varying significantly, from -2.38‰ in southern Sweden, to -7.9‰ in Eastern Siberia (Fan et al., 2011). This study provides evidence for ROECE anomalies on the order of -2.89‰ and -4.03‰, which is consistent with published ROECE anomalies elsewhere (Zhu et al., 2006; Faggetter et al., 2017). In detail, Gidgealpa 7 record provides a ROECE excursion identical to the one described by Fan et al. (2011); however, $\delta^{13}\text{C}$ data from Kalladeina 1 indicate possible bimodal ROECE excursion. Importantly, Guo et al. (2010) and Zhu et al. (2004) in China (Wuliu-Zengjiayan, Jianshan & Wangcun Sections) also observed such bimodal $\delta^{13}\text{C}$ pattern for the ROECE excursions with similar amplitude (see Figure 19). The ROECE is thought to be caused by a global transgressive event, causing

extensive flooding of shelf areas worldwide and upwelling of deeply anoxic water on shelves during transgression (Guo et al., 2010; Fan et al., 2011).

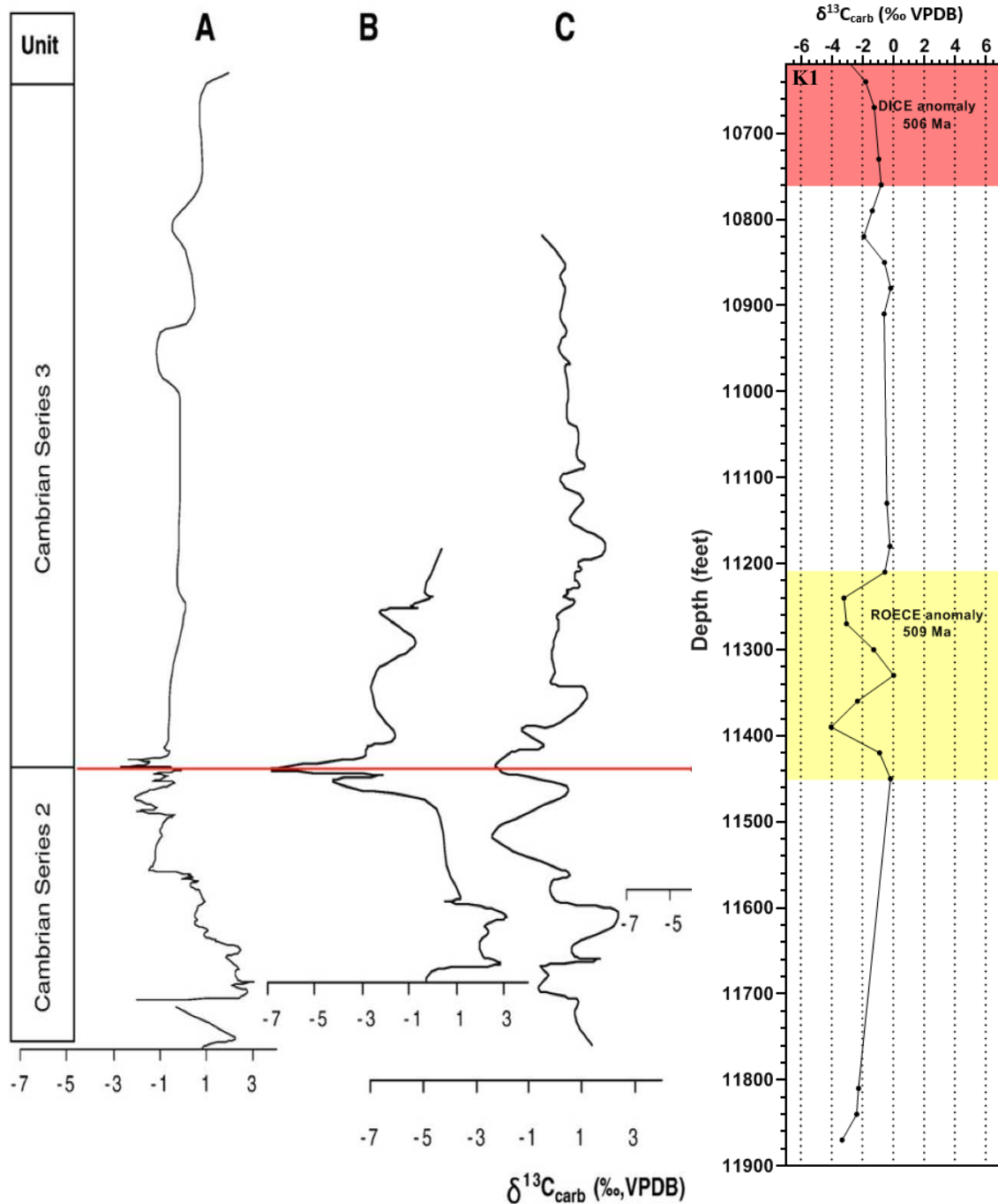


Figure 19. Published $\delta^{13}\text{C}$ records with ROECE plotted versus stratigraphic depth. Data sets A, B, C are from Guo et al. (2010) from the Yangtze Platform, South China, and the data set on the right is the $\delta^{13}\text{C}$ data from Kalladeina 1, in this the ROECE excursion from Kalladeina 1 and Chinese excursions are apparent, specifically the existence of a double-peak or bimodal nature of the observed $\delta^{13}\text{C}$ trends.

The integration of $\delta^{13}\text{C}$ data from this study with available sedimentary/gamma logs provided by SANTOS, suggest the ROECE in both wells reside in an interval associated with regression or LST just prior to a transgression, which is somewhat consistent with literature. As to palaeo-redox, Ce anomalies for the ROECE excursion in Gidgealpa 7 are dominantly close to 1, with possible indication for minor negative Ce anomaly in a couple samples, perhaps suggesting more oxic marine conditions, contrary to Guo et al. (2010) and Fan et al. (2011), (see Figure 20). ROECE redox analysis was restricted to Gidgealpa 7 data, due to alteration of primary REE signal in Kalladeina 1.

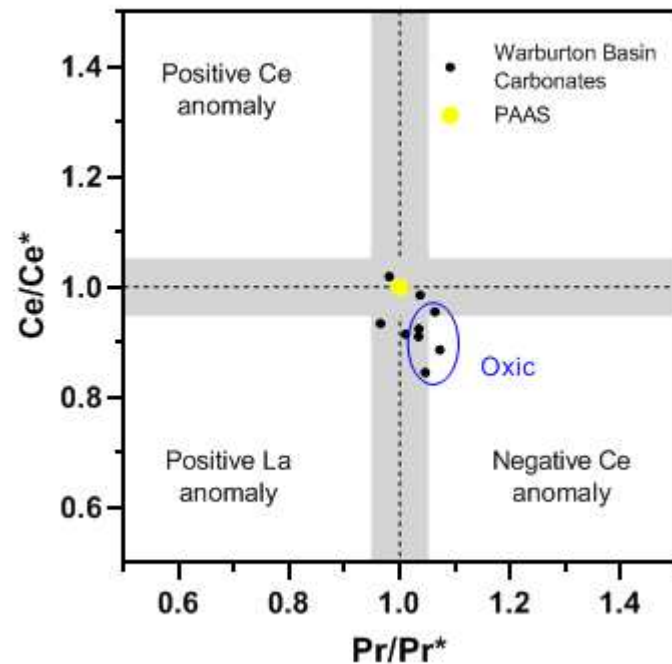


Figure 20. A cross-plot of shale-normalized (PAAS) Ce/Ce^* and Pr/Pr^* anomalies for the identified ROECE interval Gidgealpa 7. Some samples tend to be plotted within negative Ce anomaly space, perhaps indicating slightly more oxic conditions during ROECE.

5.2 Assessment of Diagenesis and Clay Contamination on $^{87}\text{Sr}/^{86}\text{Sr}$

Marine carbonates are valuable geological archives, particularly with respect to their $^{87}\text{Sr}/^{86}\text{Sr}$ ratios, which can be a proxy for i) tectonic history of our planet (i.e., continental weathering vs. hydrothermal inputs), ii) restriction of the basin from coeval

open ocean, and also ii) determining age of marine carbonate sequences based on Sr isotope stratigraphy (McArthur & Howarth 2004). However, the above constraints are only viable if the primary paleo-seawater isotope signature is preserved. Marine carbonates are prone to secondary processes such as meteoric diagenesis, recrystallisation and/or clay contamination, potentially altering their primary Sr isotopic signatures. To assess these effects, $^{87}\text{Sr}/^{86}\text{Sr}$ values are plotted against selected indices for diagenesis and/or detrital contamination. Specifically, Sr/Mn ratios of carbonates can assess degree of meteoric diagenesis (i.e., water rock interactions), and the concentrations of Al and Rb (which are enriched in detrital phases) can be indicators for clay contamination (Montañez et al., 1996, Banner & Hanson 1990). Accordingly, lower Sr/Mn ratios of marine carbonates typically point to diagenetic resetting, and elevated Al and Rb in bulk carbonates are typically the product of contamination by detrital phases and clay particle dissolution (Montañez et al., 1996). Thus, unaltered and well-preserved marine carbonates tend to have elevated Sr/Mn ratios, as progressive diagenesis typically increases Mn and lowers Sr concentrations in carbonates until the geochemical signature equilibrates with that of diagenetic/meteoric waters (Banner and Hanson 1990).

Using the above proxies, i.e., Sr/Mn and Al and Rb, the carbonates most likely to preserve the primary paleo-seawater isotopic signal should be those with the highest Sr/Mn ratio ($\geq 0.5-2$) and lowest Rb/Sr (< 0.001) and Al concentrations (< 10 ppm) (Edwards et al., 2015 & Montañez et al., 1996). Our results indicate from all carbonates analysed for $^{87}\text{Sr}/^{86}\text{Sr}$ ratios, only 1 sample in Gidgealpa 7 has a Rb/Sr < 0.001 , whereas Kalladeina 1 ratios are all in excess of 0.001 (minimum of 0.0106). Such significant

difference in Rb/Sr ratio between wells (average of ~0.03 for Gidgealpa 7 and ~0.2 for Kalladeina 1) is likely related to the shallower marine depositional environment of Kalladeina 1 (Copp 2019) receiving higher inputs of continental-derived Sr and detrital phases with elevated Rb and $^{87}\text{Sr}/^{86}\text{Sr}$ ratios. Similarly, Al concentrations are elevated in both wells, with an average value of ~437 ppm in Gidgealpa 7, and ~1125 ppm in Kalladeina 1, the concentration difference between wells likely a function of differing depositional environments, as mentioned previously. Sr/Mn ratios for majority of the analysed carbonates are in excess of 0.5, with only 6 from Gidgealpa 7 having a Sr/Mn ratio below 2. This indicates meteoric diagenesis had little effect on altering the primary trace element and Sr isotope signal of these Cambrian marine carbonates, however clay contamination is likely a major contributor. As to sample coverage, it is important to note that $^{87}\text{Sr}/^{86}\text{Sr}$ values were obtained throughout the whole of Gidgealpa 7 (Figure 7), whereas was restricted to the SPICE and sections above in Kalladeina 1. Comparing criteria for $^{87}\text{Sr}/^{86}\text{Sr}$ values specifically for the SPICE (Table 7), values are slightly more comparable between studied cores. Interestingly, similar to the pre-SPICE comparison, the Sr/Mn ratio is two times higher in Gidgealpa 7, suggesting a greater degree of diagenesis in Gidgealpa 7 marine carbonates. This is likely the product of the structural complexity and faulting present in Gidgealpa 7 (see Figure 21 below) creating local fluid-flow mechanism pathways and increasing the potential for diagenetic resetting by meteoric and/or basinal fluids, compared to the relatively undeformed Kalladeina 1.

Table 7. Elemental statistical summary between SPICE intervals from Gidgealpa 7 and Kalladeina for meteoric diagenesis and clay contamination indices, in conjunction with Sr isotope signature.

Selected Indicator	Gidgealpa 7				Kalladeina 1			
	Low	Average	High	No of Samples	Low	Average	High	No. of Samples
Sr/Mn	0.587	1.443	2.167	13	0.119	0.647	1.234	24
Rb/Sr	0.004	0.025	0.079	13	0.011	0.112	0.698	24
Al	96.77	409.57	1436.98	13	130.26	888.49	1957.70	24
⁸⁷Sr/⁸⁶Sr	0.70992	0.71054	0.71198	12	0.71078	0.71306	0.71906	17

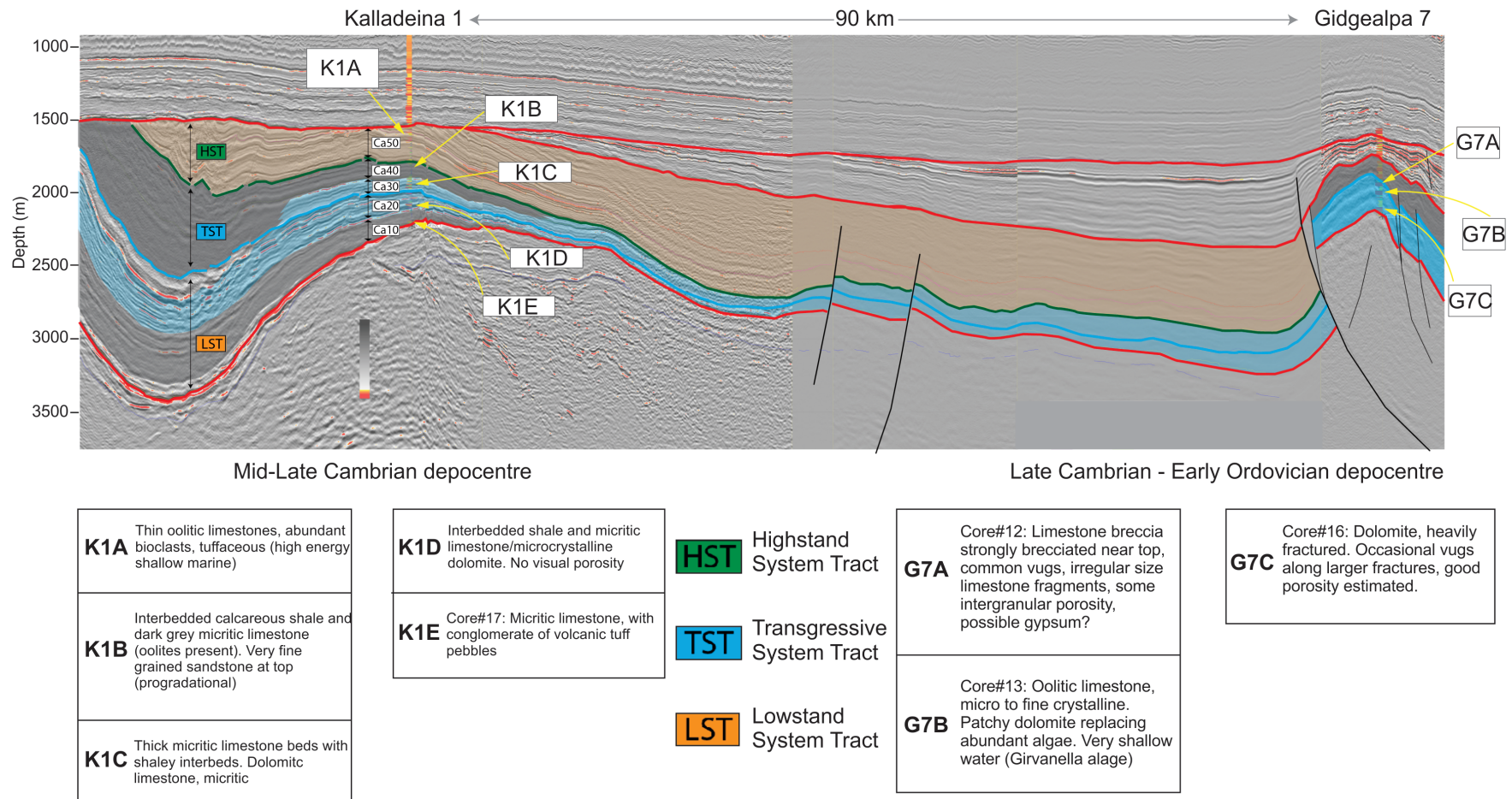


Figure 21. Modified seismic cross-section provided by SANTOS of the two main wells in this study; Gidgealpa 7 and Kalladeina 1. Correlations have been made based on the seismics and sequence boundaries identified throughout the cross-section, including the identification of a lowstand system tract (LST), transgressive system tract (TST) and highstand system tract (HST). Displays the structural geology of the two wells, particularly the significant faulting and uplift experienced in Gidgealpa 7 relative to the more undeformed Kalladeina 1. Ca? (e.g. Ca50) indicate the different interpreted sequence boundaries, with brief lithological descriptions provided (K1? And G7?). Yellow arrows indicate position in the stratigraphy lithological description is derived from.

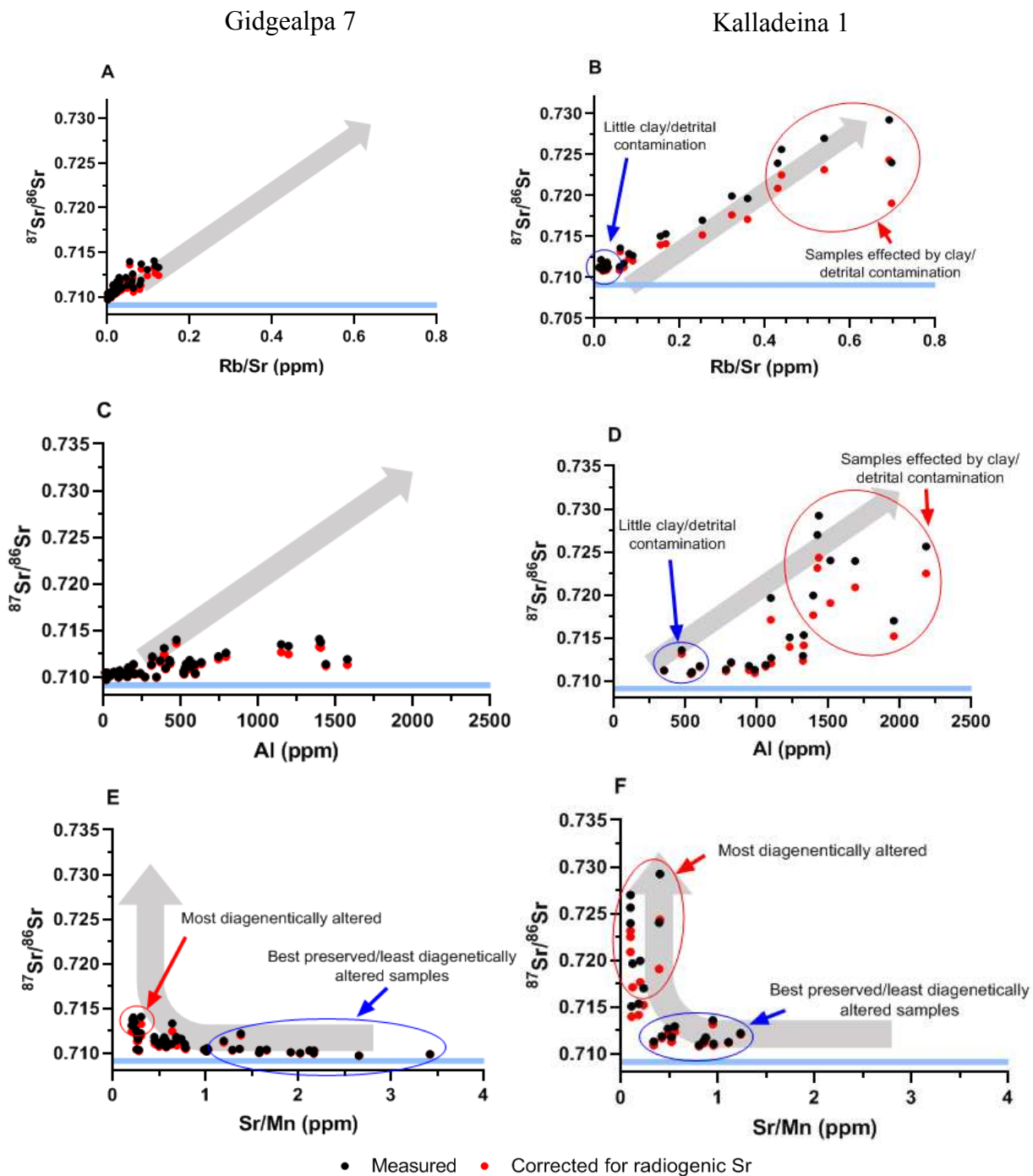


Figure 22. Cross-plot of elemental concentrations (Al) and ratios (Rb/Sr and Sr/Mn) versus Sr isotope signatures ($^{87}\text{Sr}/^{86}\text{Sr}$), as measured for both wells. a) $^{87}\text{Sr}/^{86}\text{Sr}$ values plotted against Rb/Sr for Gidgealpa 7. b) $^{87}\text{Sr}/^{86}\text{Sr}$ values plotted against Rb/Sr for Kalladeina 1. c) $^{87}\text{Sr}/^{86}\text{Sr}$ values plotted against Al concentration (ppm) for Gidgealpa 7. d) $^{87}\text{Sr}/^{86}\text{Sr}$ values plotted against Al concentration (ppm) for Kalladeina 1. The grey arrow indicates trend line for increasing clay contamination, as indicated by annotations. e) $^{87}\text{Sr}/^{86}\text{Sr}$ values plotted against Sr/Mn data for Gidgealpa 7. f) $^{87}\text{Sr}/^{86}\text{Sr}$ values plotted against Sr/Mn data for Kalladeina 1. The grey arrow indicates trend for increased meteoric diagenesis, similarly represented in annotations. All diagrams display measured $^{87}\text{Sr}/^{86}\text{Sr}$ values, in conjunction with corrected values. The blue line represents the $^{87}\text{Sr}/^{86}\text{Sr}$ composition of Cambrian seawater (~509 to ~497 Ma; 0.7089-0.7093). Scales are constant between wells for easier comparison.

5.3 Comparison of $^{87}\text{Sr}/^{86}\text{Sr}$ Values: Implications on Paleo-Depositional Environment

$^{87}\text{Sr}/^{86}\text{Sr}$ values in well-preserved marine carbonates can be used to constrain the palaeo-depositional environment during carbonate deposition, providing constraints on connectivity of a basin with respect to the global ocean, assuming approximate depositional ages of samples are known. This is due to Sr concentration and isotopic composition of the global ocean, including $^{87}\text{Sr}/^{86}\text{Sr}$ signatures being relatively homogenous. Such uniformity is due to the long residence time of Sr in oceans (10^6 years), which is far longer than the current average mixing time of the global ocean (10^3 years). However, over longer timescales and/or in restricted depositional settings (e.g. lagoons, epeiric seas) the marine $^{87}\text{Sr}/^{86}\text{Sr}$ ratio can be significantly influenced by local continental weathering inputs into these semi-closed systems. Particularly, the Cambrian global ocean was highly affected by the Pan-African orogeny (McArthur et al., 2012; Montañez et al., 1996; 2000; Peng et al., 2012), which significantly impacted Sr isotope composition of global seawater and coeval epeiric seas. Specifically, highest seawater $^{87}\text{Sr}/^{86}\text{Sr}$ isotope values (~ 0.7095) over the last ca. 4 billion years of the Earth's history are recorded during the latest Middle Cambrian time (Montañez et al., 1996). This study presents $^{87}\text{Sr}/^{86}\text{Sr}$ values that are all higher than this radiogenic marine Sr isotope threshold (~ 0.7095), with closest values to the latter signature found in Gidgealpa 7 samples with $^{87}\text{Sr}/^{86}\text{Sr}$ values of ~ 0.7097 . For Kalladeina 1 the lowest $^{87}\text{Sr}/^{86}\text{Sr}$ value was ~ 0.7108 , with locally extreme radiogenic values up to ~ 0.7243 (above the SPICE). A comparison of $^{87}\text{Sr}/^{86}\text{Sr}$ values between wells seems to support the "local depositional environment" scenario (Figure 23), as Sr isotope data through SPICE indicate the presumably shallower Kalladeina 1 yielded more radiogenic

$^{87}\text{Sr}/^{86}\text{Sr}$ than the relatively deeper Gidgealpa 7, possibly reflecting greater continental influence and restriction characteristic of shallower depositional settings.

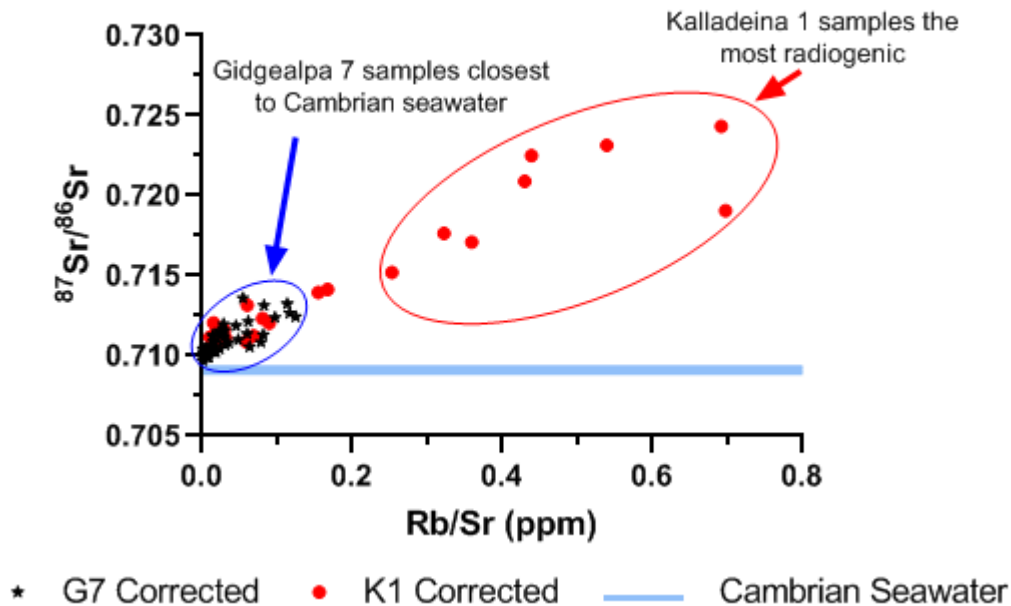


Figure 23. A cross-plot of elemental ratios, including $^{87}\text{Sr}/^{86}\text{Sr}$ values (corrected values) versus Rb/Sr ratio for all samples analysed from Gidgealpa 7 and Kalladeina 1. The blue line indicates the expected $^{87}\text{Sr}/^{86}\text{Sr}$ composition of the Late Cambrian seawater (0.7089-0.7093).

5.4 Rare Earth Element (REE) Constraints on Paleo-Redox and Hydrothermalism

The REE concentration pattern in modern seawater and precipitated marine carbonates is very specific, with archives used to reconstruct REE patterns in palaeo-seawater, the latter having implications for changes in marine redox and/or hydrothermal inputs into the oceans through geologic time (Tostevin et al., 2016; Bau & Dulski 1996). In particular, Ce has a unique chemistry amongst the REEs existing in two valence states, as Ce^{3+} and Ce^{4+} , where the latter oxidised species is readily produced in more oxic waters, but Ce^{4+} is less soluble and thus removed from seawater.

(Tostevin et al., 2016). This Ce removal due to redox processes can be quantified via Ce/Ce* anomalies, by comparing abundance of redox-sensitive Ce to concentrations of neighbouring and redox-neutral REEs. Gidgealpa 7 samples provide REE patterns with evidence for negative Ce/Ce* anomalies, indicating transient and relatively more oxic conditions, the latter also identified in a few samples from Kalladeina 1, but smaller magnitudes despite expectations of a presumably more oxic depositional setting compared to Gidgealpa 7 (see Figure 24).

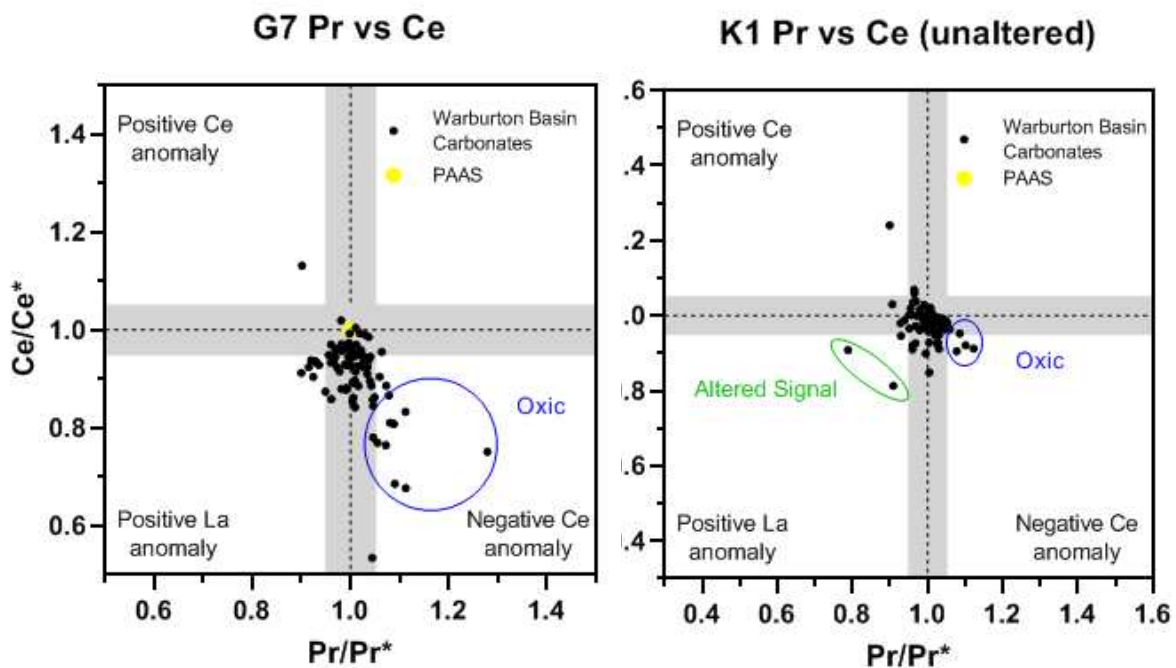


Figure 24. A cross-plot of shale-normalized (PAAS) Ce/Ce* and Pr/Pr* anomalies for Gidgealpa 7 (left) and Kalladeina 1 (right). For Gidgealpa 7 all measured Ce and Pr data are shown, but for Kalladeina 1 the plot displays only data from unaltered, or “best preserved” samples, i.e., from the upper half of the well indicated by Figure 10 (above 10400’). Negative Ce/Ce* anomaly indicates more oxic conditions, as annotated, and alternatively a positive Ce/Ce* anomaly suggest marine anoxia.

In addition to redox sensitive Ce/Ce* proxy, the Eu anomaly (Eu/Eu*) can also be used as an indicator of hydrothermal activity in marine settings. Hydrothermal input represents a large flux of REE’s to the ocean (10-10⁴ times ambient seawater),

particularly Eu, with specific REE pattern related to complex seawater-rock interactions. At temperatures exceeding 200 degrees, Eu^{3+} is dominated by its divalent counterpart, consequently the large Eu^{2+} is more efficiently desorbed during fluid-rock interactions, causing a positive Eu/Eu^* anomaly in the fluid and precipitates (i.e., marine carbonates), (Bau & Möller 1992). Because of this, large positive Eu/Eu^* anomalies present locally in seawater are typically a product of hydrothermal fluid alteration of submarine volcanic rocks, and/or a newly formed oceanic crust, consequently the Eu/Eu^* can be used as a sensitive proxy for past hydrothermalism and volcanic activity in marine settings (Bau & Dulski 1996; Tostevin et al., 2016).

Kalladeina 1 displays a significant positive Eu anomaly at the base of the well (depth of 11900') spanning about 150' with bimodal peaks, the dominant of the two showing a positive Eu/Eu^* of +2.01 (see Figure 11). The boundary between the Kalladeina Formation and the uncoformably underlying Mooracoochie volcanics is ~11810' (Sun 1996), indicating that the above positive Eu/Eu^* anomaly is present at the boundary of both formations. As a result, this anomaly is likely the product of hydrothermal activity associated with the upper layer of the underlying Mooracoochie volcanics, that possibly interacted with the ambient Late Cambrian seawater that percolated through this active volcanic system.

5.5 Geochronological Constraints on Early Cambrian Mooracoochie Volcanics

The Mooracoochie Volcanics as described in ‘Geological Background’ refers to a suite of volcanic rocks encountered in the Warburton Basin, which includes predominantly felsic and intermediate volcanic sequences (e.g. rhyolite, trachyte and andesite), with later occurrences of more mafic rocks (Sun 1996; Gatehouse 1986). This study focuses on the early Cambrian volcanics, composed of felsic tuffs and ignimbrites that unconformably underlie the Kalladeina Formation. Using carbon chemostratigraphy as an age constraint, these early volcanics must be older than the ROECE event dated at ~509 Ma (Peng et al., 2012; Fan et al., 2011; Zhu et al., 2006). Previous geochronology work on the Warburton Basin (Stewart 2010) yielded U-Pb zircon ages of 517 ± 9 Ma, with the lower boundary incorporating the ROECE. Previous studies by Sun (1996) and Gatehouse (1986) documented the early phase of Mooracoochie volcanics to be a rapidly and widely deposited unit within the basin. From this, expectations are that the geochronological ages from the correlative Kalladeina 1 and Gidgealpa 7 wells will be consistent with one another, and also with the above published age for Mooracoochie volcanics. This has been confirmed, as Gidgealpa 7 yielded U/Pb zircon age of 509.1 ± 2.1 Ma, while Kalladeina 1 volcanics yielded ages of 510.8 ± 3 Ma and 513 ± 13 Ma. These new ages are consistent with Stewart (2010) geochronological age of 517 ± 9 Ma, and also indicate that the volcanic units recorded and sampled in both wells are quite likely the same, representing a larger-scale regional (?) volcanic eruption event, yielding a combined age of 510 ± 1.6 Ma. Additionally, all acquired ages are consistent with our chemostratigraphic ROECE marker, which suggest the age of Mooracoochie

volcanics to be older than ~509 Ma, which has been confirmed by our U/Pb zircon dating (considering the errors on acquired ages).

5.6 Vuggy Dolomite: Isotope Constraints on the Origin of Dolomitization

‘Vuggy’ dolomite as described in ‘Geological Background’ refers to a dolomitic layer located within the lower part of Kalladeina Formation, typically exposed at the base of the formation just above the Mooracoochie volcanics. Its distribution is however not consistent, as it is restricted only to several wells in the Gidgealpa area, thus not present in Kalladeina 1 (Sun 1996). The dolomitic layer is originally interpreted to have been deposited in a shallow shelf environment, with complete dolomitization and secondary vuggy porosity believed to be linked to karstification providing potentially excellent reservoirs capable of trapping hydrocarbons and petroleum resources (Sun 1996; 1997). Although karstification is depicted in literature to be linked to the dolomitization (Sun 1996; 1997; Roberts et al., 1990), more recent sedimentology work by Copp (2019) suggests no clear evidence for meteoric karstification in the studied cores.

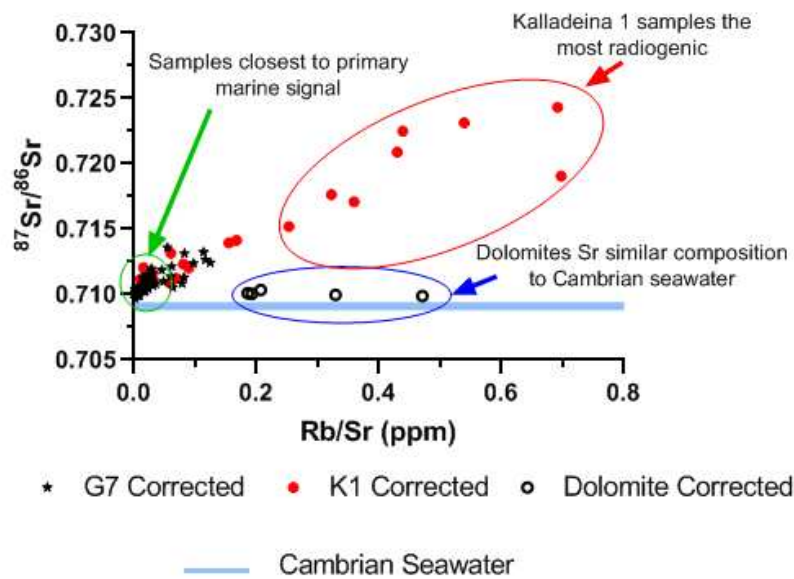


Figure 25. Cross-plot of elemental ratios, including $^{87}\text{Sr}/^{86}\text{Sr}$ values (corrected values) versus Rb/Sr ratio for all samples analysed for $^{87}\text{Sr}/^{86}\text{Sr}$, including Gidgealpa 7, Kalladeina 1 and Vuggy Dolomite samples from Gidgealpa 5, as depicted in the legend. The blue line indicates $^{87}\text{Sr}/^{86}\text{Sr}$ composition of Cambrian seawater (~509 to ~497 Ma; 0.7089-0.7093). Provides a comparison between wells/sequences, indicating radiogenic differences and samples closest to composition of Cambrian seawater.

Thus, it is more likely that an alternative scenario for dolomitization of Kalladeina limestones is plausible, involving hydrothermal dolomitization by relatively hot Mg-rich fluids derived from nearby volcanics and ongoing seawater-rock interactions between Late Cambrian seawater and the Mooracoochie volcanic system, acting as the thermal source and trigger for dolomitising fluids (Copp 2019; Roberts et al., 1990).

This study identifies a strong similarity in the Sr isotope signal between the vuggy dolomite and the best-preserved (i.e., least radiogenic) $^{87}\text{Sr}/^{86}\text{Sr}$ data from the Gidgealpa 7 Kalladeina limestones, suggesting local marine-derived fluids (i.e., Warburton-basin seawater), or modified Late Cambrian seawater were the primary source for dolomitization and formation of the vuggy dolomites. Importantly, the identification of

positive Eu/Eu* anomalies in a number of dolomitic samples (from Gidgealpa 5), and their vuggy porosity, also supports such hydrothermal origin for dolomitization.

Finally, although the vuggy dolomite has not been directly identified in Kalladeina 1 well, elevated Mg concentrations and positive Eu/Eu* anomalies at the base of the Kalladeina Formation also supports such hydrothermal dolomitization scenario. On the other hand, data from Gidgealpa 7 where vuggy dolomite is identified, show no obvious positive Eu/Eu* anomaly, which could argue against the hydrothermal origin for vuggy dolomite. Hence, this study suggests an interplay between two possible dolomitization models, i.e., hydrothermal and karstic/meteoric scenarios, representing combined effects of local volcanism/hydrothermalism, topography and structural geology of the basin. The karst model can be applied to parts of the depositional system where Kalladeina limestones have been exposed and uplifted during times of regression (i.e., LST), thus creating an interaction between marine/meteoric fluids and marine carbonates leading to generation of vuggy texture and possible later dolomitization due to subsequent burial. This is supported by SANTOS gamma/sedimentary logs, indicating the vuggy dolomite in Gidgealpa 7 and partially dolomitised section in Kalladeina 1 reside in a LST prior to a transgression. The second model, or hydrothermal scenario, suggests early dolomitization of Kalladeina limestones caused by the circulation of hydrothermal fluids (i.e., modified Late Cambrian seawaters) through volcanic systems (Mooracoochie volcanics) in the Warburton Basin. The hot and Mg-rich hydrothermal fluids would create vuggy porosity and high permeability leading to eventual early dolomitization of the Kalladeina limestones.

6. CONCLUSIONS

The paleo-depositional environment, past redox conditions and the chronostratigraphic framework of the East Warburton Basin during the Middle-Upper Cambrian (~510 to ~495 Ma) were constrained based on (i) C & Sr isotope chemostratigraphy, (ii) elemental concentrations (major and REE), and (iii) U/Pb zircon geochronology applied to sedimentary sequences from two wells; Kalladeina 1 and Gidgealpa 7. The high-resolution C isotope data ($\delta^{13}\text{C}$) collected from the above cores provided unprecedented chronostratigraphic resolution for the Kalladeina Formation in both wells, which allowed the identification of several global C isotope excursions (CIEs) in the studied records. These include a major positive C isotope anomaly called SPICE, and two negative DICE and ROECE anomalies. Additionally, different thickness of CIEs in studied wells suggest different sedimentation rates within the Warburton Basin, where results suggest local depositional/sedimentation rates up to three times greater in generally shallower Kalladeina 1 region, compared to the more distal Gidgealpa 7 settings. Furthermore, the integration of carbon data (i.e., chemostratigraphy) with SANTOS sedimentary/gamma logs (i.e., sequence stratigraphy) provides support for a transgression or relative sealevel rise during the SPICE. As to Sr isotope data, these yielded consistently more radiogenic $^{87}\text{Sr}/^{86}\text{Sr}$ values expected for Late Cambrian paleo-seawater, indicating either (i) a local basin restriction/partial restriction, or (ii) post-depositional alteration of $^{87}\text{Sr}/^{86}\text{Sr}$ signatures due to interactions with diagenetic fluid and/or effects of clay contamination (i.e., in-situ Rb decay). Overall, a comparison of elemental and Sr and C isotope data between studied wells reiterates the difference in their depositional environment, with the shallower Kalladeina 1 and relatively deeper

(distal) Gidgealpa 7. As to REE data, the Ce/Ce* anomaly in best preserved samples provided valuable insight into local palaeo-redox conditions. Evidence for negative Ce/Ce* anomalies has been found in both Gidgealpa 7 and Kalladeina 1, suggesting locally oxic conditions, although redox analysis in Kalladeina 1 was restricted to above the DICE due to likely alteration of primary REE signal. In conjunction with the chemostratigraphy C isotope work, the U/Pb zircon geochronology work done on the Mooracoochie Volcanics provided high precision, absolute age constraints on studied volcano-sedimentary sequences, which are consistent with the C isotope chemostratigraphy constraints. Specifically, ages from Gidgealpa 7 and Kalladeina 1 yielded best ages of, 509.1 ± 2.1 Ma and 510.8 ± 3 respectively, which are consistent with published Early/Middle Cambrian geochronological ages reported for Mooracoochie Volcanics (Stewart, 2010). As to the problem of dolomitization and the origin of “vuggy dolomite”, which represents the primary reservoir rock in the Warburton Basin, the combination of Sr isotope data ($^{87}\text{Sr}/^{86}\text{Sr}$) and REE analysis (Eu anomalies) on selected samples from the vuggy dolomite layer (from Gidgealpa 5 well) provided evidence for hydrothermal dolomitization, linked to local volcanic systems (i.e., Mooracoochie Volcanics), but local karstification as a cause for vuggy texture cannot be ruled out as well. Nevertheless, the documented positive Eu/Eu* anomalies and close-to palaeo-seawater $^{87}\text{Sr}/^{86}\text{Sr}$ data in vuggy dolomites points to a process where the circulation of Late Cambrian palaeo-seawater (or modified local seawater) through volcanic systems could generate hot and Mg-rich fluids that would then cause the dissolution of carbonates (i.e., Kalladeina limestones), producing their vuggy texture and eventual dolomitization. Overall, the integration of the above isotope and dating techniques applied to volcano-sedimentary sequences from the East Warburton Basin

provides an unprecedented chemostratigraphy framework of the Early to Late Cambrian basin evolution, and its different palaeo-depositional environments.

ACKNOWLEDGMENTS

I would like to thank everyone that helped throughout the year, both academically and personally. Huge mention goes to my supervisor, senior lecturer Dr Juraj Farkas for his assistance and mentorship throughout the year and also to my other supervisor Professor Alan Collins. Other acknowledgements go out to David Bruce, Dr Robert Klæbe and Dr Sarah Gilbert for their substantial help and guidance in the realm of geochemistry. A massive thankyou goes out to Dr Morgan Blades for the support and personal time she allocated towards the geochronology component of this project. Thanks to SANTOS for supplying the funding and providing great experiences and learning opportunities, hopefully this paper was worth the investment. Lastly, I would like to thank those in my honours cohort, specifically Liam Scarabotti and Chris Lowczak for the consistently long hours that we have all devoted.

REFERENCES

- ABDULLAH, R., NUGROHO, R., ROSENBAUM, G., DOUBLIER, M. P., SHAANAN, U., & ZWINGMANN, H. (2019). Evidence for Deformation in the Cambrian-Ordovician Warburton Basin and Implications for the Evolution of the Tasmanides (Eastern Australia). *Tectonics*, 38(5), 1532-1555.
- AHLBERG, P., AXHEIMER, N., BABCOCK, L. E., ERIKSSON, M. E., SCHMITZ, B., & TERFELT, F. (2009). Cambrian high-resolution biostratigraphy and carbon isotope chemostratigraphy in Scania, Sweden: first record of the SPICE and DICE excursions in Scandinavia. *Lethaia*, 42(1), 2-16.
- AHMAD, M. C., MUNSON, T. J. C., & Northern Territory Geological Survey, i. b. (2013). *Geology and mineral resources of the Northern Territory*: Northern Territory Geological Survey.
- AL-BUSAIDI, Q. A. (2018). Chemostratigraphy of Cambrian carbonates from the Amadeus Basin: implications for paleo-depositional environments and marine redox. *University of Adelaide Honours Degree Geology*, 1-31.
- AMANDA, M. O., & PETER, K. S. (2014). Interpreting carbonate and organic carbon isotope covariance in the sedimentary record. *Nature Communications*, 5.
- ANDREY YU, Z., & RACHEL, A. W. (2018). The two phases of the Cambrian Explosion. *Scientific Reports*, 8(1), 1-10.
- BABCOCK, L., ROBISON, R., REES, M., PENG, S. C., & SALTZMAN, M. (2007). The global boundary stratotype section and point (GSSP) of the drumian stage (Cambrian) in the drum mountains, Utah, USA. *Episodes*, 30(2), 85-95.
- BAILEY, T. R., MCARTHUR, J. M., PRINCE, H., & THIRLWALL, M. F. (2000). Dissolution methods for strontium isotope stratigraphy: whole rock analysis. *Chemical Geology*, 167(3), 313-319.
- BANNER, J. L., & HANSON, G. N. (1990). Calculation of simultaneous isotopic and trace element variations during water-rock interaction with applications to carbonate diagenesis. *Geochimica et Cosmochimica Acta*, 54(11), 3123-3137.
- BAO, X. (2007). Two Trends of Composition Variation of Zircons and Their Significance in Origin Discrimination.
- BAU, M., & DULSKI, P. (1996). Distribution of yttrium and rare-earth elements in the Penge and Kuruman iron-formations, Transvaal Supergroup, South Africa. *Precambrian Research*, 79(1-2), 37-55.
- BAU, M., & MÖLLER, P. (1992). Rare earth element fractionation in metamorphogenic hydrothermal calcite, magnesite and siderite. *Mineralogy and Petrology*, 45(3), 231-246.

- CARR, L. K., KORSCH, R. J., PALU, T. J., & REESE, B. (2016). Onshore basin inventory; the McArthur, South Nicholson, Georgina, Wiso, Amadeus, Warburton, Cooper and Galilee basins, central Australia. *Geoscience Australia*, 2016(04), 1-174.
- CHANG, C., HU, W., WANG, X., YU, H., YANG, A., CAO, J., & YAO, S. (2017). Carbon isotope stratigraphy of the lower to middle Cambrian on the eastern Yangtze Platform, South China. *Palaeogeography, Palaeoclimatology, Palaeoecology*, 479, 90-101.
- CHEW, D. M., PETRUS, J. A., KENNY, G. G., & MCEVOY, N. (2017). Rapid high-resolution U-Pb LA-Q-ICPMS age mapping of zircon. *Journal of Analytical Atomic Spectrometry*, 32(2), 262-276.
- COOK, H. E., TAYLOR, M. E., ZHEMCHUZHNIKOV, S. V., APOLLONOV, M. K., ERGALIEV, G. K., SARGASKAEV, Z. S., & DUBININA, S. V. (1991). Comparison of two early Paleozoic carbonate submarine facies - Western United States and Southern Kazakhshtan, Soviet Union. *Paleozoic Paleogeography of the Western United States - II: Pacific Section, SEPM*, 67, 847-872.
- CORFU, F., HANCHAR, J. M., HOSKIN, P. W. O., & KINNY, P. (2003). Atlas of zircon textures. *Reviews in Mineralogy and Geochemistry*, 53.
- CRISTIAN, G., MARLY, B., GUSTAVO MACEDO DE, P. S., & ANTONIO CARLOS, P. S. (2017). C, O, and Sr isotopic variations in Neoproterozoic-Cambrian carbonate rocks from Sete Lagoas Formation (Bambuá Group), in the Southern São Francisco Basin, Brazil. *Brazilian Journal of Geology*, 47(3), 521-543.
- DERRY, L. A., BRASIER, M. D., CORFIELD, R. M., ROZANOV, A. Y., & ZHURAVLEV, A. Y. (1994). Sr and C isotopes in Lower Cambrian carbonates from the Siberian craton: A paleoenvironmental record during the 'Cambrian explosion. *Earth and Planetary Science Letters*, 128(3), 671-681.
- DIREEN, N. G., & CRAWFORD, A. J. (2003). The Tasman Line: Where is it, what is it, and is it Australia's Rodinian breakup boundary? *Australian Journal of Earth Sciences*, 50(4), 491-502.
- EDWARDS, C. T., SALTZMAN, M. R., LESLIE, S. A., BERGSTRÖM, S. M., SEDLACEK, A. R., HOWARD, A., BAUER, J. A., SWEET, W. C., & YOUNG, S. A. (2015). Strontium isotope ($^{87}\text{Sr}/^{86}\text{Sr}$) stratigraphy of Ordovician bulk carbonate: Implications for preservation of primary seawater values. *Bulletin of the Geological Society of America*, 127(9-10), 1275-1289.
- ERIKSSON, M. E., & TERFELT, F. (2007). Anomalous facies and ancient faeces in the latest middle Cambrian of Sweden. *Lethaia*, 40(1), 69-84.
- FABRE, S., LÉZIN, C., & LEBEDEL, V. (2018). Paleooceanographic significance of cerium anomalies during the oae 2 on the NW African margin. *Journal of Sedimentary Research*, 88(11), 1284-1299.
- FAGGETTER, L. E., WIGNALL, P. B., PRUSS, S. B., NEWTON, R. J., SUN, Y., & CROWLEY, S. F. (2017). Trilobite extinctions, facies changes and the ROECE carbon isotope excursion at the Cambrian Series 2–3 boundary, Great Basin, western USA. *Palaeogeography, Palaeoclimatology, Palaeoecology*, 478, 53-66.
- FAN, R., DENG, S., & ZHANG, X. (2011). Significant carbon isotope excursions in the Cambrian and their implications for global correlations. *Science China Earth Sciences*, 54(11), 1686-1695.
- GATEHOUSE, C. G. (1986). The geology of the Warburton Basin in South Australia. *Australian Journal of Sciences*, 33(2), 161-180.
- GLIKSON, A. Y., MEIXNER, A. J., RADKE, B., UYSAL, I. T., SAYGIN, E., VICKERS, J., & MERNAGH, T. P. (2015). Geophysical anomalies and quartz deformation of the Warburton West structure, central Australia. *Tectonophysics*, 643(C), 55-72.
- GLUMAC, B. (1998). A late cambrian positive carbon-isotope excursion in the southern Appalachians: Relation to biostratigraphy, sequence stratigraphy, environments of deposition, and diagenesis. *Journal of Sedimentary Research*, 68(6).
- GUO, Q., STRAUSS, H., LIU, C., ZHAO, Y., YANG, X., PENG, J., & YANG, H. (2010). A negative carbon isotope excursion defines the boundary from Cambrian Series 2 to Cambrian Series 3 on the Yangtze Platform, South China. *Palaeogeography, Palaeoclimatology, Palaeoecology*, 285(3), 143-151.
- HALLMANN, C. O. E., AROURI, K. R., MCKIRDY, D. M., & SCHWARK, L. (2006). A NEW PERSPECTIVE ON EXPLORING THE COOPER/EROMANGA PETROLEUM PROVINCE—EVIDENCE OF OIL CHARGING FROM THE WARBURTON BASIN. *The APPEA Journal*, 46(1), 261.

- HANCHAR, J. M., & MILLER, C. F. (1993). Zircon zonation patterns as revealed by cathodoluminescence and backscattered electron images: Implications for interpretation of complex crustal histories. *Chemical Geology*, 110(1-3), 1-13.
- HANSON, G. N. (1980). Rare Earth Elements in Petrogenetic Studies of Igneous Systems. *Annu. Rev. Earth Planet. Sci.*, 8(1), 371-406.
- HENDERSON, R. A. (1976). Stratigraphy of the Georgina limestone and a revised zonation for the early upper Cambrian Idamean Stage. *Journal of the Geological Society of Australia*, 23(4), 423-433.
- HOWLEY, R. A., & JIANG, G. (2010). The Cambrian Drumian carbon isotope excursion (DICE) in the Great Basin, western United States. *Palaeogeography, Palaeoclimatology, Palaeoecology*, 296(1), 138-150.
- HUA, G., YUANSHEG, D., LIAN, Z., JIANGHAI, Y., HU, H., MIN, L., & YUAN, W. (2013). Trace and rare earth elemental geochemistry of carbonate succession in the Middle Gaoyuzhuang Formation, Pingquan Section: Implications for Early Mesoproterozoic ocean redox conditions. *Journal of Palaeogeography*, 2(2), 209-221.
- JONES, D. S., MALOOF, A. C., HURTGEN, M. T., RAINBIRD, R. H., & SCHRAG, D. P. (2010). Regional and global chemostratigraphic correlation of the early Neoproterozoic Shaler Supergroup, Victoria Island, Northwestern Canada. *Precambrian Research*, 181(1), 43-63.
- KHAIR, H. A., COOKE, D., & HAND, M. (2013). *Present-day-in-situ stresses versus paleo-stresses for locating sweet spots in unconventional reservoirs*: Australian Petroleum Production and Exploration Association.
- KOUCHINSKY, A., BENGTSON, S., GALLET, Y., KOROVNIKOV, I., PAVLOV, V., RUNNEGAR, B., SHIELDS, G., VEIZER, J. A. N., YOUNG, E., & ZIEGLER, K. (2008). The SPICE carbon isotope excursion in Siberia: a combined study of the upper Middle Cambrian–lowermost Ordovician Kulyumbe River section, northwestern Siberian Platform. *Geol. Mag.*, 145(5), 609-622.
- KRABBENHÖFT, A., FIETZKE, J., EISENHAEUER, A., LIEBETRAU, V., BÖHM, F., & VOLLSTAEDT, H. (2009). Determination of radiogenic and stable strontium isotope ratios ($^{87}\text{Sr}/^{86}\text{Sr}$) by thermal ionization mass spectrometry applying an $^{87}\text{Sr}/^{84}\text{Sr}$ double spike. *Journal of Analytical Atomic Spectrometry*, 24(9), 1267-1271.
- LEROY, M. A., & GILL, B. C. (2019). Evidence for the development of local anoxia during the Cambrian SPICE event in eastern North America. *Geobiology*.
- LIU, C., WANG, Z., & RAUB, T. D. (2013). Geochemical constraints on the origin of Marinoan cap dolostones from Nuccaleena Formation, South Australia. *Chemical Geology*, 351, 95.
- LIU, H., MA, T., TAN, X., ZENG, W., HU, G., XIAO, D., LUO, B., SHAN, S., & SU, C. (2016). Origin of structurally controlled hydrothermal dolomite in epigenetic karst system during shallow burial: An example from Middle Permian Maokou Formation, central Sichuan Basin, SW China. *Petroleum Exploration and Development Online*, 43(6), 1000-1012.
- LUDWIG, K. R. (2003). User's Manual for Isoplot 3.00: a geochronological toolkit for Microsoft Excel. *Berkeley Geochronology Center*.
- MATTHEW, R. S., SETH, A. Y., LEE, R. K., BENJAMIN, C. G., TIMOTHY, W. L., & BRUCE, R. (2011). Pulse of atmospheric oxygen during the late Cambrian. *Proceedings of the National Academy of Sciences*, 108(10), 3876.
- MCARTHUR, J. M., & HOWARTH, R. J. (2004). Strontium Isotope Stratigraphy. *The Geologic Time Scale*, 1, 96-105.
- MCARTHUR, J. M., HOWARTH, R. J., & BAILEY, T. R. (2001). Strontium Isotope Stratigraphy: LOWESS Version 3: Best Fit to the Marine SrIsotope Curve for 0509 Ma and Accompanying Lookup Table for Deriving Numerical Age. *The Journal of Geology*, 109(2), 155-170.
- MCARTHUR, J. M., HOWARTH, R. J., & SHIELDS, G. A. (2012). *Strontium Isotope Stratigraphy* (Vol. 1-2).
- MEYER, E. E., QUICKSALL, A. N., LANDIS, J. D., LINK, P. K., & BOSTICK, B. C. (2012). Trace and rare earth elemental investigation of a Sturtian cap carbonate, Pocatello, Idaho: Evidence for ocean redox conditions before and during carbonate deposition. *Precambrian Research*, 192-195(1), 89-106.
- MIDDLETON, A. W., UYSAL, I. T., & GOLDING, S. D. (2015). chemical and mineralogical characterisation of illite-smectite: implications for episodic tectonism and associated fluid flow, central Australia. *Geochemica et Cosmochimica Acta*, 148, 284-303.

- MONATANEZ, I. P., OSLEGER, D. A., BANNER, J. L., MACK, L. E., & MUSGROVE, M. (2000). Evolution of the Sr and C isotope composition of Cambrian Oceans. *GSA Today*, 10(5), 1-7.
- MONTANEZ, I., BANNER, J., OSLEGER, D., BORG, L., & BOSSERMAN, P. (1996). Integrated Sr isotope variations and sea-level history of Middle to Upper Cambrian platform carbonates: Implications for the evolution of Cambrian seawater $^{87}\text{Sr}/^{86}\text{Sr}$. *Geology*, 24(10), 917-920.
- NANCE, W. B., & TAYLOR, S. R. (1976). Rare earth element patterns and crustal evolution—I. Australian post-Archean sedimentary rocks. *Geochimica et Cosmochimica Acta*, 40(12), 1539-1551.
- NURGALIEVA, N. G., NOURGALIEV, D., & PONOMARCHUK, V. A. (2007). Strontium isotope stratigraphy: Possible applications for age estimation and global correlation of Late Permian carbonates of the Pechishchi type section, Volga River. *Russian Journal of Earth Sciences*, 9(1002).
- OEHLERT, A. M., & SWART, P. K. (2014). Interpreting carbonate and organic carbon isotope covariance in the sedimentary record. *Nature Communications*, 5, 4672.
- OLIVAREZ, A. M., & OWEN, R. M. (1991). The europium anomaly of seawater: implications for fluvial versus hydrothermal REE inputs to the oceans. *Chemical Geology*, 92(4), 317-328.
- PAGÈS, A., & SCHMID, S. (2016). Euxinia linked to the Cambrian Drumian carbon isotope excursion (DICE) in Australia: Geochemical and chemostratigraphic evidence. *Palaeogeography, Palaeoclimatology, Palaeoecology*, 461, 65-76.
- PATON, C., WOODHEAD, J. D., HELLSTROM, J. C., HERGT, J. M., GREIG, A., & MAAS, R. (2010). Improved laser ablation U-Pb zircon geochronology through robust downhole fractionation correction. *Geochemistry, Geophysics, Geosystems*, 11(3).
- PENG, S., BABCOCK, L. E., & COOPER, R. A. (2012). *The Cambrian Period* (Vol. 1-2): The Geologic Timescale.
- PETERS, S. E., & GAINES, R. R. (2012). Formation of the 'Great Unconformity' as a trigger for the Cambrian explosion. *Nature*, 484, 363-366.
- PURDY, D. J., HEGARTY, R., & DOUBLIER, M. P. (2018). Basement geology of the southern Thomson Orogen. *Australian Journal of Earth Sciences*, 65(7-8), 893-916.
- RADKE, B. (2009). Hydrocarbon and Geothermal Prospectivity of Sedimentary Basins in Central Australia. *Geoscience Australia*, 25, 1-172.
- REINERS, P. W., CARLSON, R. W., RENNE, P. R., COOPER, K. M., GRANGER, D. E., MCLEAN, N. M., & SCHOENE, B. (2018). *U-Th-Pb geochronology and thermochronology*. John Wiley & Sons Ltd.: John Wiley & Sons Ltd.
- ROBERTS, D. C., CARROLL, P. G., & SAYERS, J. (1990). The Kalladeina formation - a Warburton Basin Cambrian carbonate play. *The Australian Petroleum Exploration Association*, 1-18.
- SALTZMAN, M. R., COWAN, C. A., RUNKEL, A. C., RUNNEGAR, B., STEWART, M. C., & PALMER, A. R. (2004). The Late Cambrian SPICE ($\delta^{13}\text{C}$) event and the Sauk II-Sauk III regression: New evidence from Laurentian basins in Utah, Iowa, and Newfoundland. *Journal of Sedimentary Research*, 74(3), 366-377.
- SALTZMAN, M. R., DAVIDSON, J. P., HOLDEN, P., RUNNEGAR, B., & LOHMANN, K. C. (1995). Sea-level-driven changes in ocean chemistry at an Upper Cambrian extinction horizon. *Geology*, 23(10), 893-896.
- SALTZMAN, M. R., RIPPERDAN, R. L., BRASIER, M. D., LOHMANN, K. C., ROBISON, R. A., CHANG, W. T., PENG, S., ERGALIEV, E. K., & RUNNEGAR, B. (2000). A global carbon isotope excursion (SPICE) during the Late Cambrian: relation to trilobite extinctions, organic-matter burial and sea level. *Palaeogeography, Palaeoclimatology, Palaeoecology*, 162(3), 211-223.
- SCHILDGEN, T. F., COSENTINO, D., FRIJIA, G., CASTORINA, F., DUDAS, F. Ö., IADANZA, A., SAMPALMIERI, G., CIPOLLARI, P., CARUSO, A., BOWRING, S. A., & STRECKER, M. R. (2014). Sea level and climate forcing of the Sr isotope composition of late M iocene M editerranean marine basins. *Geochemistry, Geophysics, Geosystems*, 15(7), 2964-2983.
- SCHMID, S. (2017). Chemostratigraphy and palaeo-environmental characterisation of the Cambrian stratigraphy in the Amadeus Basin, Australia. *Chemical Geology*, 451, 169-182.
- SCHMID, S., SMITH, M. P., & WOLTERING, M. (2018). A basin-wide record of the Late Cambrian Steptoean positive carbon isotope excursion (SPICE) in the Amadeus Basin, Australia. *Palaeogeography, Palaeoclimatology, Palaeoecology*, 508, 116-128.

- SIAL, A. N., PERALTA, S., GAUCHER, C., TOSELLI, A. J., FERREIRA, V. P., FREI, R., PARADA, M. A., PIMENTEL, M. M., & SILVA PEREIRA, N. (2013). High-resolution stable isotope stratigraphy of the upper Cambrian and Ordovician in the Argentine Precordillera: Carbon isotope excursions and correlations. *Gondwana Research*, 24(1), 330-348.
- SLAMA, J., KOSLER, J., CONDON, D., CROWLEY, J., GERDES, A., HANCHAR, J., HORSTWOOD, M., MORRIS, G., NASDALA, L., NORBERG, N., SCHALTEGGER, U., SCHOENE, B., TUBRETT, M., & WHITEHOUSE, M. (2008). Plesovice zircon - A new natural reference material for U-Pb and Hf isotopic microanalysis. *Chemical Geology*, 249(1-2), 1-35.
- SUBARKAH, D. (2018). The forgotten Mesoproterozoic of Northern Australia: a chemostratigraphy and detrital zircon study of the greater McArthur Basin. *University of Adelaide Honours Degree Geology*, 1-81.
- SUN, X. (1996). *Sequence stratigraphy, sedimentology, biostratigraphy and palaeontology of the eastern Warburton Basin (Palaeozoic), South Australia*.
- SUN, X., & JAGO, J. B. (2009). An Iverian (Furongian, Cambrian) Trilobite Faunule from the Subsurface Warburton Basin, South Australia. *Memoirs of the Association of Australasian Palaeontologists*(37), 1-8.
- SUN, X. W., BENTLEY, C. J., & JAGO, J. B. (2017). The significance of Cambro-Ordovician trilobites from the Kalladeina 1 drill hole, Warburton Basin, South Australia. *Australian Journal of Earth Sciences*, 64(4), 471-485.
- SWART, P. K. (2015). The geochemistry of carbonate diagenesis: The past, present and future. *Sedimentology*, 62(5), 1233-1304.
- TAYLOR, S. R. (1985). *The continental crust, its composition and evolution : an examination of the geochemical record preserved in sedimentary rocks*. Oxford Melbourne: Blackwell Scientific Publications.
- TOSTEVIN, R., SHIELDS, G. A., TARBUCK, G. M., HE, T., CLARKSON, M. O., & WOOD, R. A. (2016). Effective use of cerium anomalies as a redox proxy in carbonate-dominated marine settings. *Chemical Geology*, 438(C), 146-162.
- VEIZER, J., ALA, D., AZMY, K., BRUCKSCHEN, P., BUHL, D., BRUHN, F., GARDEN, G. A. F., DIENER, A., EBNETH, S., GODDERIS, Y., JASPER, T., KORTE, C., PAWELLEK, F., PODLAHA, O. G., & STRAUSS, H. (1999). 87 Sr/ 86 Sr, $\delta^{13}\text{C}$ and $\delta^{18}\text{O}$ evolution of Phanerozoic seawater. *Chemical Geology*, 161(1), 59-88.
- VERMEESCH, P. (2013). Multi-sample comparison of detrital age distributions. *Chemical Geology*, 341(C), 140-146.
- VONLANTHEN, P., GERALD, J., RUBATTO, D., & HERMANN, J. (2012). Recrystallization rims in zircon (Valle d'Arbedo, Switzerland): An integrated cathodoluminescence, LA-ICP-MS, SHRIMP, and TEM study. *The American Mineralogist*, 97(2-3), 369.
- WOOD, R., LIU, A. G., BOWYER, F., WILBY, P. R., DUNN, F. S., KENCHINGTON, C. G., CUTHILL, J. F. H., MITCHELL, E. G., & PENNY, A. (2019). Integrated records of environmental change and evolution challenge the Cambrian Explosion. *Nature Ecology and Evolution*, 3(4), 528-538.
- WOODS, M., WILBY, P., LENG, M., RUSHTON, A., & WILLIAMS, M. (2011). The Furongian (late Cambrian) Steptoean Positive Carbon Isotope Excursion (SPICE) in Avalonia. *Journal of the Geological Society*, 168, 851-861.
- WOPFNER, H. (1969). Depositional History and Tectonics of South Australian Sedimentary Basins. *Mineral Resources Review*, 133.
- WOTTE, T., & STRAUSS, H. (2015). Questioning a widespread euxinia for the Furongian (Late Cambrian) SPICE event: indications from $\delta^{13}\text{C}$, $\delta^{18}\text{O}$, $\delta^{34}\text{S}$ and biostratigraphic constraints.(Author abstract). 152(6), 1085.
- WRIGHT, A. M., RATCLIFFE, K. T., ZAITLIN, B. A., & WRAY, D. S. (2010). The Application of Chemostratigraphic Techniques to Distinguish Compound Incised Valleys in Low-Accommodation Incised-Valley Systems in a Foreland-Basin Setting: an Example from the Lower Cretaceous Mannville Group and Basal Colorado Sandstone (Colorado Group), Western Canadian Sedimentary Basin. *Society for Sedimentary Geology*(94), 93-107.
- ZHANG, X., & SHU, D. (2014). Causes and consequences of the Cambrian explosion. *Science China Earth Sciences*, 57(5), 930-942.

- ZHU, M. Y., BABCOCK, L. E., & PENG, S. C. (2006). Advances in Cambrian stratigraphy and paleontology: Integrating correlation techniques, paleobiology, taphonomy and paleoenvironmental reconstruction. *Palaeoworld*, 15(3), 217-222.
- ZHU, M., YANG, A., YUAN, J., LI, G., ZHANG, J., ZHAO, F., AHN, S. Y., & MIAO, L. (2019). Cambrian integrative stratigraphy and timescale of China. *Science China Earth Sciences*, 62(1), 25-60.
- ZUO, J., PENG, S., QI, Y., ZHU, X., BAGNOLI, G., & FANG, H. (2018). Carbon-Isotope Excursions Recorded in the Cambrian System, South China: Implications for Mass Extinctions and Sea-Level Fluctuations. *Journal of Earth Science*, 29(3), 479-491.

APPENDIX A: EXTENDED METHODS

Samples for elemental analysis were analysed at Adelaide Microscopy, using the Agilent 8900x (QQQ) Inductively Coupled Plasma Mass Spectrometer (ICP-MS). Characteristically, plasma conditions were: RF (Radio Frequency) Power 1550W, Ar carrier gas flow rate 1.09 L/min, with a Micro Mist nebuliser and Scott Type spray chamber and sample depth of 8mm. The collision cell was run in O and He mode, the latter of the two was run for majority of elements [Mg, Al, Sc, Ti, V, Cr, Mn, Co, Ni, Cu, Zn, Ga, Rb, Y, Zr, Nb, Mo, Cd, Cs, Ba, La, Ce, Pr, Nd, Sm, Gd, Er, Tb, Dy, Ho, Er, Tm, Yb, Lu, Hf, Ta, Pb, Th, U]. The oxygen (30% flow rate) collision cell was used to measure P, Ca and Fe. Addition of In was used as an internal standard element and a series of mixed calibration standard [0, 10, 20, 50, 100, 200 and 500 ppb] were used for quantification.

Isotope Chemostratigraphy – Carbon & Strontium

- **Ring Milling**
 - Room and tungsten ring mill is cleaned using compressed air hose and ethanol
 - Ring mill goes through quartz rinse for 1 minute and cleaned with air hose and ethanol
 - Sample (rock chips) is placed into ring mill and milled for ~35 seconds
 - Powdered sample is placed into sample bag for isotopic analysis
 - Repeat each step, ensuring quartz rinse and multiple air hose/ethanol cleans between samples

CARBON ISOTOPES: $\delta^{13}\text{C}$

- **Cleaning**
 - Glass vials, caps and septa are placed in beakers of hot water and sonicated for ~15 minutes
 - The vials are scrubbed and sequentially triple rinsed with deionised water
 - Lastly, cleaned vials are heated in an oven over night
- **Prior to Loading into IRMS**
 - Samples (~2mg, depending on carbonate content) are flooded with helium (purged)
 - Using a needle, 8 drops of 10.5% phosphoric acid are added to each sample (including blanks and standards)

RADIOGENIC STRONTIUM ISOTOPES: $^{87}\text{SR}/^{86}\text{SR}$

- **Cleaning Centrifuge Tubes**
 - 15ml centrifuge tubes were used to leach the carbonates for strontium and major/trace element analysis
 - Prior to use, ~2ml of SD 6M HCl is added to each tube and placed on a hot plate (~80°C) overnight to reflux
 - Waste acid is removed, and tubes/lids are triple rinsed with DI H₂O
 - Then placed back on the hot plate for DI H₂O to evaporate (>30 mins) and ready for sample

- **Cleaning Teflon**
 - Teflon needs to be completely clear of previous users labels, using ethanol and wipes
 - HCl is added to all teflon vials (~1-2ml) and placed hot plate overnight (140°C)
 - Following HCl rinse, teflon is triple rinsed with DI H₂O and evaporated on hot plate
 - They are then refluxed in 6M Nitric acid on a hot plate (170°C) for 2 days
 - After nitric rinse, teflon is triple rinsed with DI H₂O and refluxed in 6M HCl on a hot plate (170°C) for a day
 - After HCl rinse, teflon is triple rinsed with DI H₂O and are capped and refluxed on a hot plate (140°C) with a small amount of 6M SD HCl for a day
 - HCl is removed to waste and teflon is left to evaporate on a hot plate

- **Cleaning ICP tubes**
 - The plastic tubes used for major/trace element (ICP) analysis follow the same cleaning protocol as the centrifuge tubes (above)

- **Chromatography in polyprep columns, using Eichrom Sr resin to extract the pure fraction of Sr from each sample. The following method was used:**
 - Wash resin and column with 3 ml of 8M HNO₃ SD (single distilled)
 - Wash resin and column with 3 ml of DI H₂O
 - Wash resin and column with 3 ml of 8M HNO₃ SD
 - Wash resin and column with 3 ml of DI H₂O
 - Wash resin and column with 3 ml of 8M HNO₃ SD
 - Wash resin and column with 3 ml of DI H₂O
 - Load samples in 1 ml 8M HNO₃ SD
 - Wash with 1 ml 8M HNO₃ SD x 5
 - Collect Sr with 1 ml of 0.05M HNO₃ SD x 6
 - Add 1 drop of H₃PO₄ to Sr vial
 - Evaporate down on hot plate at 140°C
 - Add a small amount (~1-2ml) of 15M HNO₃ to oxidise any organics
 - Cap vials and heat at 110°C for ~5 hours
 - Evaporate on hot plate at 140°C, repeat oxidising stage as necessary if Sr fraction is still dark

- **Spiking of Procedural Blanks**
 - Following chromatography, procedural blanks were spiked with Sr spike F; which were weighed out, diluted and dried down to homogenise spike
 - After spiking, blanks followed the same procedure as a regular sample for $^{87}\text{Sr}/^{86}\text{Sr}$ analysis
- **Cleaning/Making Rhenium Filaments**
 - Rhenium filaments from previous user are recycled and the rods supporting the filaments sequentially stripped using a Dremel
 - Stripped filaments are boiled in 30% H_2O_2 (hydrogen peroxide) for 1 hour at 80°C
 - Are then triple rinsed using DI H_2O
 - Following rinse, are placed in a beaker/jar of $\text{C}_3\text{H}_6\text{O}$ (acetone) and sonicated for 1 minute
 - After sonication, filaments are dried down in the oven
 - Dried filaments have a small strip of rhenium welded to them in preparation for loading

Geochronology – U/Pb Zircon Dating

- **Mineral Preparation**
 - Clean rock crusher and disk mill prior to use, using compressed air gun and ethanol
 - Crush rock using jaw crusher
 - Use disk mill for additional crushing
 - Separate fractions with a sieve; using 79 μm and 479 μm mesh to separate fractions
 - Can be sieved manually or using an Endcotts EPL2000 super shaker
 - Coarse sample >479 μm is taken and re-crushed, using either disk mill or ring mill and re-sieved
 - Repeat and divide for each sample, aiming to maximise sample between 79 μm and 479 μm (zircon fraction)
- **Mineral Separation**
 - Separation was done at The University of Adelaide, in B29 Mawson Laboratories
 - Clean room and equipment before and after use with ethanol
 - Pan samples to separate light and heavy grains from zircon fraction
 - Heavy aliquot is panned to ~20mg
 - Both light and heavy aliquots are filtered, heated and kept so no sample is lost
 - A magnet is run over the heavy aliquot to remove magnetic minerals
 - The remaining fraction is placed into a vial
- **Zircon Picking & Mount Preparation**
 - Clean petri dish with ethanol and place under light microscope
 - Transfer zircon fraction from sample onto dish

- Use a pick to take zircon and place onto Teflon mount base with double sided tape
- Repeat from sufficient number of grains (~100)
- Reconnect Teflon base with enclosure
- Coat with vaseline to ease removal in later steps
- Create epoxy mixture (epoxy 5g, hardener 0.5g) and add into mount, stirring slowly to homogenise mixture and ensure air pockets do not form
- Leave epoxy to cool and set over a 24 hour period
- Remove epoxy mount containing zircons from the Teflon holder
- Bring grains to surface using sand paper and polishing

APPENDIX B: FULL DATASET

Table 1. Colours representing different $\delta^{13}\text{C}$ isotope chemostratigraphy intervals and CIE's identified from this study. This colour scheme is used for all Gidgealpa 7 and Kalladeina 1 datasets in the following tables.

	Above SPICE
	SPICE
	Between DICE & SPICE
	DICE
	Between ROECE & DICE
	ROECE
	Below ROECE

Major and Trace Element Data Sets for Gidgealpa 7 and Kalladeina

Elements; Niobium (Nb), Hafnium (Hf), Molybdenum and Tantalum (Ta) were removed from data sets due to limited data (detection limits).

Table 2. Gidgealpa 7 data set of major and trace elements.

Depth (feet)	Mg_ppm	Al_ppm	P_ppm	Ca_ppm	Sc_ppm	Ti_ppm	V_ppm	Cr_ppm	Mn_ppm	Fe_ppm	Co_ppm	Ni_ppm
7660	5463.152	1575.900	62.046	501682.017	8.861	9.655	1.985	15.460	2348.973	9416.470	118.733	9.218
7680	3018.149	66.300	32.985	608519.197	0.231	2.125	1.117	2.076	607.862	1216.467	9.867	0.778
7701	15960.531	1436.975	60.524	553528.956	9.322	7.137	3.473	4.492	999.246	18904.346	33.270	3.502
7720	1080.051	533.438	104.280	62013.465	1.102	2.729	0.996	7.162	175.508	1730.452	13.451	1.604
7750	4847.342	591.683	44.384	470912.675	3.435	8.095	1.043	4.299	486.457	4475.251	9.350	1.309
7800	2619.643	314.000	46.755	132240.852	1.143	3.583	0.784	3.222	147.681	2062.705	10.177	1.001
7820	3223.118	520.198	36.291	415469.101	4.717	5.247	1.014	5.779	727.068	4213.163	17.106	1.772

7850	486.771	158.878	33.836	52313.329	1.101	3.902	0.409	1.853	220.245	768.306	6.737	<1.195
7910	1904.975	559.012	40.800	226529.471	4.692	7.042	0.844	3.457	847.914	2652.945	9.894	1.362
7940	4455.799	130.471	<1.111	439422.031	1.603	1.566	0.327	3.192	422.068	1719.731	8.646	0.657
7960	4465.032	202.029	7.239	392333.097	1.885	1.254	0.541	2.510	378.885	1486.568	9.129	1.195
7980	1585.029	192.660	29.600	94364.232	0.734	1.965	0.661	2.455	106.705	879.212	4.654	0.616
8010	2203.081	96.773	30.369	172389.052	0.769	0.900	0.592	1.750	141.878	1088.166	6.249	0.804
8040	3241.512	341.616	54.718	405204.025	1.961	30.116	0.768	3.415	373.272	1461.863	7.098	<0.987
8072	2564.783	246.653	35.349	211056.299	1.060	6.452	0.635	1.847	171.254	924.286	5.826	<0.889
8090	4115.549	237.151	56.878	284656.969	1.531	4.167	1.380	3.854	395.647	2471.433	5.984	1.426
8120	4623.540	267.461	32.706	441015.723	2.770	5.063	0.731	3.612	549.809	2018.867	8.370	1.259
8180	783.784	95.175	48.758	46184.048	0.439	1.735	0.400	2.286	409.683	502.875	3.315	<0.606
8230	4299.112	153.189	36.685	550339.941	2.647	3.106	0.694	3.942	709.349	1805.748	7.378	0.957
8250	2336.569	62.973	31.052	254216.876	1.402	1.834	0.901	2.776	596.476	2434.909	4.658	1.128
8280	1018.942	103.667	45.626	61787.021	0.733	0.345	0.228	1.271	287.437	723.797	2.685	0.281
8310	3126.849	429.545	181.252	124669.354	2.730	2.277	0.666	4.007	570.582	2077.493	16.281	1.425
8340	2516.316	555.568	158.903	92988.739	2.605	2.849	0.877	2.836	489.835	2230.321	13.983	1.923
8370	5226.608	366.139	98.481	108037.786	1.484	5.083	2.807	4.813	579.214	4231.134	11.991	2.486
8400	4010.980	400.267	62.321	164287.338	3.013	0.981	0.889	3.241	971.177	3202.610	11.602	1.570
8430	2223.752	517.453	97.415	118699.998	1.548	2.964	1.084	10.508	512.664	1513.728	23.674	2.740
8460	2960.791	528.608	61.323	176495.140	2.830	0.903	0.635	3.590	812.310	1846.317	14.903	1.314
8500	5171.417	308.345	89.537	182736.259	1.821	0.948	1.751	3.907	819.373	4356.044	18.073	2.004
8520	4344.568	1147.680	157.992	135349.622	3.455	3.457	1.351	4.931	1141.742	4292.517	13.822	2.260
8550	4112.525	192.671	104.476	167303.876	1.806	1.123	1.397	3.643	569.079	3368.533	8.978	2.070
8580	4880.933	297.261	79.677	143988.116	1.606	3.076	2.211	4.134	706.897	4221.949	8.250	2.296
8610	3114.836	155.893	56.277	143127.699	1.509	1.097	0.815	2.289	857.349	2237.382	5.319	0.763
8640	1969.079	28.857	33.482	213473.465	0.301	0.542	0.234	1.659	931.037	759.337	0.433	0.453
8670	4251.610	588.875	107.863	174962.139	2.039	1.969	1.187	4.560	837.903	4184.404	30.184	2.367
8760	4474.866	722.492	89.487	38556.326	2.584	2.224	1.548	3.719	429.308	5564.025	17.379	4.369
8793	917.535	12.025	11.355	161524.958	0.115	<0.221	0.172	0.617	90.963	141.085	10.530	0.599
8820	2955.630	577.915	61.028	110880.359	0.991	3.123	0.665	3.831	256.289	1736.493	18.965	1.688

Chemostratigraphy and geochronology of Cambrian sequences in East Warburton Basin, South Australia

8850	6099.617	34.661	11.208	124571.104	0.109	0.769	0.661	1.749	110.280	610.445	5.438	<0.547
8880	6228.797	47.991	12.232	252416.053	0.230	0.526	0.718	7.742	202.959	805.028	6.769	0.570
8900	1112.627	14.268	6.002	89975.408	<0.064	<0.221	0.246	2.315	29.728	112.814	4.214	<0.503
8930	2666.266	16.618	5.011	181307.259	0.124	0.170	0.247	2.024	68.651	162.142	3.382	0.210
8970	3151.008	47.746	11.263	158254.387	0.145	0.655	0.746	2.747	70.384	287.935	10.534	<0.384
9000	1355.680	39.454	20.135	134996.409	0.116	0.184	0.500	3.306	77.328	301.942	6.532	0.390
9030	5194.365	35.932	5.455	178562.690	0.207	0.269	0.155	2.279	180.194	369.867	7.290	0.536
9059	743.753	31.563	31.887	177637.954	0.213	0.185	0.533	0.794	291.988	1137.104	7.156	0.398
9074	1808.598	1652.258	127.184	25872.685	1.414	8.739	1.604	3.775	303.078	1386.921	31.981	4.132
9080	1369.172	14.631	2.235	185883.424	0.109	0.128	0.069	1.624	259.790	293.301	5.639	0.434
9100	1212.673	23.331	10.883	210340.575	0.265	0.321	0.239	2.686	420.507	965.844	2.397	0.658
9120	1559.788	73.448	41.486	221801.114	0.379	0.684	0.685	2.535	363.948	1574.630	10.027	0.861
9150	1305.147	106.848	45.724	116221.568	0.453	1.127	0.441	4.360	189.611	948.655	8.883	1.045
9250	2745.043	67.343	12.634	257869.695	0.311	0.621	0.376	2.796	185.097	817.320	5.569	0.958
9270	786.634	49.556	27.163	152620.563	0.305	0.274	0.136	2.423	84.404	285.152	3.302	0.587
9290	2093.472	325.001	57.027	336746.671	0.487	6.366	0.736	7.144	260.545	1060.214	9.793	1.170
9310	3721.114	169.654	50.906	376393.898	0.434	1.115	0.875	4.971	291.027	1149.532	4.296	1.061
9330	4231.791	224.848	36.553	230546.882	0.341	1.478	1.222	5.199	195.799	950.769	8.971	1.005
9350	2767.051	118.052	21.964	168925.031	0.230	0.534	0.610	1.758	129.881	640.262	5.392	0.854
9380	5497.347	51.752	16.745	221417.262	0.147	0.307	0.401	1.654	101.763	560.760	5.201	0.629
9410	4036.207	129.900	31.009	252990.253	0.248	0.767	0.460	3.298	134.153	700.992	8.706	0.601
9430	2764.537	45.578	19.677	205873.049	0.167	0.277	0.389	2.140	140.867	432.153	4.214	0.382
9450	2745.507	451.471	82.887	172479.358	0.809	2.711	1.067	3.940	272.812	1774.276	3.933	1.591
9530	1190.250	954.383	91.275	42130.322	0.966	6.860	1.238	1.550	147.670	1201.231	6.610	1.805
9560	3518.559	441.465	49.138	107342.679	1.730	1.350	1.020	2.639	616.954	2724.051	7.396	0.969
9580	3378.218	630.995	133.221	258036.210	3.180	3.513	1.292	4.917	1143.576	2174.338	14.782	2.253
9610	2084.433	1194.997	121.923	128179.961	0.834	11.043	1.941	2.938	209.667	1487.142	6.513	2.181
9630	2785.102	166.197	47.582	214336.174	0.917	3.058	0.960	3.239	704.059	1236.526	4.003	0.793
9650	2187.173	1404.164	222.150	117536.813	1.942	7.969	2.693	5.078	621.025	2088.072	18.635	3.211
9750	2494.447	599.944	74.726	132260.707	0.837	5.148	1.109	3.357	379.165	1413.119	20.160	1.876

9760	1743.982	1398.556	149.458	111182.447	1.638	21.534	2.274	2.973	541.110	2187.975	16.763	4.413
9780	2504.323	742.532	107.183	160461.652	1.377	5.907	1.411	2.936	813.750	2019.491	7.784	2.731
9800	2016.906	791.299	100.017	144300.036	1.778	22.130	1.367	3.407	721.890	2220.449	11.868	2.331
9831	1991.358	470.051	74.711	88863.474	0.925	5.459	0.708	1.158	453.998	1142.352	8.412	1.137
9850	1926.324	1017.749	97.213	135155.933	2.101	9.225	1.846	1.777	874.702	1854.727	10.079	2.502
9870	779.732	391.093	39.672	41519.766	0.518	3.966	0.637	0.770	233.043	704.790	4.268	0.912
9900	7392.700	372.318	46.223	147877.964	2.084	2.611	1.167	2.048	345.760	3071.750	4.931	1.133
9920	3374.791	1498.618	86.662	256751.280	4.164	8.873	1.600	5.121	1542.282	2666.528	20.296	5.466
9950	1077.746	301.085	121.967	15494.697	0.621	3.178	0.523	0.924	62.090	506.078	1.310	0.986
9970	2459.180	145.248	134.263	182514.175	0.315	3.072	0.919	1.942	263.013	826.861	5.319	0.597
10100	40416.294	425.527	42.851	102672.376	0.334	3.325	1.404	3.080	179.388	1561.671	11.175	2.300
10110	8209.618	941.620	169.687	185546.481	2.127	6.641	2.737	4.797	370.060	4195.141	16.870	4.790
10120	7995.510	1170.911	81.360	175204.537	1.686	12.303	1.800	1.903	288.925	4263.225	18.525	4.066
10140	8338.048	1395.128	192.251	95482.216	2.523	7.775	4.675	5.173	510.351	6163.799	13.999	4.440
10210	46356.641	505.632	39.249	129084.298	0.566	3.990	1.853	4.792	223.594	2363.044	18.672	2.033
10270	37341.094	170.993	20.626	84812.948	0.317	1.609	1.828	1.580	108.782	1290.947	7.104	1.266
10290	52492.018	367.881	24.994	127245.144	0.599	2.655	1.712	4.698	200.093	2893.920	24.295	2.593
10320	55554.351	265.701	21.976	119140.907	0.392	1.729	1.822	2.129	243.979	3558.247	16.016	3.228
10340	75073.364	92.741	7.374	169660.293	0.167	0.770	0.623	3.163	301.042	1733.049	20.639	1.720
10370	76190.424	410.739	18.829	205478.658	1.281	1.437	2.232	6.498	311.428	3233.566	27.826	2.861

Table 3. Continue/ Gidgealpa 7 data set of major and trace elements.

Depth (feet)	Cu_ppm	Zn_ppm	Rb_ppm	Sr_ppm	Y_ppm	Zr_ppm	Cd_ppm	Cs_ppm	Ba_ppm	Pb_ppm	Th_ppm	U_ppm
7660	5.564	<54.872	16.501	569.782	38.103	0.422	0.489	1.325	369.692	7.863	2.541	1.233
7680	0.243	<9.250	1.285	577.947	7.253	0.089	<0.062	0.085	61.529	0.395	0.059	0.923
7701	1.587	<25.460	11.282	1115.718	40.360	0.166	0.530	1.176	273.125	14.773	4.347	0.944
7720	1.122	<38.303	3.936	141.331	4.897	<0.161	1.065	0.259	46.218	2.441	0.305	0.168
7750	1.892	<28.449	4.290	771.216	15.852	0.182	<0.190	0.361	81.993	3.596	1.559	0.361

7800	1.551	<20.806	2.340	230.417	4.806	0.325	<0.139	0.151	27.238	1.407	0.341	0.154
7820	3.765	<29.785	4.336	890.429	19.593	0.150	0.264	0.480	75.524	11.058	1.813	0.387
7850	1.154	<35.821	4.385	195.111	5.372	<0.151	0.592	0.522	26.336	2.707	0.263	0.095
7910	4.413	<38.570	5.956	477.186	20.032	<0.162	<0.258	0.857	82.488	5.736	1.888	0.434
7940	0.562	<8.699	1.189	862.889	12.665	0.043	0.330	0.103	39.098	2.133	0.687	0.313
7960	0.528	<10.503	1.779	536.568	13.092	<0.044	<0.070	0.082	39.019	1.441	0.798	0.623
7980	0.543	<15.602	0.949	153.510	3.451	0.068	<0.104	<0.096	11.063	0.813	0.369	0.139
8010	0.279	<18.627	0.941	351.995	4.984	0.104	<0.125	<0.115	19.526	0.807	0.547	0.155
8040	1.207	<29.561	2.382	746.363	10.999	<0.125	<0.198	0.196	37.606	1.992	1.052	0.343
8072	0.661	<26.633	1.676	390.887	6.404	<0.112	<0.178	<0.164	14.731	0.590	0.640	0.214
8090	0.625	<21.779	1.697	395.534	8.819	0.105	<0.146	0.166	26.948	0.999	0.706	0.332
8120	1.263	<24.609	1.827	964.885	16.157	0.112	<0.165	0.238	44.629	1.882	1.268	0.474
8180	0.336	<18.164	0.722	109.629	1.963	0.081	<0.122	<0.112	7.007	0.709	0.164	0.039
8230	0.564	<14.878	1.342	1039.825	18.586	<0.063	<0.100	0.181	44.675	1.401	0.992	0.571
8250	0.229	<25.387	0.893	279.293	6.108	<0.107	<0.170	<0.156	22.075	1.195	0.418	0.165
8280	0.261	4.283	0.602	149.981	3.934	0.025	<0.019	0.086	11.055	1.004	0.371	0.125
8310	0.899	21.036	3.428	379.401	14.863	0.076	1.065	0.649	45.386	3.733	1.091	0.325
8340	1.466	19.803	3.623	340.458	12.037	<0.088	0.852	0.767	35.558	2.742	0.988	0.226
8370	0.945	93.532	2.404	289.663	8.595	0.091	0.336	0.336	26.475	1.707	0.823	0.324
8400	1.285	27.747	3.037	511.678	17.059	<0.052	0.309	0.497	40.087	3.636	1.011	0.289
8430	3.623	550.350	3.066	370.380	9.361	0.164	0.357	0.414	49.882	13.774	0.618	0.313
8460	1.253	12.883	2.633	465.215	21.273	0.057	0.031	0.295	38.449	3.766	0.920	0.524
8500	1.232	11.872	1.983	372.159	11.275	0.067	0.067	0.262	28.247	1.707	0.970	0.509
8520	6.020	43.023	10.100	244.052	9.627	0.245	0.651	2.179	56.849	5.057	1.539	0.410
8550	0.670	17.509	1.558	303.532	10.719	0.058	0.415	0.275	25.874	1.718	0.576	0.453
8580	0.669	21.907	1.970	315.169	9.281	0.072	0.087	0.322	27.229	2.002	0.901	0.278
8610	0.746	9.695	0.644	253.789	8.871	0.022	0.041	0.102	16.954	1.446	0.339	0.416
8640	0.171	6.519	0.154	249.265	2.890	0.028	0.037	0.043	13.221	2.719	0.087	0.297
8670	1.849	301.665	5.860	342.615	9.484	0.085	0.214	0.612	30.905	4.058	0.777	0.371
8760	6.568	62.567	9.063	119.978	4.815	0.203	<0.094	2.201	50.793	2.151	1.001	0.237

8793	0.138	5.947	0.088	128.586	1.275	<0.049	<0.040	0.024	6.212	0.983	0.115	0.229
8820	2.293	42.437	8.793	154.142	2.865	0.072	0.646	0.902	25.903	1.904	0.363	0.245
8850	0.375	7.391	0.233	146.956	1.143	<0.053	0.696	0.060	6.382	1.290	0.119	0.214
8880	0.296	28.520	0.191	245.916	2.252	0.033	<0.026	0.066	15.210	1.676	0.144	0.325
8900	0.214	5.513	0.095	106.400	0.630	<0.049	0.225	<0.009	8.897	0.329	<0.040	0.177
8930	0.188	9.791	0.057	177.987	1.413	0.028	0.024	0.010	5.969	0.398	0.032	0.260
8970	0.335	9.548	0.289	155.407	1.183	<0.037	<0.030	0.033	9.407	0.594	0.099	0.588
9000	0.436	8.373	0.147	154.374	1.024	0.054	<0.028	0.028	9.166	0.768	0.092	0.578
9030	0.383	9.560	0.114	167.135	1.908	0.033	0.017	0.027	9.693	0.759	0.067	0.377
9059	0.203	5.407	0.133	122.929	2.146	0.175	0.050	0.074	7.610	10.174	0.184	0.347
9074	1.826	116.326	18.494	219.101	5.223	<0.338	0.385	9.848	182.120	5.510	0.719	0.282
9080	0.127	27.357	0.096	158.567	2.297	0.117	0.034	0.023	11.914	0.094	0.016	0.374
9100	0.318	14.142	0.094	133.729	2.645	0.152	0.035	0.053	13.210	0.500	0.080	0.432
9120	0.468	22.012	0.530	162.890	2.858	0.192	0.107	0.235	14.001	2.253	0.205	0.541
9150	0.578	28.774	0.865	123.750	2.415	0.135	0.108	0.199	18.610	1.363	0.239	0.280
9250	0.451	49.795	0.262	205.224	1.864	0.318	0.025	0.054	19.423	0.789	0.109	0.706
9270	0.287	64.194	0.313	109.807	1.625	<0.040	1.404	0.109	12.890	1.522	0.112	0.229
9290	0.921	41.782	1.222	229.428	2.707	0.192	0.122	0.300	22.465	2.673	0.291	0.693
9310	1.060	31.436	0.716	276.757	2.959	0.125	0.457	0.240	26.940	2.268	0.219	0.831
9330	0.486	27.995	1.176	204.447	2.236	0.105	0.131	0.218	21.833	2.129	0.195	0.574
9350	0.432	24.043	0.833	135.209	1.321	<0.041	0.145	0.258	20.771	2.102	0.085	0.353
9380	0.265	26.557	0.295	199.351	1.333	<0.034	0.527	0.072	8.601	0.680	0.126	0.581
9410	0.587	12.455	0.502	219.192	1.548	0.036	0.066	0.080	9.723	1.130	0.197	0.846
9430	0.386	14.555	0.180	169.648	1.607	0.029	0.102	0.027	9.039	6.090	0.080	0.690
9450	1.671	19.623	1.957	160.260	3.589	0.069	0.092	0.278	14.964	2.910	0.556	0.704
9530	2.021	84.440	5.357	54.671	3.133	<0.054	0.409	0.891	13.925	1.302	0.554	0.161
9560	1.351	30.157	1.377	124.094	5.976	<0.019	0.294	0.147	17.149	3.571	0.310	0.334
9580	9.427	450.703	2.847	292.333	13.879	<0.050	0.126	0.547	38.724	9.712	0.725	0.677
9610	3.204	82.002	6.533	147.866	3.637	0.095	1.078	1.042	21.068	3.406	0.729	0.354
9630	0.883	31.295	0.639	218.248	5.785	<0.028	<0.037	0.159	26.033	2.335	0.287	0.851

9650	2.546	88.081	4.394	150.255	8.868	0.179	0.854	0.764	33.163	4.511	0.929	0.430
9750	5.498	971.933	3.240	140.615	4.147	<0.055	0.145	0.636	17.310	8.055	0.444	0.299
9760	5.187	194.470	6.140	129.389	7.016	0.134	1.056	1.280	23.881	4.380	1.010	0.320
9780	3.043	65.354	3.634	226.652	7.324	0.056	<0.068	0.719	22.507	3.902	0.979	0.551
9800	2.765	93.960	3.693	169.239	7.511	0.103	0.611	0.691	18.059	4.315	0.790	0.374
9831	2.819	18.685	1.771	91.722	4.951	0.077	0.036	0.223	12.961	2.173	0.422	0.234
9850	3.421	37.371	4.970	163.169	9.463	0.076	0.593	0.784	18.641	4.227	0.865	0.364
9870	0.837	21.182	1.727	50.308	2.456	<0.025	0.140	0.277	7.639	1.327	0.276	0.118
9900	1.633	9.521	1.588	316.029	10.165	0.046	<0.018	0.092	21.116	2.412	0.676	0.514
9920	18.065	124.203	11.149	405.044	22.384	0.100	0.280	1.576	72.067	8.119	1.443	0.781
9950	1.360	7.597	1.112	35.113	2.027	0.025	0.054	0.117	5.659	0.954	0.403	0.166
9970	0.441	5.908	0.593	250.033	5.488	0.060	<0.013	0.074	20.347	0.900	0.104	0.803
10100	1.503	37.880	1.836	86.031	1.418	0.085	0.546	0.465	17.270	10.310	0.339	0.350
10110	1.893	55.702	4.157	235.924	12.392	0.102	0.626	0.788	26.075	5.296	1.478	2.344
10120	1.152	38.298	5.450	192.128	7.454	0.231	0.168	1.042	35.034	7.313	1.565	0.824
10140	2.892	41.536	6.573	163.542	12.231	0.091	0.134	0.985	30.325	5.402	1.392	0.518
10210	1.089	34.626	2.124	111.331	1.601	0.070	0.269	0.287	19.996	18.825	0.321	0.449
10270	1.220	16.844	0.562	51.256	0.848	<0.025	0.092	0.086	7.036	8.939	0.187	0.219
10290	0.818	44.647	1.584	88.145	1.583	<0.066	0.564	0.324	13.008	26.793	0.307	0.252
10320	0.842	74.097	0.935	84.993	1.040	<0.059	0.589	0.118	12.181	23.045	0.205	0.293
10340	0.908	40.377	0.231	91.270	0.609	<0.026	0.093	0.036	5.841	25.518	0.117	0.145
10370	1.776	43.697	1.810	158.026	3.873	0.034	0.068	0.254	26.820	10.964	0.395	0.405

Table 4. Gidgealpa 7 REE data set.

Depth (feet)	La_ppm	Ce_ppm	Pr_ppm	Nd_ppm	Sm_ppm	Eu_ppm	Gd_ppm	Tb_ppm	Dy_ppm	Ho_ppm	Er_ppm	Tm_ppm	Yb_ppm	Lu_ppm
7660	16.094	38.758	5.121	21.403	5.859	1.110	6.636	1.059	6.450	1.259	3.469	0.466	2.722	0.449
7680	5.852	11.681	1.338	5.239	1.030	0.205	1.032	0.156	0.983	0.207	0.612	0.085	0.482	0.084
7701	22.172	51.926	6.855	27.495	6.418	1.255	6.298	1.005	6.441	1.290	3.634	0.514	2.669	0.444

Chemostratigraphy and geochronology of Cambrian sequences in East Warburton Basin, South Australia

7720	2.595	6.515	0.924	3.882	1.057	0.194	0.938	0.134	0.807	0.166	0.401	0.046	0.288	0.039
7750	11.839	24.598	3.005	11.551	2.635	0.444	2.546	0.391	2.472	0.501	1.412	0.196	0.981	0.175
7800	3.509	7.646	0.958	3.699	0.955	0.146	0.824	0.127	0.756	0.154	0.397	0.053	0.335	0.046
7820	11.599	24.793	3.249	13.342	3.799	0.727	3.690	0.561	3.288	0.645	1.757	0.241	1.409	0.219
7850	1.826	4.355	0.610	2.832	1.046	0.207	1.212	0.159	0.951	0.180	0.481	0.063	0.350	0.053
7910	5.716	14.537	2.069	9.758	3.656	0.808	3.972	0.578	3.443	0.670	1.865	0.258	1.419	0.230
7940	5.974	15.664	2.111	8.944	2.330	0.445	2.247	0.342	2.099	0.418	1.171	0.161	0.895	0.146
7960	8.039	17.032	2.097	8.129	1.849	0.331	1.931	0.322	2.065	0.440	1.255	0.173	0.971	0.154
7980	2.232	4.791	0.590	2.323	0.512	0.086	0.542	0.082	0.532	0.109	0.298	0.041	0.200	0.034
8010	3.731	7.785	0.954	3.581	0.716	0.126	0.737	0.115	0.713	0.151	0.443	0.059	0.411	0.050
8040	9.139	18.826	2.320	8.565	1.789	0.316	1.687	0.268	1.671	0.337	0.994	0.131	0.800	0.112
8072	5.448	10.745	1.309	4.885	0.993	0.193	0.956	0.145	0.956	0.197	0.547	0.075	0.400	0.065
8090	6.697	13.697	1.675	6.215	1.299	0.265	1.307	0.195	1.304	0.267	0.757	0.107	0.644	0.087
8120	12.025	25.135	2.931	11.100	2.364	0.380	2.197	0.364	2.372	0.506	1.414	0.210	0.933	0.176
8180	1.381	2.986	0.379	1.426	0.321	0.072	0.324	0.049	0.313	0.056	0.172	0.020	0.078	0.016
8230	14.171	28.844	3.371	12.658	2.589	0.511	2.445	0.411	2.695	0.563	1.606	0.214	1.118	0.193
8250	4.635	10.789	1.330	5.074	1.038	0.192	0.870	0.153	0.919	0.191	0.507	0.073	0.427	0.065
8280	3.339	7.731	0.955	3.578	0.669	0.132	0.602	0.095	0.615	0.120	0.334	0.046	0.329	0.045
8310	9.038	19.090	2.356	9.015	2.051	0.418	1.980	0.340	2.205	0.453	1.289	0.197	1.293	0.188
8340	7.134	15.309	1.836	7.335	1.882	0.340	1.791	0.290	1.843	0.385	1.112	0.156	0.978	0.133
8370	7.285	14.534	1.716	6.586	1.367	0.305	1.225	0.188	1.208	0.250	0.731	0.096	0.654	0.093
8400	10.785	21.658	2.557	9.640	2.120	0.433	2.020	0.339	2.349	0.487	1.468	0.207	1.310	0.194
8430	6.593	13.819	1.669	6.684	1.629	0.310	1.412	0.224	1.383	0.282	0.819	0.113	0.771	0.103
8460	16.937	31.572	3.602	13.394	2.887	0.577	2.732	0.470	3.066	0.625	1.892	0.266	1.674	0.243
8500	9.961	19.492	2.261	7.880	1.707	0.334	1.442	0.233	1.537	0.330	1.006	0.138	0.887	0.129
8520	3.962	8.977	1.202	5.807	2.257	0.443	2.152	0.291	1.686	0.311	0.812	0.104	0.654	0.095
8550	8.787	17.042	1.956	7.267	1.459	0.344	1.472	0.236	1.630	0.328	0.986	0.146	0.877	0.130
8580	8.062	15.909	1.788	6.598	1.374	0.283	1.200	0.183	1.243	0.257	0.751	0.106	0.653	0.095
8610	6.881	13.701	1.532	5.415	1.110	0.238	1.040	0.182	1.189	0.248	0.740	0.107	0.692	0.099
8640	2.894	5.506	0.585	2.178	0.412	0.082	0.360	0.057	0.362	0.077	0.230	0.031	0.210	0.028

Chemostratigraphy and geochronology of Cambrian sequences in East Warburton Basin, South Australia

8670	7.078	14.041	1.661	6.328	1.375	0.290	1.361	0.216	1.342	0.281	0.818	0.116	0.770	0.103
8760	1.177	3.050	0.459	2.172	1.088	0.232	1.224	0.168	0.922	0.159	0.397	0.055	0.327	0.048
8793	0.758	1.485	0.177	0.651	0.118	0.032	0.142	0.019	0.139	0.026	0.067	0.012	0.059	0.009
8820	1.555	3.299	0.426	1.956	0.530	0.117	0.566	0.075	0.446	0.090	0.237	0.030	0.177	0.026
8850	0.687	1.265	0.161	0.715	0.144	0.020	0.165	0.019	0.120	0.027	0.081	0.010	0.063	<0.010
8880	1.220	2.176	0.282	1.148	0.252	0.053	0.251	0.040	0.225	0.050	0.142	0.020	0.128	0.018
8900	0.285	0.493	0.069	0.258	0.045	0.014	0.065	0.006	0.060	<0.012	0.040	<0.006	0.037	<0.009
8930	1.141	2.101	0.272	0.977	0.202	0.037	0.172	0.028	0.163	0.034	0.098	0.013	0.086	0.011
8970	0.806	1.457	0.187	0.699	0.131	0.035	0.134	0.018	0.139	0.028	0.081	0.010	0.076	0.008
9000	0.555	1.024	0.130	0.532	0.112	0.030	0.120	0.016	0.113	0.022	0.063	0.008	0.056	0.007
9030	1.061	1.954	0.258	0.995	0.227	0.041	0.213	0.032	0.204	0.042	0.128	0.017	0.106	0.016
9059	1.113	1.618	0.271	1.105	0.219	0.043	0.223	0.032	0.216	0.045	0.126	0.017	0.113	0.015
9074	1.158	3.428	0.524	2.513	0.954	0.281	1.460	0.190	1.003	0.182	0.465	0.047	0.307	<0.063
9080	1.197	1.922	0.275	1.108	0.247	0.049	0.226	0.035	0.238	0.049	0.144	0.019	0.121	0.017
9100	1.251	2.029	0.297	1.183	0.258	0.054	0.268	0.040	0.247	0.055	0.167	0.022	0.129	0.020
9120	1.710	2.787	0.394	1.597	0.320	0.067	0.311	0.043	0.308	0.064	0.190	0.023	0.163	0.020
9150	1.193	2.342	0.325	1.389	0.354	0.076	0.345	0.056	0.304	0.064	0.182	0.023	0.125	0.019
9250	1.040	1.988	0.252	1.010	0.222	0.044	0.241	0.038	0.245	0.054	0.153	0.019	0.110	0.016
9270	0.993	1.385	0.217	0.876	0.175	0.045	0.186	0.026	0.172	0.042	0.126	0.019	0.109	0.011
9290	1.482	2.680	0.361	1.499	0.327	0.076	0.379	0.057	0.354	0.075	0.203	0.025	0.159	0.021
9310	1.480	3.649	0.371	1.504	0.368	0.072	0.411	0.059	0.350	0.081	0.236	0.034	0.182	0.025
9330	1.080	2.081	0.303	1.127	0.276	0.063	0.317	0.048	0.249	0.055	0.161	0.024	0.124	0.018
9350	0.633	1.202	0.154	0.608	0.165	0.037	0.192	0.027	0.145	0.031	0.094	0.009	0.062	0.011
9380	0.738	1.381	0.176	0.741	0.129	0.035	0.176	0.024	0.133	0.030	0.086	0.013	0.072	0.011
9410	1.010	1.881	0.238	0.976	0.220	0.042	0.196	0.029	0.188	0.038	0.103	0.014	0.083	0.012
9430	0.916	1.592	0.222	0.843	0.188	0.039	0.292	0.029	0.184	0.036	0.115	0.014	0.089	0.012
9450	1.484	3.044	0.441	2.082	0.601	0.145	0.633	0.091	0.527	0.105	0.260	0.035	0.180	0.030
9530	0.800	2.233	0.357	1.963	0.841	0.163	0.840	0.109	0.601	0.109	0.262	0.031	0.169	0.032
9560	2.208	5.273	0.764	3.513	0.963	0.229	0.984	0.157	0.936	0.181	0.509	0.073	0.468	0.066
9580	4.178	10.111	1.424	6.989	2.040	0.469	2.144	0.357	2.143	0.436	1.204	0.178	1.147	0.168

9610	1.573	3.763	0.537	2.719	0.825	0.161	0.822	0.110	0.573	0.105	0.264	0.035	0.254	0.029
9630	2.966	6.579	0.881	3.778	0.851	0.215	0.936	0.148	0.918	0.186	0.470	0.064	0.490	0.060
9650	2.742	22.318	1.139	5.704	1.869	0.377	1.707	0.266	1.509	0.281	0.757	0.107	0.654	0.094
9750	1.544	3.699	0.509	2.303	0.633	0.155	0.801	0.109	0.645	0.129	0.317	0.042	0.273	0.039
9760	1.943	5.300	0.860	4.013	1.280	0.287	1.309	0.194	1.058	0.207	0.505	0.072	0.388	0.068
9780	3.505	8.287	1.218	4.952	1.234	0.260	1.214	0.175	1.089	0.205	0.560	0.080	0.475	0.071
9800	2.956	7.113	1.016	4.365	1.223	0.274	1.245	0.192	1.158	0.240	0.687	0.091	0.534	0.088
9831	1.860	4.431	0.621	3.028	0.846	0.198	0.905	0.147	0.811	0.164	0.458	0.057	0.362	0.054
9850	2.951	7.822	1.121	5.196	1.531	0.338	1.674	0.262	1.504	0.288	0.788	0.099	0.704	0.098
9870	0.787	1.971	0.400	1.458	0.471	0.106	0.483	0.071	0.431	0.078	0.216	0.026	0.174	0.024
9900	8.029	14.723	1.776	6.400	1.349	0.297	1.265	0.200	1.292	0.273	0.781	0.110	0.698	0.096
9920	5.998	14.880	2.256	11.603	3.944	0.983	4.461	0.646	3.639	0.722	1.843	0.250	1.515	0.216
9950	1.324	3.214	0.472	2.073	0.449	0.090	0.400	0.057	0.320	0.064	0.164	0.020	0.110	0.015
9970	3.568	7.691	1.015	3.981	0.809	0.187	0.752	0.113	0.733	0.152	0.430	0.059	0.386	0.053
10100	1.161	2.380	0.309	1.200	0.277	0.041	0.247	0.035	0.193	0.038	0.113	0.015	0.086	0.015
10110	10.181	17.763	2.293	8.653	1.724	0.446	1.773	0.270	1.739	0.369	0.979	0.135	0.843	0.141
10120	6.803	14.162	1.498	5.324	1.134	0.233	1.115	0.165	1.028	0.217	0.616	0.094	0.608	0.099
10140	9.650	18.566	2.400	8.667	2.041	0.418	1.948	0.296	1.832	0.358	1.000	0.144	0.941	0.118
10210	3.376	2.811	0.379	1.486	0.365	0.074	0.307	0.048	0.276	0.049	0.135	0.019	0.089	0.014
10270	0.697	1.621	0.203	0.756	0.174	0.028	0.140	0.023	0.142	0.023	0.076	0.009	0.063	0.008
10290	1.330	3.238	0.443	1.700	0.326	0.049	0.305	0.042	0.263	0.049	0.127	0.016	0.103	0.016
10320	1.061	2.111	0.254	1.052	0.225	0.045	0.193	0.037	0.178	0.045	0.082	0.024	0.068	0.017
10340	0.589	1.100	0.138	0.514	0.113	0.021	0.111	0.017	0.103	0.020	0.051	0.008	0.033	0.006
10370	2.591	6.579	0.851	3.427	0.764	0.137	0.705	0.112	0.602	0.123	0.338	0.049	0.253	0.038

Table 5. Kalladeina 1 data set of major and trace elements.

Depth (feet)	Mg_ppm	Al_ppm	P_ppm	Ca_ppm	Sc_ppm	Ti_ppm	V_ppm	Cr_ppm	Mn_ppm	Fe_ppm	Co_ppm	Ni_ppm
7150	2697.994	1458.369	493.064	141126.875	2.006	14.957	2.363	19.930	1406.249	26420.515	290.015	19.422

7180	1643.293	242.385	109.804	208925.783	1.161	3.120	0.517	4.308	1042.140	5795.674	54.619	4.107
7200	932.757	69.630	57.736	42228.000	0.190	0.402	0.176	0.587	266.456	1079.994	8.286	0.558
7300	2540.405	1501.770	408.993	89730.973	2.499	11.061	1.794	2.861	909.743	2983.620	129.444	4.675
7330	1724.056	532.945	107.925	134262.403	1.620	0.633	0.878	38.917	1150.839	21790.185	165.291	32.496
7360	1532.212	44.020	18.765	386667.250	0.858	0.529	0.296	0.513	1313.382	500.209	17.109	1.204
7390	3915.671	199.701	12.208	281675.688	0.892	2.072	0.194	11.695	663.693	6724.524	31.610	18.840
7420	5525.022	81.931	16.137	165016.909	0.370	<0.453	0.161	<0.797	389.147	1408.821	10.603	0.812
7450	2893.786	365.150	279.051	247131.194	2.034	10.170	0.757	2.228	1569.312	1803.266	47.158	1.851
7480	2088.211	608.306	199.927	105501.207	0.746	4.058	0.478	2.100	728.066	1383.175	77.319	9.568
7500	3373.476	3107.700	484.970	208009.519	10.139	7.882	2.389	306.975	2604.535	7111.088	272.821	18.641
7900	2116.512	3242.651	488.461	144529.739	3.807	30.263	3.482	6.894	3012.009	4301.278	95.618	6.016
7930	2305.504	3510.938	453.939	23898.843	2.742	30.205	4.323	<8.088	662.156	4282.875	158.165	6.926
7950	2144.444	3399.146	456.672	17604.870	2.169	33.775	4.815	5.873	529.281	4220.984	93.719	6.393
7970	1803.841	3034.852	409.327	28667.222	2.425	31.411	4.269	10.370	812.558	4215.315	166.518	7.625
7990	2313.711	3242.921	378.332	20460.090	2.640	34.095	4.284	<6.338	464.786	3808.355	102.459	6.413
8190	1661.810	1228.746	377.134	118383.828	1.413	11.838	1.336	2.882	2080.675	1873.631	23.173	2.185
8160	1484.611	1432.732	153.605	7232.555	1.243	14.838	1.346	3.749	314.141	1631.354	13.650	3.696
8220	1627.043	2184.373	241.800	33171.534	2.630	9.419	2.048	6.660	1272.494	2510.767	91.596	3.994
8250	1149.537	1423.002	88.516	13006.759	1.597	5.856	1.151	4.539	672.786	1706.674	47.208	2.990
8280	1496.465	1686.508	169.803	30212.707	2.076	12.495	1.681	5.108	1397.089	2096.502	62.984	3.789
8310	805.234	1096.713	149.716	14861.466	1.039	3.952	0.794	4.212	415.332	1772.187	20.213	2.862
8340	1562.973	1394.096	147.201	40612.031	1.343	15.277	1.085	3.870	858.704	1831.707	25.012	2.747
8370	1666.360	1327.053	88.084	74746.803	1.436	13.101	1.255	2.108	1407.951	1708.751	13.281	3.012
8400	3744.076	983.536	130.129	143048.532	1.998	5.397	1.121	3.111	1281.353	2490.930	23.133	2.409
8430	4190.839	1320.892	133.001	74527.452	2.821	12.514	1.794	3.601	480.543	2916.679	30.028	2.321
8460	2985.330	349.117	28.448	199123.677	0.909	3.808	0.480	1.714	569.195	2127.804	12.360	0.976
8488	2403.733	1512.881	52.345	11067.882	1.716	10.159	1.487	3.644	288.427	1894.974	28.837	2.797
8520	3889.484	943.765	35.070	115535.282	1.422	5.052	0.468	5.316	632.853	2342.698	17.782	2.209
8550	1943.169	1099.129	87.103	68356.817	2.408	11.758	1.155	2.010	573.227	1896.621	10.358	1.534
8580	3897.380	1060.136	122.803	173344.006	5.738	5.491	1.079	3.734	1304.729	3542.637	39.714	1.951

Chemostratigraphy and geochronology of Cambrian sequences in East Warburton Basin, South Australia

8600	2787.988	1957.695	155.166	88430.637	3.597	11.041	2.309	3.768	1463.233	3101.936	32.249	3.661
9150	5265.514	818.864	45.855	170705.736	2.892	4.919	0.938	1.467	495.651	2378.169	8.069	1.816
9180	1485.353	473.204	63.752	21685.037	0.828	3.348	0.593	0.751	116.508	1031.833	3.939	0.870
9210	2803.305	599.642	23.684	148238.829	2.464	1.467	0.491	1.371	466.341	2171.709	7.928	1.147
9240	3809.580	782.923	52.987	213561.371	3.291	3.187	0.918	1.957	525.082	2701.245	11.066	1.259
9270	2692.360	545.147	38.990	207331.149	2.732	2.078	0.556	1.487	422.127	1868.290	10.525	0.805
9300	3204.949	536.274	42.800	213751.226	3.253	1.338	0.568	1.528	523.504	2338.408	10.412	0.842
9330	3472.425	476.923	30.761	179575.590	3.045	4.434	0.603	1.255	388.922	2813.075	7.046	0.848
9360	3096.187	1085.165	122.063	188488.962	2.919	7.779	1.457	2.251	395.721	3444.447	8.262	1.685
9390	3285.810	647.981	43.844	217799.517	3.959	2.855	0.706	1.402	546.499	3029.397	10.347	1.077
9420	3174.021	452.165	18.076	267725.280	4.168	3.114	0.411	1.646	619.394	1823.462	14.707	0.635
9450	2840.110	130.263	9.493	322833.488	1.955	2.091	0.256	0.907	611.219	987.835	19.110	0.688
9480	2723.172	271.381	53.617	186161.385	1.606	1.717	0.409	1.219	252.752	1339.633	5.633	0.524
9510	2160.850	1458.927	20.398	46142.111	1.039	5.048	0.588	3.322	167.854	1889.456	8.700	2.887
9540	2833.117	513.633	73.561	143867.766	1.905	2.743	0.646	1.182	392.147	2081.647	6.856	1.105
9570	2399.026	477.761	63.002	67424.555	1.257	3.055	0.682	1.103	235.142	1853.014	4.633	1.039
9600	3786.052	641.508	14.954	139021.592	2.837	3.714	0.523	2.271	549.342	4166.169	6.535	1.748
9630	2287.353	302.033	35.282	18874.251	1.196	2.860	0.760	0.724	69.400	2077.779	2.890	0.621
9660	2793.802	222.977	38.064	167401.759	1.116	2.554	0.611	0.892	205.327	1580.594	3.532	0.461
9690	2422.913	110.787	10.649	200834.103	0.926	2.983	0.449	0.809	173.527	925.560	2.813	0.308
9720	4443.149	156.680	37.476	253491.888	0.796	2.621	0.693	0.861	257.950	1558.317	5.265	0.488
9750	2852.631	395.791	107.232	63250.305	1.115	2.070	0.771	0.885	154.223	1695.678	8.402	1.299
9780	3769.778	324.424	39.839	342139.241	2.389	5.660	0.591	1.235	730.972	2374.827	14.251	0.906
9810	5334.910	470.978	94.971	257843.368	1.307	13.797	1.291	1.452	306.769	2295.069	7.701	1.186
9840	5084.826	409.102	83.785	284428.761	3.147	4.448	0.761	1.404	1064.893	3013.472	13.119	1.196
9870	5432.966	679.158	115.778	225084.019	2.209	12.532	1.568	2.200	415.789	2979.107	12.659	2.400
9900	6162.867	228.065	112.460	250588.590	1.037	3.688	0.992	1.186	182.966	1614.332	6.709	0.952
9930	5495.534	145.094	46.014	168301.235	0.545	0.972	0.487	0.987	266.720	1025.175	3.406	0.366
9960	6827.788	68.305	41.249	78793.264	0.367	0.693	0.464	0.374	697.349	925.921	1.898	0.198
9990	5433.361	149.872	132.083	206155.685	1.066	1.880	0.829	1.028	761.818	2124.678	6.592	1.440

Chemostratigraphy and geochronology of Cambrian sequences in East Warburton Basin, South Australia

10020	8324.113	267.238	61.593	129909.896	1.046	1.609	0.797	1.173	988.992	3675.033	6.500	1.296
10050	4875.238	1300.052	150.386	31661.664	2.817	7.865	1.643	5.067	774.440	5951.742	11.269	3.892
10170	4031.718	3045.815	210.707	43658.095	2.955	23.637	3.680	67.296	846.437	5802.087	15.387	5.046
10190	2524.256	1944.789	124.880	19161.485	1.991	8.023	1.892	3.867	507.688	4102.349	11.235	3.668
10220	2095.676	332.664	76.045	24842.802	0.423	1.169	0.601	0.477	200.045	1858.625	2.051	0.483
10250	5306.747	3250.031	229.165	69594.224	4.524	31.801	3.976	4.423	962.977	7790.884	17.958	5.215
10280	6390.442	4279.386	245.290	97215.630	6.667	31.352	5.199	5.927	1492.580	11472.216	19.912	6.690
10310	5534.086	1468.512	183.201	124172.384	4.395	6.885	2.957	4.339	819.334	7340.804	20.988	6.267
10340	5972.799	169.580	102.932	216127.936	0.429	1.714	0.991	0.600	228.829	758.118	6.295	0.694
10400	995.343	99.833	24.292	16388.496	0.462	0.307	0.272	0.200	72.610	919.501	6.295	0.609
10430	5646.107	1578.716	160.075	94394.604	2.487	7.370	2.423	2.476	490.514	6669.648	16.773	3.518
10460	4629.954	2744.477	131.978	26099.410	2.751	5.868	2.671	4.698	493.888	7973.712	22.089	6.575
10490	5615.192	1044.896	106.047	25251.474	3.078	2.588	1.957	2.623	783.052	11103.326	13.163	4.309
10520	10087.365	5356.543	71.962	152612.523	7.818	11.611	4.295	14.537	1338.673	22003.353	34.769	14.540
10550	3919.708	1620.886	130.034	26689.918	3.149	12.269	1.878	2.510	354.176	7382.185	23.220	6.053
10580	6843.661	1841.205	161.003	41829.178	5.477	5.926	2.780	3.562	640.135	13742.933	36.404	7.182
10610	8257.352	2082.568	198.939	59974.614	7.468	6.585	3.410	3.643	818.860	15351.868	54.400	11.662
10640	8666.088	1580.648	203.715	90500.947	3.932	12.365	2.426	3.692	624.138	11610.771	53.702	8.502
10670	28367.448	1487.218	221.104	126752.594	1.673	5.476	3.322	3.697	717.445	7414.256	58.205	8.195
10700	38854.097	1024.274	112.334	102235.532	3.653	11.650	4.120	4.434	552.304	9904.244	37.288	6.714
10730	29465.449	1808.647	133.696	79723.938	4.750	6.618	4.641	3.889	730.329	17035.775	43.620	10.967
10760	21262.310	1981.044	218.251	59347.969	4.870	11.891	4.242	5.665	801.821	20994.327	89.378	13.830
10790	8750.042	3142.977	197.812	54609.508	2.754	8.241	4.377	5.910	398.239	10850.383	30.303	8.376
10820	13494.738	3279.347	140.450	64391.365	6.476	9.785	3.228	13.296	1178.751	16489.323	41.879	13.828
10850	6650.932	1215.966	48.981	86251.434	2.007	8.481	1.168	4.882	796.669	8097.753	18.442	6.920
10880	10108.733	1940.652	102.525	168124.472	3.151	6.266	2.527	4.426	998.236	10392.545	30.231	4.655
10910	8911.558	1727.075	149.072	103597.066	3.631	5.925	2.627	3.221	830.690	9839.276	21.115	5.836
10940	8063.008	172.818	28.909	239459.198	0.519	1.108	0.943	0.818	864.599	1951.665	9.454	0.609
10970	12591.040	119.851	25.835	67067.482	0.295	0.377	1.255	0.685	479.020	2436.411	1.988	0.219
11000	8789.002	146.429	67.876	157909.903	0.388	0.677	1.326	<0.617	529.966	1249.299	13.462	0.789

11020	13304.468	235.063	102.052	182563.473	0.529	0.928	2.005	<1.005	720.940	1960.849	32.771	2.032
11050	9909.371	162.092	95.772	177025.770	0.715	1.095	1.458	1.741	612.664	1530.483	10.109	1.070
11080	9528.330	321.030	82.523	274804.516	1.902	0.436	1.913	2.303	890.816	2921.774	12.547	2.226
11100	7875.890	72.767	25.164	215278.629	0.652	0.567	0.858	0.974	767.829	1466.437	6.399	0.808
11130	9271.764	1445.285	69.517	30876.990	3.264	3.165	2.827	4.030	658.715	12589.357	14.553	5.090
11160	8928.128	222.500	28.835	47889.976	1.094	0.749	1.344	1.862	778.721	7845.518	5.179	1.572
11180	6499.549	1354.170	121.480	110124.933	1.580	8.077	2.306	2.730	739.288	5128.496	21.681	3.371
11210	7385.774	1210.116	134.223	150569.189	2.582	2.822	2.487	2.283	991.904	6029.314	64.877	3.387
11240	4879.295	3756.259	196.702	49589.245	5.419	18.421	4.231	6.789	1264.315	9393.095	27.545	7.893
11270	4634.608	2452.996	124.830	118932.423	4.064	10.118	2.631	4.562	1460.583	6360.387	31.688	5.446
11300	6126.022	2268.390	193.777	95548.566	2.673	10.191	3.260	3.818	1063.034	5233.807	29.726	4.945
11330	5450.722	2141.071	142.738	83201.509	1.877	10.462	2.658	3.284	569.947	4027.432	12.215	4.040
11360	6951.771	2810.386	164.831	75143.439	3.551	22.548	3.888	5.120	1072.928	7030.132	29.126	5.594
11390	7862.911	3113.123	148.269	43983.760	6.504	18.097	3.952	5.440	1446.709	8889.268	41.549	7.301
11420	5504.678	1614.618	112.169	92514.672	2.212	10.932	2.463	2.699	1030.923	4056.130	22.217	3.814
11450	4661.679	1045.000	80.798	26734.844	1.389	3.191	1.464	2.274	518.756	3016.511	9.009	2.196
11750	1380.952	411.619	15.623	19263.155	0.795	1.151	0.817	0.573	932.603	3252.731	7.178	0.701
11780	2036.999	619.849	28.037	64845.288	1.022	2.512	1.353	0.825	1369.023	3319.627	21.104	1.180
11810	11011.268	918.160	32.778	103541.249	1.408	16.294	1.594	1.131	3332.956	9096.340	44.401	2.014
11840	10431.025	991.597	65.177	34359.655	2.903	1.413	2.660	7.463	1950.869	9336.612	22.415	3.260
11870	12642.678	2426.853	134.197	122806.262	7.359	2.158	3.083	10.888	2648.395	15605.893	206.133	5.254
11900	6317.970	1348.603	207.384	108893.356	3.568	2.253	2.221	5.396	1609.903	4559.054	82.671	3.782

Table 6. Continue/ Kalladeina 1 data set of major and trace elements.

Depth (feet)	Cu_ppm	Zn_ppm	Rb_ppm	Sr_ppm	Y_ppm	Zr_ppm	Cd_ppm	Cs_ppm	Ba_ppm	Pb_ppm	Th_ppm	U_ppm
7150	1.811	1825.233	11.035	257.175	21.422	<0.127	1.263	2.220	179.866	51.253	1.129	1.129
7180	0.522	49.106	2.177	196.189	10.677	<0.072	0.347	0.509	32.293	7.035	0.550	0.550
7200	0.195	10.713	0.407	46.815	2.522	<0.016	0.084	0.043	7.780	1.288	0.213	0.213

7300	1.663	197.183	12.538	113.974	19.219	0.121	1.130	1.542	35.996	9.293	1.486	0.326
7330	20.950	81.361	3.168	145.996	21.150	<0.045	0.138	0.128	39.697	22.834	0.359	0.191
7360	0.390	28.613	0.444	250.453	11.075	<0.018	0.033	0.078	8.822	3.582	0.519	0.407
7390	2.300	1755.065	3.022	342.822	7.953	<0.054	0.346	0.499	27.812	316.020	0.603	0.169
7420	0.202	64.329	0.714	176.257	2.808	<0.032	0.575	0.075	6.665	25.810	0.301	0.058
7450	0.853	82.227	1.305	203.087	24.342	0.177	0.441	0.179	18.810	45.831	1.067	0.326
7480	11.047	585.028	7.941	133.369	8.754	<0.080	1.838	1.093	66.324	67.608	0.406	0.226
7500	21.667	894.484	8.234	227.982	77.089	0.755	3.131	0.692	117.665	1597.582	2.748	1.078
7900	10.073	551.851	24.827	202.853	47.015	0.267	0.270	3.324	233.078	49.655	2.654	0.765
7930	14.485	1483.883	44.189	143.836	28.099	0.976	0.547	7.983	62.014	17.324	2.559	1.101
7950	22.063	43.516	24.811	76.242	24.305	0.231	0.492	4.466	121.505	4.706	1.630	0.731
7970	3.946	397.126	14.564	82.018	30.706	0.282	<0.290	1.755	303.143	11.858	1.667	0.621
7990	13.718	47.000	38.055	111.795	27.070	<0.256	0.491	6.501	65.716	5.022	2.059	0.770
8190	1.705	27.613	12.221	222.747	17.599	0.441	0.428	2.240	18.638	14.458	1.537	0.262
8160	7.994	102.082	30.903	126.078	12.195	<0.229	0.223	5.084	12.909	1.302	1.121	0.771
8220	5.777	123.939	18.990	122.123	25.195	<0.256	0.231	3.312	193.953	2.671	1.213	0.458
8250	4.603	150.300	12.468	65.247	8.936	<0.226	0.364	2.446	51.136	24.334	0.712	0.329
8280	5.970	1707.093	20.745	136.106	18.052	<0.245	0.546	4.204	57.420	179.581	1.011	0.280
8310	2.575	933.251	6.325	49.681	7.413	0.096	0.100	0.600	31.026	130.919	0.634	0.152
8340	2.662	225.064	19.387	169.792	8.932	0.207	0.294	2.107	78.034	19.827	1.260	0.212
8370	2.964	1831.302	15.188	256.243	10.029	0.154	0.150	2.450	20.641	38.750	0.977	0.274
8400	2.641	1293.327	8.965	432.384	11.969	0.165	0.427	1.313	28.675	121.619	1.168	0.169
8430	3.028	773.465	7.590	265.913	13.746	0.331	0.219	1.530	25.468	32.106	1.253	0.157
8460	1.775	239.243	2.382	632.018	5.556	0.104	0.188	0.355	44.030	34.851	0.575	0.090
8488	38.179	417.051	27.999	113.297	4.870	<0.251	<0.204	5.008	94.130	1.450	0.690	0.527
8520	7.114	862.038	8.015	329.213	6.929	0.082	0.337	0.906	78.083	371.026	0.684	0.242
8550	2.965	115.456	8.800	277.688	10.409	0.119	0.140	1.314	124.279	11.061	1.083	0.224
8580	3.918	275.765	5.663	548.556	27.615	0.072	0.178	1.003	254.041	88.162	1.138	0.225
8600	15.188	428.675	30.537	340.634	16.987	0.248	0.276	5.276	213.517	40.675	1.439	0.600
9150	4.538	124.047	3.359	611.470	10.090	0.457	0.103	0.434	143.257	30.656	0.907	0.498

9180	1.439	64.542	2.364	110.479	2.585	<0.038	<0.031	0.225	38.057	2.969	0.463	0.071
9210	1.778	79.716	2.787	407.976	10.157	<0.027	0.036	0.255	75.148	7.093	0.789	0.174
9240	1.220	108.573	4.958	448.762	13.647	0.127	0.443	0.709	54.215	13.396	1.340	0.206
9270	0.773	81.185	3.884	402.617	11.312	0.066	0.466	0.428	66.654	14.956	0.997	0.151
9300	0.786	275.406	2.918	421.896	13.299	<0.037	0.091	0.357	30.316	11.340	1.001	0.209
9330	0.845	55.574	2.593	286.953	11.092	0.070	0.198	0.274	31.107	6.562	0.960	0.960
9360	1.034	92.323	3.172	291.514	10.955	0.164	0.943	0.250	27.824	8.681	1.621	1.621
9390	3.500	321.138	4.476	378.223	13.083	0.150	0.871	0.671	40.869	10.264	1.098	1.098
9420	2.561	31.604	2.954	460.801	17.135	0.098	0.537	0.380	93.581	9.087	1.086	1.086
9450	0.413	5.972	2.686	492.377	15.338	0.064	0.114	0.248	60.671	2.716	0.191	0.191
9480	0.502	96.235	1.275	283.936	7.245	0.059	0.079	0.131	17.828	4.358	0.887	0.887
9510	3.095	104.574	8.555	108.548	2.591	0.082	0.229	0.395	29.964	29.422	0.554	0.554
9540	1.430	45.322	2.719	311.914	8.123	0.065	0.070	0.375	25.688	10.380	0.724	0.724
9570	1.627	27.283	2.720	153.320	4.652	0.034	0.885	0.272	17.760	4.407	0.560	0.560
9600	1.463	13.556	3.150	293.946	7.786	0.072	0.218	0.228	40.254	5.704	0.808	0.808
9630	1.165	3.286	0.774	41.094	1.810	0.020	0.075	0.086	7.695	1.081	0.599	0.599
9660	0.567	6.308	0.874	279.869	4.432	0.055	0.033	0.095	16.956	2.301	0.618	0.618
9690	0.182	6.932	0.570	303.359	4.672	0.027	0.050	0.042	12.913	2.622	0.201	0.201
9720	0.166	3.937	0.662	490.408	4.494	0.083	0.389	0.092	19.039	2.183	0.369	0.369
9750	0.746	11.764	1.836	241.283	4.392	0.055	1.020	0.253	18.970	3.583	0.549	0.549
9780	0.600	11.972	1.763	652.228	14.911	0.063	0.261	0.260	58.017	5.306	0.316	0.316
9810	1.248	7.291	2.358	477.421	5.455	0.217	0.905	0.316	17.751	5.103	0.906	0.906
9840	1.085	33.103	2.073	536.573	12.775	0.049	0.052	0.359	23.457	7.048	0.896	0.896
9870	1.145	20.566	3.219	364.806	9.092	0.143	0.117	0.309	39.024	6.211	0.986	0.986
9900	0.366	6.492	1.064	440.141	4.005	0.082	0.663	0.178	18.504	1.768	0.589	0.589
9930	0.485	22.809	0.483	299.295	2.058	0.021	0.109	0.057	12.098	7.546	0.211	0.211
9960	0.490	3.110	0.214	114.648	2.180	0.024	0.128	0.026	8.611	2.296	0.263	0.263
9990	0.912	634.242	0.741	352.239	6.633	0.029	0.398	0.169	17.905	16.315	0.397	0.397
10020	1.288	27.617	1.102	237.002	4.326	0.021	0.050	0.160	22.603	30.059	0.364	0.364
10050	11.412	41.849	7.180	140.238	4.476	<0.066	0.448	1.122	73.034	44.614	0.892	0.892

10170	3.008	53.963	20.617	149.780	3.843	0.179	3.605	3.861	41.724	10.255	1.331	1.331
10190	4.072	21.366	7.834	56.658	3.157	<0.070	2.660	0.837	17.140	23.213	0.789	0.789
10220	0.612	1.916	1.284	46.226	0.897	<0.016	0.963	0.155	34.291	2.822	0.176	0.176
10250	3.266	13.634	21.940	190.477	7.012	0.196	4.814	4.460	145.780	24.582	1.468	1.468
10280	4.806	18.657	26.404	208.842	12.369	0.238	0.634	4.808	60.754	6.360	2.763	2.763
10310	3.185	23.048	11.503	231.668	10.978	0.106	0.185	2.435	55.337	7.839	1.722	1.722
10340	0.433	19.280	0.936	272.855	1.668	<0.031	0.283	0.205	14.031	2.114	0.275	0.275
10400	0.357	3.058	1.584	21.193	0.887	<0.011	0.014	0.501	6.766	0.886	0.116	0.116
10430	2.698	52.867	16.078	153.498	4.858	0.212	2.771	3.637	92.713	4.800	0.889	0.889
10460	8.422	39.386	16.849	81.313	3.837	<0.101	0.185	2.091	146.803	8.204	1.179	1.179
10490	4.173	26.432	5.406	133.695	4.289	<0.046	0.037	0.577	104.456	15.186	0.814	0.814
10520	11.560	1226.302	41.834	445.574	10.782	0.166	5.671	3.913	308.975	677.558	1.257	1.257
10550	5.096	76.600	25.347	150.780	3.073	0.141	0.125	3.925	78.492	26.481	0.880	0.880
10580	3.584	45.505	22.980	132.046	5.797	0.198	1.667	3.578	97.390	8.486	1.347	1.347
10610	2.968	41.964	22.957	193.900	6.439	0.147	0.104	5.187	46.876	8.502	1.939	1.939
10640	2.181	26.621	17.177	210.681	6.314	<0.100	0.383	2.773	46.405	11.975	1.348	1.348
10670	2.144	68.362	9.657	333.447	5.139	0.101	0.035	1.478	96.386	16.328	0.784	0.784
10700	2.441	80.588	7.686	481.502	6.522	<0.081	0.320	1.873	37.719	17.537	0.852	0.852
10730	3.400	63.868	21.148	418.764	7.799	0.138	0.236	4.571	125.062	31.161	1.097	1.097
10760	6.904	271.956	27.578	213.150	7.079	0.829	0.067	7.473	79.976	32.089	1.449	1.449
10790	20.578	57.508	24.790	186.389	4.615	0.132	5.467	4.928	77.097	5.306	1.586	1.586
10820	11.282	104.388	34.578	254.230	6.669	0.202	1.929	6.028	86.766	14.371	1.527	1.527
10850	4.587	687.611	12.019	191.016	5.132	0.096	0.576	1.182	53.777	286.677	0.544	0.544
10880	3.602	88.468	16.260	273.325	6.992	0.084	1.964	2.203	70.753	46.861	1.010	1.010
10910	3.975	113.183	29.447	215.707	6.255	0.103	5.258	5.510	78.822	16.810	1.409	1.409
10940	0.187	25.370	0.979	279.556	2.606	<0.020	0.100	0.219	40.087	21.237	0.344	0.344
10970	0.177	9.907	0.311	65.514	0.766	<0.016	0.016	0.045	6.175	2.937	0.229	0.229
11000	0.171	6.945	1.601	188.656	1.753	<0.056	0.096	0.357	29.785	5.620	0.260	0.260
11020	0.306	14.244	4.011	216.076	2.156	<0.091	0.556	0.939	12.213	4.800	0.087	0.087
11050	0.635	559.696	1.420	185.997	2.744	<0.037	0.230	0.329	53.474	77.998	0.336	0.336

11080	0.341	10.186	2.206	243.919	7.523	<0.032	0.024	0.689	13.367	13.380	0.722	0.722
11100	0.149	5.326	0.328	184.652	3.785	<0.013	0.015	0.057	22.067	3.606	0.249	0.249
11130	6.501	7.762	7.471	40.348	4.905	0.069	1.015	0.932	45.367	3.102	0.953	0.953
11160	0.375	14.101	1.073	128.050	2.781	<0.022	0.108	0.151	108.202	15.242	0.305	0.305
11180	1.980	133.089	16.654	336.198	4.021	0.105	2.079	1.995	63.605	7.902	0.763	0.763
11210	1.010	930.940	13.690	252.973	6.534	<0.103	6.092	3.958	54.686	56.239	0.635	0.635
11240	5.283	259.396	35.845	156.733	9.845	0.314	1.017	9.629	47.107	13.323	1.886	1.886
11270	5.640	923.184	20.423	204.607	9.828	<0.088	4.108	6.767	39.764	84.822	1.273	1.273
11300	2.766	600.620	21.957	166.932	7.086	0.120	1.090	6.291	45.635	38.914	1.289	1.289
11330	2.452	9.375	19.364	129.666	4.295	0.145	0.710	5.550	31.391	3.107	1.209	1.209
11360	2.574	54.657	16.749	124.879	6.848	0.176	0.966	3.347	39.881	38.207	1.311	1.311
11390	3.942	104.487	27.780	134.068	7.394	<0.148	0.805	8.150	59.003	81.768	1.355	1.355
11420	2.170	187.737	17.057	170.272	4.919	0.150	1.058	3.993	61.792	43.093	0.866	0.866
11450	2.160	74.168	6.120	54.850	2.342	<0.047	0.303	0.921	19.658	15.022	0.526	0.526
11750	1.483	3.427	1.450	19.410	1.243	<0.022	0.104	0.158	66.567	102.977	0.288	0.288
11780	5.773	43.259	4.581	72.650	3.376	0.060	0.441	0.836	1685.034	338.477	0.425	0.425
11810	6.018	17.267	6.798	163.967	5.972	0.188	0.139	1.325	1786.343	743.376	0.601	0.601
11840	3.259	77.327	4.850	72.666	4.720	<0.077	1.246	0.714	1362.441	81.897	0.243	0.243
11870	3.263	172.315	31.956	253.947	13.904	<0.149	1.026	8.942	1082.479	43.196	0.835	0.835
11900	2.814	73.749	18.124	299.340	13.664	<0.156	0.429	5.309	483.029	39.549	0.316	0.316

Table 7. Kalladeina 1 REE data set.

Depth (feet)	La_ppm	Ce_ppm	Pr_ppm	Nd_ppm	Sm_ppm	Eu_ppm	Gd_ppm	Tb_ppm	Dy_ppm	Ho_ppm	Er_ppm	Tm_ppm	Yb_ppm	Lu_ppm
7150	12.454	31.168	4.052	16.863	3.914	0.894	3.929	0.660	3.897	0.799	2.206	0.317	2.105	0.346
7180	9.886	21.988	2.607	9.621	1.929	0.403	1.852	0.297	1.802	0.384	1.137	0.166	1.062	0.176
7200	2.136	5.073	0.605	2.293	0.449	0.094	0.450	0.076	0.429	0.089	0.252	0.038	0.248	0.037
7300	8.668	22.686	3.006	13.633	3.521	0.800	3.896	0.651	3.487	0.679	1.793	0.266	1.959	0.305
7330	11.732	26.420	3.136	12.432	2.728	0.698	2.968	0.503	3.166	0.688	2.165	0.312	2.153	0.324

7360	11.032	23.516	2.562	9.392	1.750	0.345	1.773	0.288	1.742	0.350	1.050	0.156	1.013	0.140
7390	7.478	16.308	1.810	6.440	1.231	0.252	1.330	0.207	1.237	0.238	0.779	0.109	0.686	0.094
7420	2.813	5.787	0.658	2.425	0.449	0.094	0.412	0.072	0.464	0.088	0.259	0.039	0.249	0.038
7450	21.213	44.878	5.014	17.762	3.250	0.693	3.427	0.561	3.722	0.811	2.452	0.374	2.661	0.418
7480	5.501	13.076	1.568	6.581	1.379	0.328	1.505	0.243	1.466	0.275	0.813	0.115	0.737	0.111
7500	34.418	75.307	9.179	38.064	10.161	2.225	11.579	2.048	12.697	2.536	7.614	1.193	8.495	1.265
7900	33.245	72.565	8.351	31.742	6.575	1.306	6.924	1.214	7.322	1.442	4.370	0.691	4.288	0.632
7930	45.077	101.667	11.235	42.686	8.435	1.343	6.668	0.989	4.779	0.991	2.644	0.327	2.142	0.377
7950	30.520	64.588	7.202	28.220	5.136	1.175	5.294	0.731	4.047	0.772	1.997	0.310	1.930	0.292
7970	51.242	107.262	12.014	43.261	7.172	1.468	6.800	0.930	5.234	0.977	2.719	0.374	2.310	0.385
7990	56.397	110.654	13.324	51.133	9.376	1.525	7.287	1.010	4.764	0.784	2.064	0.277	1.680	0.308
8190	11.344	25.747	3.093	11.735	2.731	0.527	2.577	0.412	2.705	0.538	1.568	0.233	1.583	0.220
8160	4.221	10.318	1.388	6.364	1.949	0.379	2.201	0.374	2.111	0.399	0.983	0.108	0.752	0.098
8220	7.201	17.927	2.631	11.270	3.422	0.841	4.079	0.628	3.983	0.774	2.011	0.282	1.817	0.282
8250	3.238	7.347	1.007	4.548	1.573	0.334	1.525	0.245	1.539	0.273	0.745	0.101	0.801	0.087
8280	5.098	12.116	1.764	7.465	2.356	0.569	2.553	0.444	2.687	0.549	1.455	0.217	1.457	0.188
8310	2.630	7.911	1.145	5.315	1.319	0.302	1.505	0.219	1.265	0.228	0.559	0.078	0.456	0.066
8340	4.031	11.580	1.544	6.926	1.827	0.364	1.848	0.279	1.505	0.315	0.783	0.113	0.666	0.091
8370	3.798	10.279	1.330	6.451	1.627	0.329	1.775	0.270	1.529	0.323	0.885	0.107	0.815	0.114
8400	5.482	14.508	1.929	8.030	1.730	0.417	1.944	0.301	1.987	0.378	1.122	0.161	1.006	0.147
8430	4.558	13.560	2.033	9.008	2.535	0.663	2.523	0.411	2.444	0.470	1.203	0.170	1.294	0.180
8460	4.406	10.849	1.227	4.813	0.959	0.216	0.920	0.146	0.904	0.185	0.532	0.079	0.476	0.070
8488	1.035	2.740	0.508	2.922	1.418	0.383	1.653	0.191	1.067	0.177	0.413	0.047	0.447	0.055
8520	3.563	8.713	1.175	4.874	1.357	0.313	1.423	0.221	1.223	0.231	0.640	0.080	0.550	0.077
8550	4.100	10.587	1.444	6.951	2.064	0.504	2.159	0.350	1.915	0.344	0.997	0.132	0.842	0.131
8580	9.135	26.538	3.599	15.504	3.774	0.980	3.801	0.686	4.348	0.893	2.699	0.400	2.729	0.404
8600	5.425	13.835	1.982	9.813	3.209	0.836	3.621	0.544	2.788	0.549	1.487	0.226	1.383	0.215
9150	7.027	15.682	1.892	7.485	1.712	0.401	1.618	0.262	1.631	0.324	0.899	0.127	0.824	0.114
9180	1.541	4.199	0.610	2.576	0.575	0.166	0.573	0.080	0.444	0.079	0.221	0.028	0.171	0.026
9210	6.762	16.210	2.078	7.751	1.702	0.479	1.586	0.261	1.604	0.323	0.942	0.124	0.851	0.113

Chemostratigraphy and geochronology of Cambrian sequences in East Warburton Basin, South Australia

9240	8.237	20.452	2.655	10.168	2.047	0.458	1.975	0.362	2.163	0.434	1.347	0.182	1.211	0.181
9270	8.216	18.849	2.292	8.508	1.701	0.357	1.644	0.278	1.807	0.368	1.102	0.160	1.021	0.149
9300	8.865	20.441	2.537	9.603	1.874	0.391	1.902	0.327	2.080	0.421	1.241	0.184	1.216	0.176
9330	6.598	16.257	2.125	8.210	1.734	0.369	1.786	0.313	1.961	0.412	1.167	0.167	1.094	0.161
9360	7.239	17.934	2.368	9.080	1.962	0.411	1.921	0.329	1.929	0.409	1.169	0.168	1.070	0.163
9390	8.361	19.613	2.446	9.296	2.024	0.462	2.117	0.383	2.309	0.492	1.437	0.204	1.344	0.196
9420	11.123	25.515	3.272	12.196	2.569	0.574	2.657	0.474	2.979	0.636	1.856	0.273	1.763	0.251
9450	10.911	22.826	3.057	11.275	2.342	0.488	2.343	0.399	2.539	0.545	1.558	0.218	1.376	0.208
9480	7.290	16.216	1.984	7.076	1.354	0.246	1.231	0.201	1.228	0.259	0.734	0.110	0.669	0.101
9510	2.249	5.356	0.678	2.540	0.567	0.110	0.501	0.083	0.492	0.088	0.264	0.035	0.225	0.036
9540	6.674	14.747	1.826	6.725	1.472	0.319	1.460	0.238	1.430	0.290	0.820	0.116	0.732	0.118
9570	3.858	8.649	1.083	4.425	0.946	0.200	0.921	0.150	0.849	0.170	0.462	0.065	0.394	0.064
9600	5.439	13.061	1.684	6.492	1.404	0.311	1.389	0.230	1.382	0.282	0.794	0.117	0.747	0.113
9630	1.080	3.056	0.461	1.833	0.437	0.087	0.409	0.064	0.362	0.069	0.193	0.025	0.161	0.023
9660	5.062	11.021	1.360	4.832	0.926	0.183	0.831	0.132	0.774	0.159	0.445	0.065	0.402	0.057
9690	6.293	13.060	1.520	5.249	0.954	0.183	0.891	0.139	0.825	0.169	0.461	0.068	0.426	0.063
9720	4.875	10.177	1.176	4.291	0.855	0.177	0.770	0.128	0.740	0.155	0.434	0.060	0.385	0.058
9750	3.651	7.764	0.950	3.713	0.789	0.167	0.761	0.129	0.722	0.147	0.430	0.060	0.394	0.056
9780	14.913	27.723	3.150	10.963	2.161	0.446	2.083	0.377	2.409	0.519	1.508	0.247	1.580	0.249
9810	7.118	14.032	1.617	5.705	1.041	0.206	0.999	0.160	0.925	0.174	0.499	0.080	0.470	0.070
9840	13.304	24.985	2.744	9.361	1.835	0.398	1.777	0.319	2.021	0.437	1.331	0.202	1.307	0.202
9870	8.855	17.553	2.043	7.238	1.390	0.303	1.361	0.239	1.462	0.307	0.913	0.148	0.873	0.128
9900	4.368	8.673	0.982	3.279	0.624	0.119	0.608	0.104	0.625	0.133	0.399	0.058	0.382	0.055
9930	2.378	4.601	0.499	1.755	0.321	0.069	0.312	0.052	0.315	0.068	0.202	0.031	0.198	0.030
9960	1.349	3.107	0.337	1.266	0.258	0.067	0.290	0.051	0.318	0.071	0.191	0.029	0.170	0.025
9990	5.242	10.433	1.132	3.971	0.801	0.183	0.808	0.145	0.902	0.202	0.606	0.096	0.610	0.102
10020	3.522	7.541	0.842	3.035	0.647	0.135	0.610	0.102	0.668	0.139	0.412	0.065	0.406	0.062
10050	2.108	5.496	0.779	3.524	1.146	0.288	1.118	0.170	0.898	0.168	0.456	0.060	0.360	0.062
10170	1.805	4.306	0.706	3.334	1.275	0.372	1.334	0.192	0.880	0.160	0.372	0.052	0.352	0.058
10190	1.362	3.795	0.598	2.959	0.993	0.220	1.042	0.137	0.731	0.126	0.282	0.040	0.254	0.035

Chemostratigraphy and geochronology of Cambrian sequences in East Warburton Basin, South Australia

10220	0.667	1.527	0.216	0.775	0.199	0.047	0.173	0.027	0.157	0.032	0.086	0.012	0.071	0.011
10250	2.294	5.623	0.841	5.425	1.979	0.441	1.917	0.292	1.476	0.275	0.650	0.091	0.564	0.085
10280	4.006	11.025	1.545	7.429	3.468	0.801	3.774	0.502	2.544	0.448	1.153	0.148	0.991	0.148
10310	4.976	11.253	1.620	7.213	2.357	0.546	2.213	0.356	1.939	0.383	1.073	0.152	1.013	0.152
10340	1.717	3.295	0.394	1.257	0.247	0.054	0.229	0.040	0.224	0.048	0.141	0.024	0.138	0.021
10400	0.246	0.608	0.093	0.448	0.193	0.042	0.186	0.029	0.162	0.030	0.089	0.012	0.077	0.011
10430	1.489	5.119	0.560	2.773	1.164	0.290	1.258	0.178	0.924	0.173	0.444	0.058	0.397	0.056
10460	1.322	3.579	0.536	2.591	1.270	0.328	1.400	0.181	0.865	0.154	0.358	0.050	0.284	0.038
10490	1.173	3.314	0.526	2.578	1.016	0.245	0.985	0.160	0.844	0.165	0.415	0.053	0.377	0.051
10520	6.566	13.854	1.760	7.174	2.199	0.555	2.493	0.366	1.957	0.375	0.993	0.135	0.861	0.123
10550	0.997	2.566	0.436	1.961	0.946	0.257	1.063	0.154	0.709	0.123	0.303	0.035	0.240	0.035
10580	1.904	4.757	0.745	3.599	1.649	0.377	1.694	0.237	1.221	0.225	0.565	0.097	0.499	0.069
10610	1.935	4.732	0.933	4.092	1.738	0.434	1.842	0.267	1.289	0.241	0.556	0.090	0.536	0.078
10640	2.281	6.404	0.983	4.360	1.571	0.368	1.518	0.218	1.173	0.227	0.626	0.087	0.591	0.089
10670	2.168	5.088	0.715	3.162	0.927	0.254	0.959	0.151	0.860	0.169	0.507	0.072	0.435	0.068
10700	2.958	7.487	0.998	4.124	1.443	0.338	1.497	0.230	1.252	0.233	0.653	0.086	0.591	0.089
10730	3.016	7.797	1.139	4.916	1.852	0.498	2.041	0.288	1.593	0.299	0.762	0.105	0.645	0.093
10760	2.986	7.077	0.978	4.589	1.901	0.487	2.151	0.322	1.634	0.274	0.720	0.097	0.567	0.081
10790	1.728	4.250	0.646	3.187	1.727	0.411	1.897	0.235	1.105	0.171	0.426	0.057	0.323	0.054
10820	2.462	6.009	0.874	4.149	1.696	0.422	1.901	0.280	1.473	0.250	0.635	0.099	0.609	0.101
10850	3.079	6.954	0.950	4.065	1.062	0.230	1.047	0.155	0.898	0.178	0.488	0.067	0.395	0.056
10880	3.979	9.044	1.185	5.037	1.444	0.334	1.419	0.221	1.253	0.237	0.681	0.093	0.568	0.086
10910	2.210	5.810	0.870	4.173	1.688	0.365	1.680	0.248	1.235	0.230	0.562	0.083	0.499	0.082
10940	2.802	5.185	0.655	2.228	0.451	0.108	0.432	0.070	0.432	0.087	0.252	0.036	0.213	0.037
10970	0.806	1.515	0.194	0.692	0.141	0.032	0.121	0.021	0.127	0.026	0.076	0.011	0.065	0.010
11000	1.732	3.391	0.433	1.611	0.350	0.089	0.349	0.053	0.281	0.053	0.153	0.020	0.145	0.020
11020	1.868	3.625	0.474	1.764	0.397	0.110	0.406	0.063	0.352	0.064	0.210	0.024	0.176	0.028
11050	2.117	4.563	0.549	2.110	0.483	0.093	0.422	0.067	0.415	0.089	0.241	0.037	0.243	0.038
11080	5.147	11.904	1.562	6.560	1.531	0.363	1.376	0.224	1.229	0.246	0.688	0.093	0.571	0.095
11100	3.553	7.726	0.930	3.385	0.653	0.151	0.599	0.098	0.587	0.121	0.342	0.049	0.327	0.048

11130	2.123	5.625	0.843	4.016	1.328	0.308	1.325	0.197	1.044	0.194	0.480	0.059	0.361	0.053
11160	1.637	3.948	0.538	2.178	0.522	0.134	0.460	0.076	0.468	0.094	0.270	0.039	0.232	0.033
11180	2.325	5.549	0.782	3.383	0.937	0.226	0.947	0.123	0.751	0.139	0.383	0.048	0.322	0.051
11210	2.715	6.764	0.953	4.367	1.416	0.348	1.398	0.222	1.284	0.222	0.599	0.088	0.523	0.090
11240	3.482	9.576	1.459	7.606	2.610	0.652	2.926	0.420	2.154	0.366	0.915	0.126	0.692	0.119
11270	3.788	9.884	1.438	6.891	2.366	0.548	2.330	0.349	1.863	0.327	0.821	0.116	0.744	0.109
11300	2.679	6.976	1.075	5.461	1.920	0.426	1.738	0.265	1.381	0.250	0.610	0.086	0.545	0.077
11330	1.948	4.928	0.735	3.460	1.243	0.299	1.287	0.182	0.928	0.155	0.391	0.055	0.305	0.040
11360	2.696	7.131	1.032	5.041	1.797	0.396	1.732	0.279	1.355	0.253	0.671	0.089	0.555	0.079
11390	2.099	5.455	0.851	4.440	1.960	0.439	1.941	0.295	1.580	0.274	0.709	0.102	0.647	0.089
11420	2.001	4.812	0.678	3.236	1.192	0.273	1.279	0.173	0.950	0.176	0.447	0.063	0.350	0.060
11450	0.926	2.454	0.384	1.845	0.688	0.156	0.697	0.103	0.525	0.091	0.236	0.029	0.196	0.029
11750	0.526	1.328	0.194	0.897	0.236	0.074	0.260	0.044	0.235	0.047	0.119	0.015	0.099	0.018
11780	1.580	3.640	0.563	2.499	0.689	0.306	0.728	0.103	0.594	0.113	0.318	0.041	0.250	0.039
11810	3.286	7.899	1.200	5.250	1.258	0.495	1.213	0.197	1.069	0.207	0.602	0.081	0.489	0.079
11840	2.702	4.897	0.764	3.140	0.885	0.344	0.934	0.172	0.942	0.183	0.479	0.063	0.478	0.074
11870	8.618	15.074	2.131	8.638	2.516	1.141	2.739	0.469	2.765	0.519	1.504	0.223	1.505	0.241
11900	7.291	13.777	1.936	7.872	2.333	0.865	2.684	0.476	2.585	0.501	1.419	0.211	1.441	0.229

Carbon Isotope ($\delta^{13}\text{C}$) Datasets

Table 8. Carbon ($\delta^{13}\text{C}$) isotope dataset for Gidgealpa 7. (?) indicates analysis number and red text indicates outliers.

Sample	Value Used	$\delta^{13}\text{C}$ (1)	Error	$\delta^{13}\text{C}$ (2)	Error	$\delta^{13}\text{C}$ (3)	Error
7660	-3.887	-5.353		-6.353	0.281	-3.887	0.027
7680	1.350	0.038	0.142	1.350	0.074	-	-
7701	1.538	1.220	0.063	1.538	0.016	-	-

7720	0.236	-1.300	0.139	0.236	0.028	-	-
7750	3.178	-1.584	n.a.	3.178	0.039	-	-
7800	3.258	1.811	0.026	2.304	0.101	3.258	0.033
7820	2.741	2.741	0.054	-	-	-	-
7850	2.276	4.254	0.110	2.276	0.012	-	-
7910	2.110	1.305	0.063	2.110	0.040	-	-
7940	3.671	3.671	0.019	-	-	-	-
7960	0.577	1.444	0.036	0.577	0.019	-	-
7980	0.389	-0.861	0.254	0.461	0.130	0.389	0.025
8010	0.593	-1.183	0.342	0.593	0.054	-	-
8072	0.091	0.091	0.289	-	-	-	-
8090	-1.167	-1.167	0.102	-	-	-	-
8120	-1.399	-1.399	0.081	-	-	-	-
8180	-0.832	-0.832	0.098	-	-	-	-
8230	0.536	0.536	0.328	-	-	-	-
8250	-1.000	-1.000	0.052	-	-	-	-
8280	-0.784	-0.784	0.107	-	-	-	-
8310	0.876	0.876	0.129	-	-	-	-
8340	-0.765	-0.765	0.094	-	-	-	-
8370	-1.075	-1.075	0.312	-	-	-	-
8400	-0.823	-0.823	0.269	-	-	-	-
8430	-0.648	-0.648	0.102	-	-	-	-
8460	-0.565	-0.565	0.151	0.216	0.177	-	-
8500	-0.060	-0.060	0.330	-	-	-	-
8520	0.024	0.024	0.134	-	-	-	-
8550	0.644	0.644	0.302	-	-	-	-
8580	-0.580	-0.580	0.123	-	-	-	-
8610	0.140	0.140	0.072	-	-	-	-
8640	0.952	0.952	0.049	-	-	-	-
8670	0.098	0.098	0.321	-	-	-	-

8760	-1.670	-1.670	0.007	-1.651	0.037	-	-
8793	-0.504	-0.504	0.141	5.237	0.277	-	-
8820	0.719	0.719	0.076	-	-	-	-
8850	0.293	0.293	0.089	-	-	-	-
8880	0.254	0.254	0.133	-	-	-	-
8900	0.221	0.221	0.094	-	-	-	-
8930	0.532	0.532	0.135	-	-	-	-
8970	0.151	0.151	0.057	-	-	-	-
9000	-0.120	-0.120	0.209	-1.133	0.260	-	-
9030	-0.026	-0.026	0.218	-	-	-	-
9059	-0.878	-0.878	0.239	-	-	-	-
9074	-4.799	-4.799	0.343	n.a.	-	-	-
9080	-1.371	1.645	0.177	-1.371	0.018	-	-
9100	-0.247	-0.247	0.214	-	-	-	-
9120	1.177	1.177	0.128	-	-	-	-
9150	-0.632	-0.632	0.216	-	-	-	-
9250	-0.751	-0.751	0.108	-	-	-	-
9270	0.048	0.048	0.246	-	-	-	-
9290	-0.480	-0.480	0.245	-	-	-	-
9310	1.771	1.771	0.289	-10.510	0.974	-	-
9330	-1.091	-1.091	0.141	-	-	-	-
9350	-0.049	-0.049	0.182	-	-	-	-
9380	-0.080	-0.080	0.147	-	-	-	-
9410	0.355	0.355	0.163	-	-	-	-
9430	-0.996	-0.996	0.105	-	-	-	-
9450	0.800	0.800	0.831	-	-	-	-
9530	-1.671	-1.671	0.180	-	-	-	-
9560	-1.219	-1.219	0.093	-	-	-	-
9580	-1.711	-1.711	0.109	-	-	-	-
9610	-0.694	-0.694	0.118	-	-	-	-

9630	-1.513	-1.513	0.104	-	-	-	-
9650	-1.203	-1.203	0.115	-1.203	0.060	1.440	0.182
9750	-0.848	-0.717	0.147	-0.848	0.022	-	-
9760	-1.242	-1.161	0.159	-1.242	0.019	-	-
9780	-1.011	-0.912	0.159	-1.011	0.013	-	-
9800	-1.095	-0.885	0.160	-1.095	0.052	-	-
9830	-0.957	-0.956	0.226	-0.957	0.046	-	-
9850	-1.132	-1.095	0.245	-1.132	0.010	-0.912	0.014
9870	-1.008	-1.084	0.137	-1.008	0.049	-	-
9900	0.690	0.834	0.163	0.690	0.078	-	-
9920	-1.175	-1.175	0.035	-0.941	0.037	-	-
9950	-0.090	-0.090	0.040	-	-	-	-
9970	0.316	0.316	0.084	-	-	-	-
10100	-0.480	-0.480	0.155	-	-	-	-
10110	-2.888	-2.771	0.179	-2.888	0.047	-	-
10120	-2.096	-2.161	0.203	-2.096	0.041	-	-
10140	-2.771	-2.420	0.084	-2.771	0.025	-	-
10210	-0.433	-0.433	0.054	-	-	-	-
10270	-0.561	-0.561	0.096	-	-	-	-
10290	-0.439	-0.439	0.093	-	-	-	-
10320	-0.346	-0.392	0.123	-0.346	0.020	-	-
10340	0.797	0.797	0.023	-	-	-	-
10370	0.136	0.136	-	-	-	-	-

Table 9. Carbon ($\delta^{13}\text{C}$) isotope dataset for Kalladeina 1. (?) indicates analysis number and red text indicating outliers.

Sample	Value Used	$\delta^{13}\text{C}$ (1)	Error	$\delta^{13}\text{C}$ (2)	Error	$\delta^{13}\text{C}$ (3)	Error
6580	0.363	0.363	0.035	-	-	-	-
6670	1.376	1.376	0.016	-	-	-	-

6700	1.958	1.958	0.078	-	-	-	-
6790	1.001	1.001	0.050	-	-	-	-
6820	1.071	1.071	0.041	-	-	-	-
6850	1.208	1.208	0.032	-	-	-	-
6910	0.424	0.424	0.047	-	-	-	-
7000	-0.385	-0.385	0.065	-	-	-	-
7030	-0.102	-0.102	0.067	-	-	-	-
7060	0.282	0.282	0.055	-	-	-	-
7090	0.029	0.029	0.022	-	-	-	-
7180	0.279	0.279	0.019	-	-	-	-
7200	0.008	0.008	0.057	-	-	-	-
7360	-0.507	-0.507	0.060	-	-	-	-
7390	0.182	0.182	0.042	-	-	-	-
7450	0.034	-1.118	0.034	-0.767	0.073	-	-
7480	-2.675	-2.675	0.107	-	-	-	-
7900	-2.907	-2.907	0.111	-2.733	0.227	-	-
7930	-3.895	-6.522	0.268	-3.895	0.132	-	-
7950	-3.997	-6.983	0.532	-3.997	0.090	-	-
7970	-5.527	-6.357	0.593	-6.126	0.242	-5.527	0.060
7990	-4.028	-4.028	1.360	-3.481	0.098	-	-
8160	-3.278	-3.278	0.626	-9.953	1.748	-	-
8190	-0.461	-0.461	0.054	-0.381	0.121	-	-
8220	-4.505	-5.022	0.558	-4.505	0.103	-	-
8250	-6.043	-7.256	0.384	-6.043	0.344	-	-
8280	-5.863	-6.761	0.060	-5.863	0.036	-	-
8310	0.758	0.758	0.116	0.578	0.228	-	-
8340	1.769	1.769	0.107	2.037	0.131	-	-
8370	2.560	2.560	0.117	2.788	0.545	-	-
8400	3.732	3.732	0.031	4.019	0.141	-	-
8430	4.247	4.247	0.076	4.167	0.118	-	-

Chemostratigraphy and geochronology of Cambrian sequences in East Warburton Basin, South Australia

8460	5.240	4.622	0.188	5.240	0.086	-	-
8488	-	-7.745	0.557	-	-	-	-
8520	4.810	4.810	0.022	4.434	0.206	-	-
8550	3.829	3.829	0.018	3.972	0.192	-	-
8580	3.300	3.300	0.043	3.480	0.174	-	-
8600	2.796	2.796	0.037	-5.147	n.a.	-	-
9150	2.526	2.526	0.035	2.595	0.094	-	-
9180	1.112	1.112	0.058	1.788	0.128	-	-
9210	1.186	1.186	0.029	1.235	0.214	-	-
9240	1.288	1.288	0.035	1.240	0.197	-	-
9270	0.998	0.858	0.129	1.138	0.128	-	-
9300	0.782	0.782	0.036	1.149	0.175	-	-
9330	0.675	0.675	0.107	0.882	0.207	-	-
9360	0.483	0.483	0.008	0.760	0.117	-	-
9390	0.467	0.467	0.042	0.520	0.057	-5.554	1.022
9420	0.388	0.388	0.096	0.416	0.118	-	-
9450	0.410	0.410	0.035	0.197	0.232	-	-
9480	0.341	0.281	0.074	0.400	0.075	-	-
9510	0.269	0.269	0.121	-	-	-	-
9540	-0.358	-0.358	0.119	-0.661	0.200	-	-
9570	-0.273	-0.273	0.071	-0.271	0.219	-	-
9600	-0.060	-0.057	0.061	-0.060	0.048	-0.124	0.156
9630	-0.134	-0.134	0.035	-0.276	0.156	-	-
9660	0.213	0.242	0.072	0.184	0.072	-	-
9690	-0.108	-0.010	0.065	-0.207	0.058	-	-
9720	0.067	0.067	0.070	-0.266	0.127	-	-
9750	1.759	1.759	0.688	-	-	-	-
9780	0.223	0.223	0.108	-	-	-	-
9810	-0.496	-0.496	0.119	-	-	-	-
9840	-0.577	-0.577	0.204	-	-	-	-

10050	-1.003	-1.003	0.030	-	-	-	-
10150	-2.870	-2.870	0.073	-	-	-	-
10170	-0.345	-0.345	0.063	-	-	-	-
10190	-0.472	-0.472	0.057	-	-	-	-
10250	-0.668	-0.668	0.025	-0.494	0.057	-	-
10280	-0.971	-0.971	0.049	-	-	-	-
10400	-1.028	-1.028	0.110	-	-	-	-
10430	-0.397	-0.397	0.042	-	-	-	-
10460	-1.257	-1.257	0.070	-	-	-	-
10490	-2.455	-2.455	0.046	-	-	-	-
10520	-1.480	-1.480	0.058	-	-	-	-
10550	-2.641	-2.641	0.038	-	-	-	-
10580	-2.966	-2.966	0.081	-	-	-	-
10610	-3.254	-3.254	0.056	-	-	-	-
10640	-1.792	-1.792	0.135	-	-	-	-
10670	-1.231	-1.231	0.081	-	-	-	-
10730	-0.942	-0.942	0.095	-	-	-	-
10760	-0.778	-0.778	0.082	-	-	-	-
10790	-1.366	-1.660	0.055	-1.366	0.043	-	-
10820	-1.914	-1.914	0.057	-	-	-	-
10850	-0.569	-0.569	0.055	-	-	-	-
10880	-0.170	-0.170	0.054	-	-	-	-
10910	-0.589	-0.589	0.039	-	-	-	-
11130	-0.418	-0.418	0.029	-	-	-	-
11180	-0.219	-0.219	0.041	-	-	-	-
11210	-0.548	-0.548	0.022	-	-	-	-
11240	-3.200	-3.200	0.040	-	-	-	-
11270	-3.039	-3.039	0.058	-	-	-	-
11300	-1.266	-1.266	0.037	-	-	-	-
11330	0.025	0.025	0.025	-	-	-	-

11360	-2.321	-2.321	0.064	-	-	-	-
11390	-4.027	-4.027	0.059	-	-	-	-
11420	-0.885	-0.885	0.079	-	-	-	-
11450	-0.181	-0.181	0.030	-	-	-	-
11810	-2.250	-2.250	0.012	-	-	-	-
11840	-2.375	-2.375	0.014	-2.064	0.053	-	-
11870	-3.315	-3.315	0.029	-	-	-	-

Sr Isotope ($^{87}\text{Sr}/^{86}\text{Sr}$) Datasets

Table 10. Sr isotope ($^{87}\text{Sr}/^{86}\text{Sr}$) uncorrected (for in-situ Rb decay) dataset for Gidgealpa 7. (?) indicates analysis number, with (1) representing $^{87}\text{Sr}/^{86}\text{Sr}$ value used, with exceptions to those in red (outliers).

Sample	$^{87}\text{Sr}/^{86}\text{Sr}$ Value (1)	Error	$^{87}\text{Sr}/^{86}\text{Sr}$ Value (2)	Error
7660	.711875	.000004	-	-
7680	.710534	.000003	-	-
7701	.711354	.000003	-	-
7720	.711412	.000004	-	-
7750	.710367	.000003	-	-
7800	.710523	.000004	.712183	.001374
7820	.710357	.000003	-	-
7850	.711000	.000003	-	-
7910	.711058	.000003	-	-
7940	.710258	.000004	-	-
7960	.710330	.000003	.711235	.000003
7980	.710400	.000003	.726284	.008475

8010	.709969	.000003	-	-
8040	.709981	.000003	.714442	.004624
8090	.710390	.000003	-	-
8120	.709994	.000004	.709988	.000004
8180	.710356	.000003	.710385	.000062
8230	.710024	.000004	-	-
8280	.710697	.000003	-	-
8310	.711581	.000003	-	-
8340	.711797	.000005	-	-
8370	.711739	.000003	-	-
8400	.710940	.000003	-	-
8430	.710594	.000004	-	-
8460	.711036	.000003	.715837	.003700
8500	.711317	.000003	-	-
8520	.713483	.000003	-	-
8550	.711362	.000004	-	-
8580	.711528	.000003	-	-
8610	.710930	.000003	-	-
8640	.710392	.000003	-	-
8670	.711336	.000003	.711787	.000545
8760	.716027	.000003	-	-
8793	.710448	.000004	-	-
8900	.709854	.000003	-	-
8930	.709699	.000003	-	-
8970	.710283	.000524	.709866	.000004
9000	.710088	.000003	-	-
9030	.710175	.000004	-	-
9074	.720848	.000003	-	-

9080	.720848	n.a.	-	-
9530	.716472	.000003	-	-
9580	.711560	.000003	-	-
9610	.713303	.000003	-	-
9650	.713717	.000003	-	-
9780	.712194	.000003	-	-
9800	.712580	.000004	-	-
9831	.713973	.001467	-	-
9870	.713069	.000003	-	-
9970	.710383	.000003	-	-
10100	.711794	.000004	-	-
10140	.714047	.000003	-	-
10270	.710899	.000003	.734176	.008632

Table 11. Sr isotope ($^{87}\text{Sr}/^{86}\text{Sr}$) uncorrected (for in-situ Rb decay) dataset for Kalladeina 1. (?) indicates analysis number, with (1) representing $^{87}\text{Sr}/^{86}\text{Sr}$ value used.

Sample	$^{87}\text{Sr}/^{86}\text{Sr}$ Value (1)	Error	$^{87}\text{Sr}/^{86}\text{Sr}$ Value (2)	Error
8190	.715055	.000003	-	-
8160	.729228	.000004	-	-
8220	.725618	.000022	-	-
8250	.726968	.000003	-	-
8280	.723932	.000003	-	-
8310	.719646	.000004	-	-
8340	.719932	.000003	-	-
8370	.715321	.000003	-	-
8400	.711297	.000003	-	-
8430	.712905	.000003	-	-

8460	.711235	.000003	.711240	.000004
8488	.724006	.000003	-	-
8520	.711738	.000004	-	-
8550	.712663	.000003	-	-
8580	.711853	.000004	-	-
8600	.716988	.000004	-	-
9150	.712167	.000003	-	-
9180	.713578	.000003	-	-
9210	.711723	.000018	.711650	.000057
9240	.711343	.000003	-	-
9270	.711057	.000003	-	-
9300	.710916	.000003	-	-

Table 12. Sr isotope ($^{87}\text{Sr}/^{86}\text{Sr}$) uncorrected (for in-situ Rb decay) dataset for “Vuggy Dolomite” samples from Gidgealpa 5.

Sample	Depth (feet)	Position	$^{87}\text{Sr}/^{86}\text{Sr}$ Value	Error
D1	7951	Vug	.710071	.000005
D2	7951	Light	.710128	.000004
D3	8123	Light /Dark thin section	.709936	.000003
D4	8123	Vug	.710382	.000003
D5	8123	Light/Dark	.710114	.000003